A Thesis submitted for the degree of Doctor of Philosophy in the Faculty of Science

Stabilised mixed finite element methods on anisotropic meshes

Andreas Wachtel

15 December 2015

Department of Mathematics and Statistics
University of Strathclyde
Glasgow, UK

This thesis is the result of the author's original research. It has been composed by the author and has not been previously submitted for examination which has led to the award of a degree.

Signed:

Date:

Contents

List of Figures

List of Tables

Acknowledgements

I would like to express my deepest thanks to my supervisor, Dr. Gabriel Barrenechea. Thank you for the continued guidance, interest, support, motivation and actually accepting me as your PhD student.

Considering the publication [ABW15], which is based on results from Chapter 3, I would like to thank Prof. Mark Ainsworth for his contribution.

Another "thank you" goes to all my friends, in particular, Heather, Edith, Cheherazada, Stephen, and Kilian for both help and fun-time.

Furthermore, I am grateful towards some members of the staff of the Department of Mathematics and Statistics of the University of Strathclyde. In particular, to the administrative staff that made organisation of my academic time schedule not only easy, but also more pleasant.

My research was funded by the Leverhulme Trust under grant RPG-2012-483.

To my family, in particular, my wife, your love and support made this possible.

Thank you all!

Abstract

This thesis treats finite element methods for Stokes and Oseen equations on highly anisotropic meshes. The stability of the discrete saddle-point problem may be affected in a negative way by the anisotropies in the mesh $\mathcal{P}$. The reason is a required compatibility condition (inf-sup condition) between the discrete velocity space $\boldsymbol{V}_{\mathcal{P}}$ and the pressure space $M_{\mathcal{P}}$.

We identify subspaces $G \subset M_{\mathcal{P}}$ and derive uniform inf-sup conditions for the pair $\boldsymbol{V}_{\mathcal{P}} \times G$. That is, the inf-sup constant β_G is independent of properties of the mesh. These conditions are shown to be equivalent to the deficiency

$$\sup_{\boldsymbol{v}\in\boldsymbol{V}_{\mathcal{P}}} \frac{(\operatorname{div}\boldsymbol{v}, q)_\Omega}{|\boldsymbol{v}|_{1,\Omega}} \geq \beta_G \|\Pi_G q\|_{0,\Omega} - \|q - \Pi_G q\|_{0,\Omega} \quad \text{for all} \quad q \in M_{\mathcal{P}}\,,$$

where $\Pi_G \colon M_{\mathcal{P}} \to G$ is a surjective projection.

The definition of the spaces $G \subset M_{\mathcal{P}}$ relies on a set of constraints. Using these results we propose uniformly stable mixed methods, either by using the pairs $\boldsymbol{V}_{\mathcal{P}} \times G$ (i. e., strongly imposing the constraints) or by adding a stabilisation term to the formulation using $\boldsymbol{V}_{\mathcal{P}} \times M_{\mathcal{P}}$ (i. e., weakly imposing the constraints). The proposed stabilisation terms only act on the non-inf-sup stable part of the pressure, they vanish for members of G, and they are block diagonal. In addition, these properties ensure a local mass-conservation property also of the stabilised methods.

The above claims are confirmed by several numerical experiments.

Chapter 1

Introduction

In this thesis we study (stabilised) *Finite Element Methods (FEM)* applied to problems in fluid mechanics on *anisotropic* meshes, that is, meshes containing long and thin cells. Although the solution $\boldsymbol{u}$ of the problem is unknown, some of its physical properties may be known. Suppose, for example, that $\boldsymbol{u}$ is the velocity of water flowing through a pipe. At the boundary of the pipe, the magnitude of the velocity $|\boldsymbol{u}|$ is zero, whereas towards its centre $|\boldsymbol{u}|$ may increase rapidly. The velocity $\boldsymbol{u}$ is almost constant in the direction of flow and therefore the approximation error in this direction will be very small. By using meshes with long and thin cells we can exploit this fact and save computational effort when computing a discrete approximation $\boldsymbol{u}_h$ of $\boldsymbol{u}$.

A general incompressible flow problem is given by the Navier–Stokes equations:

Find a velocity $\boldsymbol{u}$ and a pressure p such that

$$\partial_t \boldsymbol{u} - \nu\Delta\boldsymbol{u} + \boldsymbol{u}\cdot\nabla\boldsymbol{u} + \sigma\boldsymbol{u} + \nabla p = \boldsymbol{f} \quad \text{and} \quad \operatorname{div}\boldsymbol{u} = 0 \tag{NS}$$

inside a domain Ω, for suitable parameters ν, σ, a body force $\boldsymbol{f}$ and subject to boundary conditions.

Here the phrase "suitable parameters" refers loosely to parameters such that a unique solution exists. One of the main references for this problem is the book by Girault and Raviart [GR86], where more precise assumptions on the parameters are given. The solution of (NS) is normally approximated by solving linearised sub-problems again and again in an iterative fashion. The iterative process is independent of anisotropies of meshes if the sub-problems can be solved independently. Therefore, we may restrict our attention to $\Omega \subset \mathbb{R}^2$ and sub-problems of the type:

For a given source $\boldsymbol{f} \in L^2(\Omega)^2$, find $\boldsymbol{u}$ and p such that

$$\begin{aligned} -\nu\Delta\boldsymbol{u} + \boldsymbol{b}\cdot\nabla\boldsymbol{u} + \sigma\boldsymbol{u} + \nabla p &= \boldsymbol{f} \quad \text{in} \quad \Omega\,, \\ \operatorname{div}\boldsymbol{u} &= 0 \quad \text{in} \quad \Omega\,, \\ \boldsymbol{u} &= \boldsymbol{0} \quad \text{on} \quad \partial\Omega\,, \end{aligned} \tag{1.1}$$

where $\nu > 0$ and $\sigma \geq 0$ are non-negative constants and $\boldsymbol{b}$ serves as a parameter.

When $\boldsymbol{b} = \boldsymbol{u}$, problem (1.1) is the stationary case of (NS), that is, $\partial \boldsymbol{u}/\partial t = 0$. For $\boldsymbol{b} \in L^\infty(\Omega)^2, \operatorname{div} \boldsymbol{b} = 0$, (1.1) is the *Oseen problem*, which arises, for example, from a linearisation of (NS) when $\boldsymbol{b}$ is an approximation of $\boldsymbol{u}$. And, for $\boldsymbol{b} \equiv \boldsymbol{0}$ it resembles the (generalised) *Stokes problem*, which also arises when the non-linear term in (NS) can be ignored, for example if the velocity is small compared to the parameters ν and σ.

The remainder of this chapter is structured as follows. We first set the necessary notation and recall sufficient conditions to solve problems of type (1.1). These conditions will also provide some structure for the subsequent literature review. Afterwards, an outline of the thesis is given.

1.1. Context for Literature review

We include this section for the sake of completeness and to motivate some detailed statements in the later review of existing literature. We will assume basic knowledge on FEMs, see for example [Cia78, BS08] for a thorough introduction to the topic.

We start with some notation, a weak formulation of (1.1), and an existence result which will be useful to refer to in the literature review. Hereafter, we use the standard notation for Sobolev spaces. The notation is aligned with [GR86], for more details we also refer to [Ada75]. Let $\omega \subseteq \Omega$ and let $L^2(\omega)$ be the set of square integrable functions on ω with the *inner product* denoted by $(u, v)_\omega \coloneqq \int_\omega uv \,\mathrm{d}\boldsymbol{x}$ and the corresponding norm $\|v\|_{0,\omega}^2 \coloneqq (v, v)_\omega$. Moreover, we use the average free subspace given by $L_0^2(\omega) \coloneqq \{q \in L^2(\omega) \colon (1, q)_\omega = 0\}$.

For $\ell \in \mathbb{N}_+$, $H^\ell(\omega) \subset L^2(\omega)$ denotes the usual Sobolev space containing functions whose weak (or distributional) derivatives exist up to order ℓ and lie in $L^2(\omega)$. The functions in $H_0^1(\omega)$ belong to $H^1(\omega)$ and vanish on the boundary $\partial\omega$. We denote the norm and seminorm in $H^\ell(\omega)$ by $\|\cdot\|_{\ell,\omega}$ and $|\cdot|_{\ell,\omega}$, respectively. Vector-valued functions and their spaces are given a bold-faced symbol, e. g. $\boldsymbol{v} \in \boldsymbol{H}_0^1(\omega) = \left[H_0^1(\omega)\right]^2$. Norms and inner products for functions in $L^2(\omega)^2$ and $L^2(\omega)^{2\times 2}$ are defined component-wise; the same notation is used.

In (1.1) the pressure p only appears as a gradient. Therefore, the solution is only unique up to a constant. This is normally solved by looking for a pressure in $L_0^2(\Omega)$ and later, if desired, adding the average of the atmospheric pressure to the obtained solution.

Now we are in the position to state the weak formulation of (1.1):

Find $(\boldsymbol{u}, p) \in \boldsymbol{V} \times M \coloneqq \boldsymbol{H}_0^1(\Omega) \times L_0^2(\Omega)$ *such that*

$$\mathfrak{B}(\boldsymbol{u}, p; \boldsymbol{v}, q) = (\boldsymbol{f}, \boldsymbol{v})_\Omega \quad \text{for all} \quad (\boldsymbol{v}, q) \in \boldsymbol{V} \times M\,, \tag{1.2}$$

where the bilinear form $\mathfrak{B}$ is defined by

$$\mathfrak{B}(\boldsymbol{u}, p; \boldsymbol{v}, q) \coloneqq a(\boldsymbol{v}, \boldsymbol{v}) - (p, \operatorname{div} \boldsymbol{v})_\Omega - (q, \operatorname{div} \boldsymbol{u})_\Omega\,, \tag{1.3}$$

with

$$a(\boldsymbol{u}, \boldsymbol{v}) \coloneqq \nu(\nabla \boldsymbol{u}, \nabla \boldsymbol{v})_\Omega + (\boldsymbol{b} \cdot \nabla \boldsymbol{u}, \boldsymbol{v})_\Omega + \sigma(\boldsymbol{u}, \boldsymbol{v})_\Omega\,. \tag{1.4}$$

We note that to obtain this formulation we integrated by parts over the domain Ω, that is, we applied Green's formula (see [GR86]). This formula is proven to be valid on domains whose boundary is *Lipschitz continuous*, which, for $\Omega \subset \mathbb{R}^2$, means that the boundary $\partial\Omega$ can be locally parametrized by a Lipschitz continuous function. A more general definition can be found in [GR86, Gri85] . All domains in this thesis have a Lipschitz continuous boundary.

We say a problem is *well-posed* if it has a unique solution. The following result restates [GR86, Corollary I.4.1] and gives criteria that are sufficient for the existence of a unique solution of (1.2).

Corollary 1.1. *Let the bilinear form* $a(\cdot, \cdot)$ *be* $\boldsymbol{V}$*-elliptic, that is, there is* $\gamma > 0$ *such that*

$$a(\boldsymbol{v}, \boldsymbol{v}) \geq \gamma \|\boldsymbol{v}\|_{\boldsymbol{V}}^2 = \gamma \|\boldsymbol{v}\|_{1,\Omega}^2 \quad \textit{for all} \quad \boldsymbol{v} \in \boldsymbol{V}\,. \tag{1.5}$$

Then, problem (1.2) *is well-posed if and only if*

$$\inf_{q \in M} \sup_{\boldsymbol{v} \in \boldsymbol{V}} \frac{(q, \operatorname{div} \boldsymbol{v})_\Omega}{\|q\|_{0,\Omega} |\boldsymbol{v}|_{1,\Omega}} \geq \beta_\Omega > 0\,. \tag{1.6}$$

Condition (1.6) has been proven to hold, see also [Gal94, Lemma III.3.1], and is called *inf-sup condition*, or *LBB condition*, where LBB are the initials of the authors Ladyzhenskaya, Babuška and Brezzi, who independently proposed the condition. Finally, the *Poincaré inequality* $\|v\|_{0,\Omega} \leq C_\Omega |v|_{1,\Omega}$ (see [BS08, Sec. 10.6]) guarantees the validity of (1.5) even for $\sigma = 0$ and $\operatorname{div} \boldsymbol{b} = 0$.

Let us now state a finite element formulation of (1.2). To this end we define some terminology. A finite element method seeks a solution in a *trial space* and tests the equality for every function in a *test space*. If trial and test spaces coincide, then the method is called *Galerkin method*, otherwise it is called *Petrov–Galerkin method*.

Now, we suppose that $\Omega \subset \mathbb{R}^2$ is an open, polygonal and bounded domain covered by a partition $\mathcal{P}$ consisting of geometrically simple and non-overlapping cells (a precise definition is given later in Section 2.1). Furthermore, let $\boldsymbol{V}_\mathcal{P} \subset \boldsymbol{V}$ and $M_\mathcal{P} \subset M$ be discrete, finite-dimensional, spaces associated with $\mathcal{P}$. Then, a Galerkin method for (1.2) reads:

Find $(\boldsymbol{u}_\mathcal{P}, p_\mathcal{P}) \in \boldsymbol{V}_\mathcal{P} \times M_\mathcal{P}$ *such that*

$$\mathfrak{B}(\boldsymbol{u}_\mathcal{P}, p_\mathcal{P}; \boldsymbol{v}, q) = (\boldsymbol{f}, \boldsymbol{v})_\Omega \quad \text{for all} \quad (\boldsymbol{v}, q) \in \boldsymbol{V}_\mathcal{P} \times M_\mathcal{P}\,, \tag{1.7}$$

where the bilinear form $\mathfrak{B}$ *is defined as in* (1.3).

Unlike an elliptic problem, (1.7) is not automatically well-posed by choosing subspaces $\boldsymbol{V}_\mathcal{P} \subset \boldsymbol{V}$ and $M_\mathcal{P} \subset M$. This is one source of instability that may occur when solving problem (1.7). At this point we elaborate on this and other sources in form of a few comments:

- The existence of the unique (discrete) solution of (1.7) follows from Corollary 1.1, if the discrete pair $\boldsymbol{V}_\mathcal{P} \times M_\mathcal{P}$ satisfies the conditions in Corollary 1.1. It is noteworthy that (1.5) remains valid for any subspace $\boldsymbol{V}_\mathcal{P} \subset \boldsymbol{V}$; in particular for any partition $\mathcal{P}$. However, the discrete equivalent of (1.6), namely

  $$\inf_{q \in M_\mathcal{P}} \sup_{\boldsymbol{v} \in \boldsymbol{V}_\mathcal{P}} \frac{(q, \operatorname{div} \boldsymbol{v})_\Omega}{\|q\|_{0,\Omega} |\boldsymbol{v}|_{1,\Omega}} \geq \beta_\mathcal{P}\,, \tag{1.8}$$

  imposes implicit constraints on the partition $\mathcal{P}$ and the relation between $\boldsymbol{V}_\mathcal{P}$ and $M_\mathcal{P}$. This is very important for the scope of the present thesis.

  Existing results concerning the behaviour of inf-sup constants and how to circumvent condition (1.8) are presented in Sections 1.2.1 and 1.2.2. Additionally, the choice of the space $\boldsymbol{V}_\mathcal{P} \times M_\mathcal{P}$ has an impact on how well the divergence constraint in (1.1) is satisfied, cf. Section 1.2.4.

- Another source of an unsatisfactory behaviour of a finite element method may be caused by dominating convection ($\nu \ll \|\boldsymbol{b}\|_\infty$) or reaction ($\nu \ll \sigma$). Such behaviour is mainly observed for high Reynolds number flows, which is a case of practical interest. A few results on this point are listed in Section 1.2.3.

- Furthermore, the approximation qualities of a discrete solution may require some regularity of the partition $\mathcal{P}$, because the proof relies on properties of interpolation operators which may require a maximum angle condition. We cover this point and its literature review in Section 2.2.3, as more detailed definitions are required.

The desire for an LBB constant $\beta_\mathcal{P}$ in (1.8) to be independent of the partition $\mathcal{P}$ has

two motivations. The first one, is given by the worst case error estimate for the Stokes problem. That is, if the inf-sup condition (1.8) is satisfied, then a standard a priori error estimate is

$$|\boldsymbol{u}-\boldsymbol{u}_{\mathcal{P}}|_{1,\Omega}+\|p-p_{\mathcal{P}}\|_{0,\Omega} \leq \left(1+\frac{C}{\beta_{\mathcal{P}}^2}\right)\left\{\inf_{(\boldsymbol{v}_{\mathcal{P}},q_{\mathcal{P}})\in \boldsymbol{V}_{\mathcal{P}}\times M_{\mathcal{P}}} |\boldsymbol{u}-\boldsymbol{v}_{\mathcal{P}}|_{1,\Omega}+\|p-q_{\mathcal{P}}\|_{0,\Omega}\right\}, \quad (1.9)$$

see for example [ESW14] or [BF91, Sec. II.2.2]. The negative power of $\beta_{\mathcal{P}}$ in this estimate is the reason why a $\beta_{\mathcal{P}}$ independent of mesh properties, such as size and shape of the elements of Partition $\mathcal{P}$, is desirable.

The second motivation is that $\beta_{\mathcal{P}}$ affects the condition number of the discrete system to be solved. For instance, the smallest eigenvalue of the discrete Stokes system behaves as $\beta_{\mathcal{P}}^2$, whereas its largest eigenvalue is independent of the partition (bounded by the continuity constant of the bilinear form). Hence, the condition number of the discrete system is related to $\beta_{\mathcal{P}}^{-2}$, which is a strong inconvenience when $\beta_{\mathcal{P}}$ is small. For a detailed discussion on the preconditioning issue for stabilised low order methods and symmetric indefinite systems we refer to [Sil94, WS93, SW94, SS11] and for a comprehensive introduction to the iterative solving process to [ESW14] or [GS00, pp. 623–639].

1.2. Literature review

In this section we perform a literature review for various sources of instability that occur when problem (1.7) is solved. These sources include inf-sup condition (1.8), and how to circumvent it, dominating convection and mass-conservation.

As observed, when solving (1.7) an *inf-sup stable pair* $\boldsymbol{V}_{\mathcal{P}} \times M_{\mathcal{P}}$ is beneficial, that is, a pair satisfying (1.8) with a positive constant $\beta_{\mathcal{P}}$ independent of mesh properties. We refer to $\beta_{\mathcal{P}}$ as the *inf-sup* or *LBB constant* of the pair $\boldsymbol{V}_{\mathcal{P}} \times M_{\mathcal{P}}$. The term *spurious (pressure) mode* refers to a (basis) function, say $\phi_s \in M_{\mathcal{P}}$, that causes $\beta_{\mathcal{P}}$ to depend on mesh quantities. Inserting any multiple of ϕ_s into (1.8) gives the same inf-sup constant $\beta_{\mathcal{P}}$. Therefore, if a spurious mode is to be removed from $M_{\mathcal{P}}$, then a whole one-dimensional subspace, span $\{\phi_s\} \subset M_{\mathcal{P}}$ or one degree of freedom (DOF), has to be removed.

In order to discuss available finite element pairs, we define (discontinuous) spaces that consist piece-wise of polynomials. To this end, for $\ell \in \mathbb{N}$ and $\omega \subseteq \overline{\Omega}$ we introduce sets of polynomials $\mathbb{P}_\ell(\omega)$ of (at most) degree ℓ and $\mathbb{Q}_\ell(\omega)$ of (at most) of degree ℓ in each variable. Furthermore, let $\mathcal{P}$ be a conforming partition of Ω into the union of closed parallelograms or triangles (defined later). Then, we define the scalar-valued

spaces

$$\mathbb{Q}_{\ell,\mathcal{P}} \coloneqq \left\{ v \in L^2(\Omega) \colon v|_K \in \mathbb{Q}_\ell(K) \quad \forall K \in \mathcal{P} \right\}$$

and

$$\mathbb{P}_{\ell,\mathcal{P}} \coloneqq \left\{ q \in L^2(\Omega) \colon q|_K \in \mathbb{P}_\ell(K) \quad \forall K \in \mathcal{P} \right\}.$$

Continuous spaces are given a superscript c, that is, we define $\mathbb{Q}^c_{\ell,\mathcal{P}} \coloneqq \mathbb{Q}_{\ell,\mathcal{P}} \cap C^0(\Omega)$ and vector-valued spaces are bold-faced, e. g. $\boldsymbol{Q}^c_{\ell,\mathcal{P}} \coloneqq [\mathbb{Q}^c_{\ell,\mathcal{P}}]^2$. In this thesis we predominantly use continuous velocity spaces and discontinuous pressure spaces. The superscript c merely serves to avoid confusion during the literature review. When using a continuous space we implicitly suppose an appropriate partition, for example $\mathbb{P}^c_{k,\mathcal{P}}$ can be defined on triangles but not on parallelograms. If we talk about inf-sup stable pairs and the spaces are defined on the same partition, then the partition symbol is left out, for instance, the pairs $\boldsymbol{P}^c_k \times \mathbb{P}^c_k$ and $\boldsymbol{Q}^c_k \times \mathbb{P}_k$ (defined on parallelograms) are not inf-sup stable.

The aim of the next two sections is to recall inf-sup stable pairs and show methods available to circumvent the inf-sup condition (1.8).

1.2.1. Inf-sup stable pairs

A thorough introduction to inf-sup stable pairs on (shape-) regular meshes and a recent summary of such pairs may be found in [BBF13]. We summarise the results most relevant to us here. For the arguments below it is worth mentioning that on regular meshes the pairs $\boldsymbol{Q}^c_k \times \mathbb{Q}^c_k$ and $\boldsymbol{P}^c_k \times \mathbb{P}^c_k$ are not inf-sup stable, as can be confirmed by numerical experiments. The pairs $\boldsymbol{Q}^c_k \times \mathbb{P}_{k-1}$ [BM99] and the Hood–Taylor pairs $\boldsymbol{P}^c_k \times \mathbb{P}^c_{k-1}$ and $\boldsymbol{Q}^c_k \times \mathbb{Q}^c_{k-1}$ are inf-sup stable for $k \geq 2$ [Bof94] and [BBF13, Sec. 8.8.2]. The latter pairs are also called *balanced-order* pairs, since the norms in (1.9) converge equally fast.

On anisotropic meshes the situation is more complicated. Here we provide a more detailed review. First, we cover *non-conforming* approaches, that is $\boldsymbol{V}_{\mathcal{P}} \not\subset \boldsymbol{V}$. The piecewise linear, non-conforming Crouzeix–Raviart element introduced in [CR73] was in [ANS01] proven to satisfy (1.8) on arbitrary conforming anisotropic meshes consisting of triangles. However, to ensure good approximation properties of the interpolant a maximum angle condition is assumed, see also [AD99]. Another non-conforming stable pair is the rotated, non-parametric $\tilde{\boldsymbol{Q}}_1 \times \mathbb{P}_0$-element introduced in [RT92]. This pair was later [BR95] shown to be stable independent of the cell aspect ratio on rectangular, conforming tensor-product meshes. Finally, in [AM08] inf-sup stable pairs on

anisotropic rectangular meshes are defined. This is done, starting from a fixed pressure space ($\mathbb{P}_{k-1}$) and a velocity space $\boldsymbol{P}_k$ that is enriched by functions belonging to $\boldsymbol{Q}_{k+1}$ until uniform stability is achieved.

In this thesis we focus on $\boldsymbol{V}_\mathcal{P} \subset \boldsymbol{V}$. For conforming spaces $\boldsymbol{V}_\mathcal{P} \subset \boldsymbol{V}$ on anisotropic meshes, a difference of two in the polynomial degree between velocity and pressure space seems to allow LBB constants independent of local aspect ratios. For example, in [SS98,SSS99] the $\boldsymbol{Q}^c_{k+1} \times \mathbb{Q}_{k-1}$ pair was proven to be uniformly inf-sup stable on meshes containing edge patches, but corner patches were excluded. If a corner patch is present, then the LBB constant may depend on a non-local quantity κ (called grading factor in [SSS99]), see Figure 1.1. The exclusion of corner patches is motivated by experiments in [SSS99, AC00, AMR03]. Furthermore, in [AC00] some spurious pressure modes that cause $\beta_\mathcal{P} = C(\kappa)$ are identified for $\boldsymbol{Q}^c_{k+1} \times \mathbb{P}_{k-1}$ and other pairs. This knowledge was used to construct velocity polynomials of degree $\kappa^{-1/2}$ (with κ given by $h_{\boldsymbol{c}}/H_{\boldsymbol{c}}$ from Figure 1.1), that, when added to $\boldsymbol{V}_\mathcal{P} = \boldsymbol{Q}^c_{k+1}$, prevent $\beta_\mathcal{P}$ from degenerating. These polynomials change with κ which complicates the implementation of this approach. Moreover, in [AN04], the stability of $\boldsymbol{Q}^c_2 \times \mathbb{P}_0$ and $\boldsymbol{P}^c_2 \times \mathbb{P}_0$ on some anisotropic meshes is justified. In detail, the assumptions on the partition in [AN04] restrict grading factors and allow any partition that can be split into a finite number of shape-regular macro elements where each of the macro elements contains cells stretched in a single direction. In [BLR12] a divergence-preserving interpolant on anisotropic meshes is constructed. Its approximation estimates, however, are not independent of local anisotropies, cf. [BLR12, estimate (1.3)], and the grading factors are restricted see [BLR12, Assumption 1].

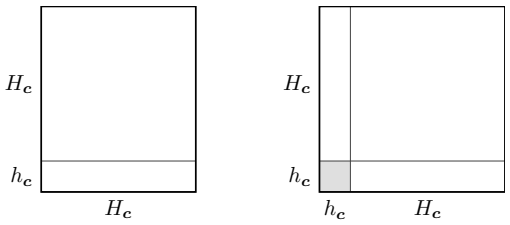

Fig. 1.1. An edge and a corner patch with aspect ratio $\varrho = h_{\boldsymbol{c}}/H_{\boldsymbol{c}}$ and grading factor $\kappa = h_{\boldsymbol{c}}/H_{\boldsymbol{c}}$.

In summary, when $\boldsymbol{V}_\mathcal{P}$ is fixed, then $\beta_\mathcal{P}$ is defined by the infimum over $M_\mathcal{P}$ and restricting this infimum to any subspace of $M_\mathcal{P}$ increases $\beta_\mathcal{P}$. On various meshes the works [SS98, SSS99, AN04] show that dependencies on local aspect ratios are cured by a velocity space that is "two polynomial degrees richer" than the pressure space, where simultaneous stretching in two spatial directions is bounded. Experiments for the

balanced-order pairs $\boldsymbol{Q}_k^c \times \mathbb{P}_{k-1}$ ($k \geq 2$) show they are not uniformly inf-sup stable, and hence loose their stability as aspect ratios decrease. Table 1.1 shows the behaviours of the LBB constant that can be expected on anisotropic meshes consisting of rectangles (for simplicity). The constant $\beta_{\mathcal{P}} = C(\ldots)$ may, in general, depend on the aspect ratio ϱ, or topological parameters κ (e. g. neighbourhood-local grading factor) and polynomial degree k. The shown dependencies have been either restricted or proven in the cited publication, for instance the result in the second row is proven for shape-regular meshes on which ϱ and κ are bounded by constants. In the course of this thesis, it will turn out that the topological dependency, indicated by κ in Table 1.1, is not local (see Chapter 3 and Remark 3.2 for details).

Table 1.1. The relation between $\boldsymbol{V}_{\mathcal{P}} \times M_{\mathcal{P}}$ and LBB constants $\beta_{\mathcal{P}}$

$\boldsymbol{V}_{\mathcal{P}} \times M_{\mathcal{P}}$, $k \geq 1$	$\beta_{\mathcal{P}}$	Comments
$\boldsymbol{Q}_{k+1}^c \times \mathbb{P}_{k+1}$	0	consequence of [BM99, Prop. 2.1]
$\boldsymbol{Q}_{k+1}^c \times \mathbb{P}_k$	$C(\varrho, \kappa, k) > 0$	consequence of [BM99, Prop. 4.1]
$\boldsymbol{Q}_{k+1}^c \times \mathbb{P}_{k-1}$	$C(\kappa, k) > 0$	consequence of [AC00]

None of the approaches [SS98, SSS99, AMR03, AN04, AM08, BLR12] allows corner patches as in [AC00], or in Figure 1.1, right. And the approach of augmenting the LBB constant proposed in [AC00] imposes difficulties when being implemented.

1.2.2. Circumventing inf-sup conditions

The observations made for inf-sup stable pairs show that equal-order pairs, for example $\boldsymbol{P}_k^c \times \mathbb{P}_k^c$, are not inf-sup stable. However, for ease of implementation such pairs are considered desirable. This is why condition (1.8) is often circumvented by penalty/decoupling techniques [GR86, Section I.4.3] or by stabilisation as follows. We skip penalty approaches here, because it is elaborated in [DB04] that penalty methods may fail to converge.

An early stabilisation approach is the *Galerkin-Least-Squares (GLS)* method designed in [HF87]. One special case is the method using the $\boldsymbol{P}_1^c \times \mathbb{P}_0$ pair, which is not inf-sup stable, and penalising jumps of the pressure across all interior edges makes the discrete problem solvable. This GLS method is included in [HF87], but also analysed in [SK90]. A simple switch of a sign in the stabilisation term resulted in the Douglas–Wang method [DJW89] which has better stability properties as analysed in [FFH92]. One form of an "incomplete" GLS-stabilised method is the Streamline Upwind Petrov–Galerkin (SUPG) method introduced in [BH82] for convection dominated flows. If the pair $\boldsymbol{V}_{\mathcal{P}} \times M_{\mathcal{P}}$ is not inf-sup stable, then such methods contain a sum of weighted

discrete gradients of the pressure to circumvent (1.8), sometimes referred to as pressure-stabilised Petrov–Galerkin (PSPG) method [HFB86, JS86]. These methods can be classified as *consistently* stabilised methods [BBGS04], that is, the stabilisation terms vanish for the exact solution if it is sufficiently smooth.

Both GLS and SUPG methods use a stabilisation term based on weighted residuals. This causes two main drawbacks. One of them is that the stabilisation term introduces additional (unphysical) couplings between velocity and pressure. This is inconvenient because the coupling terms modify the system matrix in many different places. Furthermore (to paraphrase [BBJL07, p. 864]) the physical meaning of a term in the SUPG-norm is unclear. Another drawback is that the higher-order versions are not robust with respect to over-stabilisation, which is caused by using inverse inequalities to bound the coupling terms in the proofs. In the case of the Stokes problem, these inequalities are used when $\Delta \boldsymbol{u}_{\mathcal{P}} \neq 0$ (and not in the lowest-order case with constant coefficients). The methods in their original form were proposed on isotropic meshes [BH82, HF87] using the diameter h_K of a cell K to define the stabilisation parameters. This works because cells in isotropic meshes are stretched (almost) equally in each spatial direction. For some anisotropic meshes consisting of triangles the GLS method for the pair $\boldsymbol{P}_1^c \times \mathbb{P}_1^c$ is analysed in [MPP03]. Therein, the stabilisation parameters are defined using the smallest eigenvalue of the Jacobian matrix J_K of the affine transformation onto the cell K. The SUPG/PSPG method has been extended in [AKL08] for continuous equal-order pairs $\boldsymbol{P}_k^c \times \mathbb{P}_k^c$ on meshes where the Jacobian of each cell has (block) diagonal form. In the ansiotropic case, the choice of stabilisation parameters is also restricted by inverse inequalities, see for example [AKL08, eq. (20)]. Additionally, in [AKL08, Theorem 5, Remark 6] a restriction on the local aspect ratio is made. Both approaches in [MPP03, AKL08] use one small cell-dependent stabilisation parameter for all spatial directions. The subsequent work [Bla08] significantly improves the behaviour of GLS methods by stabilising differently in each spatial direction. In this case the full Jacobian J_K, which implicitly contains stretching information about each spatial direction, is used to define the stabilisation terms in two and three space dimensions on affine meshes.

The stability of the GLS and SUPG methods is only due to their symmetric (or block-diagonal) terms. This fact and the drawbacks, mentioned in the previous paragraph, motivated the design of other methods. Reviews on these approaches for the Oseen problem on isotropic meshes are given in [BBJL07, RST08]. More recently, [MT15] gives an account of inf-sup stable and (locally) stabilised equal-order pairs used on isotropic meshes. Only a few of the methods in [MT15, BBJL07] have

been extended to anisotropic meshes. One of them is a so-called Pressure Gradient Projection (PGP) method [CB00], which is adapted to anisotropic meshes in [Bla07]. We are particularly interested in methods stabilised by adding terms in form of local fluctuations, usually called *Local Projection Stabilisation (LPS)* terms, see for example [BB01, MST07, MT15]. This approach may be used both to circumvent the LBB condition and to increase control over a convection dominated velocity, see, for instance, [Bra08] where an LPS stabilised method using the $\boldsymbol{Q}_1^c \times \mathbb{Q}_1^c$ pair is analysed for the Oseen problem on anisotropic quadrilateral meshes.

In some cases *Pressure Projection Stabilisation (PPS)* is related to LPS. For instance, if an inf-sup stable subspace $\boldsymbol{V}_{\mathcal{P}} \times G$ with $G \subseteq M_{\mathcal{P}}$ and an LBB constant β_G is known, then the following inf-sup deficiency holds

$$\sup_{\boldsymbol{v} \in \boldsymbol{V}_{\mathcal{P}}} \frac{(\operatorname{div} \boldsymbol{v}, q)_\Omega}{|\boldsymbol{v}|_{1,\Omega}} \geq \beta_G \|\Pi_G q\|_{0,\Omega} - \|q - \Pi_G q\|_{0,\Omega} \quad \text{for all} \quad q \in M_{\mathcal{P}}\,, \tag{1.10}$$

where $\Pi_G \colon M_{\mathcal{P}} \to G$ is any surjective projection (cf. Lemma 3.5 later). Then, adding a stabilisation term, say s_p satisfying $s_p(q,q) \geq \|q - \Pi_G q\|_{0,\Omega}^2$ for all $q \in M_{\mathcal{P}}$, cures the inf-sup deficiency and adds stability for the pressure modes causing the stability issue. The first (possibly minimal) PPS method may have been presented in [PS85] where local checker-board modes are removed from $\boldsymbol{Q}_1^c \times \mathbb{P}_0$ to circumvent (1.8). Additionally, optimal convergence can be achieved, provided the space $G \subset M_{\mathcal{P}}$ is large enough, that is, $\inf_{q_{\mathcal{P}} \in G} \|p - q_{\mathcal{P}}\|_{0,\Omega}$ converges fast enough, see also [Bur08, BF01]. This is particularly interesting for equal-order pairs on shape-regular meshes, where, for example, $\boldsymbol{Q}_k^c \times \mathbb{P}_k$ and $G \coloneqq \mathbb{P}_{k-1}$ (cf. Table 1.1) may be chosen, see also [DB04]. Then, since balanced-order pairs converge with optimal order, also the equal-order pair will converge, see [BF01] for other examples. An alternative approach for the pairs $\boldsymbol{P}_1^c \times \mathbb{P}_0$ and $\boldsymbol{P}_1^c \times \mathbb{P}_1^c$ is developed in [BDG06], where inf-sup deficiencies, similar to (1.10), are derived integrating by parts, and applying inverse inequalities. A unified presentation of the PPS methods above can also be found in [Bur08].

On anisotropic meshes a proof of an inf-sup deficiency as in [BDG06] does not seem to be applicable. Whereas, the difficulty in the proof of (1.10) lies in proving the uniform inf-sup condition for $\boldsymbol{V}_{\mathcal{P}} \times G$. This is because the uniformly inf-sup stable part may be even smaller and therefore the convergence of the mixed method might suffer when adding more stabilisation. In this case, coarse-scale projections may be a remedy. For example, the local jump stabilisation proposed in [SK90, KS92, Sil94], and extended to anisotropic meshes in [LS13] (without corner patches), and in [BW15] (with corner patches), converges optimally.

This PPS concept is valid for several methods in literature and can be used to derive

uniformly inf-sup stable methods, as we will do in this thesis. The methods presented in this thesis fit into this (sometimes minimal) stabilisation framework presented in [BF01].

1.2.3. Dominating convection

As mentioned before, another source of instability is dominating convection. If we remove the divergence constraint and the pressure from (1.1), then we obtain the vector-valued *Convection-diffusion-reaction (CDR)* equation. In this case, to obtain an elliptic bilinear form, the demand on $\boldsymbol{b}$ is usually $\boldsymbol{b} \in W^{1,\infty}(\Omega)^2$ and $\sigma - \frac{1}{2}\operatorname{div}\boldsymbol{b} \geq 0$. For this problem it is well known that dominating convection ($\|\boldsymbol{b}\|_{\infty,\Omega} \gg \nu$) or reaction ($\sigma \gg \nu$) may cause the solution to contain *layers*; that is, components of the solution that cause steep gradients in a very narrow region of the domain Ω. It is known that the (standard) Galerkin solution of such problems possesses spurious oscillations when layers are not resolved. If the location, orientation and width of these regions is known a priori, then the CDR problem may be solved by the Galerkin method on layer-adapted meshes (very anisotropic meshes). For a comprehensive review on this topic, see [RST08]. In [SO97] the CDR equation is solved on Shishkin meshes, and in [DL06] on graded meshes. An immediate consequence of [SO97, DL06] is that on meshes adapted to the behaviour of the solution no stabilisation is needed to achieve a good approximation. This is different in the case of non-conforming approaches with $\boldsymbol{V}_{\mathcal{P}} \not\subset \boldsymbol{V}$, since the bilinear form does not automatically inherit the ellipticity condition (1.5). Then, an appropriate choice of stabilisation parameters is required, see for instance [FRW14] where a singularly perturbed biharmonic problem is solved by a Continuous Interior Penalty (CIP) method on Shishkin meshes. These approaches require knowledge of the structure of layers which is in general unavailable. Therefore, both for CDR and Oseen problems stabilisation approaches were developed on shape-regular meshes, see for example [BH82, FFH92], the collection by Tobiska [Tob09], detailed information on LPS methods [Kno09, Kno10, KT13], a CIP method [BFH06], and the already mentioned methods in [AKL08, Bra08] and references therein.

1.2.4. Mass conservation

If the divergence constraint can be satisfied pointwise, then the error estimates for velocity and pressure can be decoupled, cf. [GR86]. Then, in particular the velocity error does not depend on the pressure or on the inf-sup constant. In [Lin14] a clever variational crime is designed to mimic these features. However, most finite element methods do not solve in a pointwise divergence-free space. Because of that, stabilisation of the divergence constraint, hereafter referred to as *grad-div* stabilisation, has been

pointed out as important for robustness, see for instance [FF92, HS90, TL91, GLOS05]. More recently, in [JJLR14] a good choice of the grad-div stabilisation parameter for the Stokes problem is developed. And in [LR13], a grad-div term with a reduced stencil is designed and analysed.

1.3. Outline

We end this chapter with the outline of this thesis. With the desire to use anisotropic meshes and in the context of anisotropic refinements one may wish to use corner patches (see Figure 1.1) and then it is interesting how to circumvent the behaviours of LBB constants depending on mesh properties, cf. Table 1.1.

Then, for rest of this thesis we have the following aims:

1. Propose alternative (possibly stabilised) methods to [AC00] for the $\boldsymbol{Q}^c_{k+1} \times \mathbb{P}_{k-1}$ pair that allow corner patches and whose implementation is independent of mesh properties. We start with these pairs and the Stokes problem, as this allows us to focus on inf-sup deficiencies caused by corner patches.

2. Extend the ideas to balanced-order pairs on meshes with corner patches.

3. Extend the results to more general problems (the Oseen and NS problem) and more general meshes.

4. Propose methods with full control over the L^2-norm of the pressure. On anisotropic meshes this is rarely proven. In [AKL08] and the appendix of [MPP03], the control seems to depend on aspect ratios. In [Bra08] only the fluctuation of the pressure gradient is controlled and a higher regularity is required to prove convergence.

The thesis is organised as follows. In Chapter 2 we introduce other notation and estimates with explicit constants valid on isotropic and anisotropic cells. Various of the presented tools, in particular trace inequalities, may be useful also outside the scope of the present thesis, for instance, when deriving a posteriori error bounds.

Then, in Chapter 3 we apply the PPS approach to achieve Aim 1 for the non-optimal order pair $\boldsymbol{V}_{\mathcal{P}} \times M_{\mathcal{P}} \coloneqq \boldsymbol{Q}^c_{k+1} \times \mathbb{P}_{k-1}$. We propose methods that circumvent the mesh-dependency of the LBB constant, cf. Table 1.1 (3rd. row). This is done by identifying a maximal-dimensional, subspace $G \subset M_{\mathcal{P}}$, such that the pair $\boldsymbol{V}_{\mathcal{P}} \times G$ is uniformly inf-sup stable. Equivalently, $M_{\mathcal{P}}$ is restricted by a minimal set of constraints to the subspace G. These constraints may be added in form of stabilisation terms to obtain a FEM whose convergence is independent of mesh properties. Approaches whose stability and

convergence analysis rely on the same type of analysis are for instance [BDG06, BF01]. The results in Chapter 3 are the basis of the publication [ABW15]; Section 3.6 gives an account of the published results.

Afterwards, in Chapter 4 we attack Aim 2 and extend the results in Chapter 3 to the balanced-order pair $\boldsymbol{Q}_1^c \times \mathbb{P}_0$. Similarly to Table 1.1 (2nd. row) this pair requires more stabilisation terms, as inf-sup deficiencies are also caused by local aspect ratios. In fact, the results here only extend the method proposed in [LS13] to meshes that contain corner patches. Results based on this chapter were accepted for publication in [BW15]. Apparently, the method for $\boldsymbol{Q}_1^c \times \mathbb{P}_0$ or $\boldsymbol{P}_1^c \times \mathbb{P}_0$ stabilised by global jumps on anisotropic meshes has not been published. The results in Chapter 4 show that such a method can be proposed, but local jumps are preferred, for the sake of local mass-conservation properties.

In Chapter 5 we will mix and extend the approaches from Chapter 4 and from [MT15, Bra08] to propose low-order methods for the Oseen equation on meshes containing further refined corner patches (Aim 3). For the analysis we use and extend results from [MT15], to the non-inf-sup stable pair $\boldsymbol{Q}_1^c \times \mathbb{P}_0$. The Oseen problem may be convection dominated, and therefore another source of instability may have to be treated. We will add velocity stabilisation in form of LPS terms to reduce the effects of this issue. More precisely, we compare the term proposed by [Bra08] with a grad-div term enhanced by a minimal fluctuation of the convective gradient when applied to a strongly convection dominated solution.

We conclude and present possible further extensions in Chapter 6. For instance, in Chapter 3 the meshes are restricted to parallelograms, and it is interesting to extend the results to meshes consisting of triangles. We present experiments and arguments for the $\boldsymbol{P}_2^c \times \mathbb{P}_0$ pair. In Chapter 4 we only propose the lowest (balanced) order pair. Extending these results to triangles and to higher (balanced) order pairs is also of interest. In fact, we show numerical evidence that this is possible for the $\boldsymbol{Q}_2^c \times \mathbb{P}_1$ and $\boldsymbol{P}_2^c \times \mathbb{P}_1$ pairs. Additionally, we apply the method proposed in Chapter 5 to the Navier–Stokes problem and show some preliminary results.

Finally, we include an appendix describing how the methods using the subspaces G can be implemented in an abstract way.

Chapter 2

Notations and preliminaries

In this chapter we introduce notations and conventions used later on. In particular, we introduce notation associated with domains and partitions, as well as their isotropic and anisotropic properties. Afterwards, we state estimates whose constants are independent of any property of the partition. Finally, we define function spaces and operators used throughout.

Throughout the thesis $\mathbb{N} \coloneqq \{0, 1, 2, \ldots\}$ and $\mathbb{N}_+ \coloneqq \mathbb{N} \setminus \{0\}$ denote the set of natural and positive natural numbers, respectively. We use $\mathbb{R}$ to denote the set of real numbers.

2.1. Geometry

Let $\Omega \subset \mathbb{R}^d$ for $d \in \{2, 3\}$ be an open, bounded and connected domain with boundary $\partial\Omega$. Then, for a set $\omega \subseteq \Omega$ we denote its *closure* by $\overline{\omega} \coloneqq \omega \cup \partial\omega$ and its *interior* by $\omega^\circ \coloneqq \omega \setminus \partial\omega$.

A *partition* $\mathcal{P}$ of a polygonal domain Ω (also called *mesh* or *triangulation*) is a finite set of closed simplices, or quadrilaterals with disjoint interiors, such that $\overline{\Omega} = \bigcup_{K \in \mathcal{P}} K$. Elements $K \in \mathcal{P}$ are called *cells*. A partition is *conforming* if every non-empty intersection of two distinct cells is either a common node or a common edge. We call a mesh $\mathcal{P}$ *axis-parallel* if every cell $K \in \mathcal{P}$ is an axis-aligned rectangle. The set $\mathcal{E}_\mathcal{P}$ contains all *interior edges* of $\mathcal{P}$.

For a finite set, say $\mathcal{P}$, $\operatorname{card}(\mathcal{P})$ is the number of elements in $\mathcal{P}$. The symbol $|\diamond|$ is defined depending on the input $\diamond$, that is, for $\omega \subset \mathbb{R}^d$, $|\omega|$ is the appropriate measure. For instance, $|\omega|$ is the length of a curve in $\mathbb{R}^d$, the area of a surface in $\mathbb{R}^3$ or cell in $\mathbb{R}^2$ and the volume of a cell in $\mathbb{R}^3$. Moreover, we denote by $|x|$ the Euclidean distance of $x \in \mathbb{R}^d$ to the origin (for $d = 1$ it is the absolute value).

2.1.1. On shape regularity and anisotropies

A common assumption is that families of partitions are (shape-) regular, that is, for every cell the ratio of its diameter and the radius of its largest inscribed ball is bounded by a common constant. An anisotropic mesh is by definition not regular. In this section, we become familiar with these notions.

In order to give the following definition we use a subscript $h \coloneqq \max_{K\in\mathcal{P}} \operatorname{diam}(K)$ for partitions. A family of partitions $\{\mathcal{P}_h\}_h$ is said to be *(shape-) regular* (also *isotropic*), if there exists a constant $\varrho_0 > 0$, such that

$$\forall K \in \{\mathcal{P}_h\}_h \colon \frac{r_K}{\operatorname{diam}(K)} \geq \varrho_0 > 0\,, \tag{2.1}$$

where r_K is the radius of the largest ball inscribed in K. By definition, an *anisotropic* mesh violates condition (2.1) which is characterised by the presence of cells K possessing small (aspect) ratios $r_K/\operatorname{diam}(K)$.

The definition of aspect ratios is not unique in literature, cf. [AC00] and [LS13]. We use the one from [AC00] as a basis for this thesis. This means for a rectangle K, of area $|K| = hH$, and edges of lengths $h \leq H$, that the aspect ratio equals $h/H = |K|/H^2$. Motivated by this relation we define the *aspect ratio* of parallelograms and triangles to be

$$\varrho_K \coloneqq h_1^{-2}|K| \quad \text{where} \quad h_1 \coloneqq \max_{e\subset\partial K}|e|.$$

We note that $\varrho_K \leq 1$ for any parallelogram and triangle. The global aspect ratio is denoted and defined by

$$\varrho \coloneqq \min_{K\in\mathcal{P}} \varrho_K\,.$$

The following remark shows that a family of meshes with bounded aspect ratio is shape-regular, and vice-versa.

Remark 2.1. *If a family $\{\mathcal{P}_h\}_h$ consists of parallelograms or triangles, then*

$$\{\mathcal{P}_h\}_h \textit{is shape regular} \iff \textit{the aspect ratio is uniformly bounded, that is,}\quad \exists\, \varrho_0 > 0 \colon \forall K \in \{\mathcal{P}_h\}_h \colon \varrho_K \geq \varrho_0 > 0.$$

Proof. The proof relies on the equivalences $r_K \sim |K|/h_1$ and $h_1 \sim \operatorname{diam}(K)$. For an arbitrary triangle K these are given by $h_1 = \operatorname{diam}(K)$ and

$$r_K = 2\frac{|K|}{|\partial K|} \quad \text{and} \quad 2\,h_1 < |\partial K| \leq 3\,h_1.$$

For parallelograms, we have $h_1 < \operatorname{diam}(K) < 2h_1$ and $2r_K = |K|/h_1$. □

A single partition $\mathcal{P}$ is shape-regular, since $\operatorname{card}(\mathcal{P})$ is finite. However, for practical reasons we may call a single partition $\mathcal{P}$ anisotropic if there is a cell $K \in \mathcal{P}$ with $\varrho_K \ll 1$.

We realise that the aspect ratio ϱ_K depends only on cell-local properties. For a mesh consisting of parallelograms we define the (neighbourhood-local) *grading factor*, denoted by κ_K, to be

$$\kappa_K \coloneqq \min_{e \subset \partial K,\, e = \partial K \cap \partial K'} \left(\min \left\{ \frac{|K|}{|K'|}, \frac{|K'|}{|K|} \right\} \right),$$

and global grading factor by

$$\kappa \coloneqq \min_{K \in \mathcal{P}} \kappa_K \,.$$

We end this section with some examples of isotropic and anisotropic meshes. In Figure 2.1a we show an isotropic mesh where ϱ and κ are bounded, Figure 2.1b shows a geometrically graded mesh ($\kappa = 1/2$) with unbounded aspect ratios and Figure 2.1c shows an *edge patch*, that is, a shape-regular domain covered by cells that are squeezed in only one spatial direction. Additionally, in Figure 2.2 we show different corner patches, which are (for now) special anisotropic meshes containing cells stretched in different directions, with small aspect ratios $\varrho_{\boldsymbol{c}} = h_{\boldsymbol{c}}/H_{\boldsymbol{c}}$ and the property $\kappa = \varrho$.

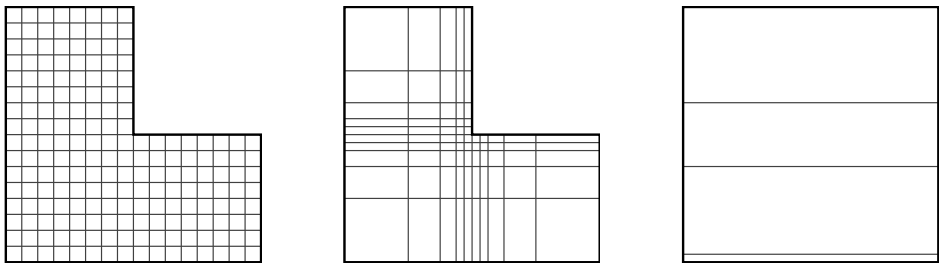

(a) $\varrho = \kappa = 1$ (b) $\varrho \ll 1, \kappa = 1/2$ (c) $\varrho \ll 1, \kappa \ll 1$

Fig. 2.1. Isotropic and anisotropic meshes with small aspect ratio ϱ and grading factor κ.

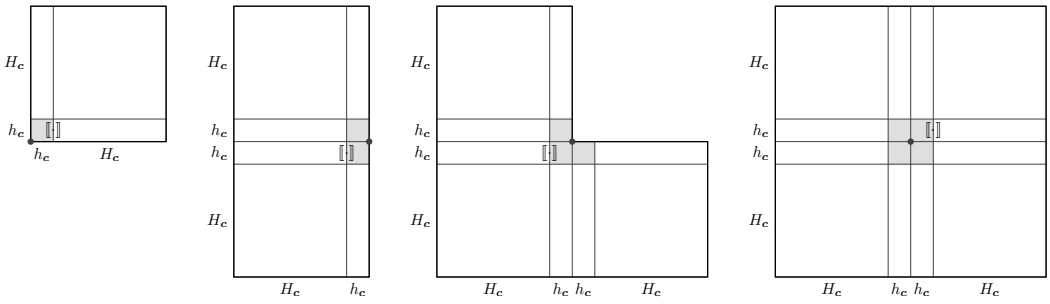

Fig. 2.2. Corner patches with aspect ratio $\varrho = h_{\boldsymbol{c}}/H_{\boldsymbol{c}}$ and grading factor $\kappa = h_{\boldsymbol{c}}/H_{\boldsymbol{c}}$.

2.2. Estimates on anisotropic meshes

In this section we report some technical results that are essential not only for performing the stability and convergence analysis of methods proposed later in this thesis, but also for methods outside this thesis. A common property of the presented estimates is that they have constants independent of properties of the mesh. Trace and inverse estimates introduce dependencies on cell-local geometric properties and have to be used with care.

We start by introducing a few standard inequalities. Probably the most used estimates in this thesis are *inequalities of Cauchy and Schwarz*, for completeness we list them here

$$(v,w)_\omega \leq \|v\|_{0,\omega}\|w\|_{0,\omega} \qquad \text{for all} \quad v,w \in L^2(\omega)\,, \tag{CS$_1$}$$

$$\sum_{i=1}^{n}|x_i y_i| \leq \left(\sum_{i=1}^{n} x_i^2\right)^{1/2}\left(\sum_{i=1}^{n} y_i^2\right)^{1/2} \qquad \text{for all} \quad x,y \in \mathbb{R}^n\,. \tag{CS$_2$}$$

Occasionally, we estimate a product by a weighted sum. This is done using *Young's inequality*

$$|ab| \leq \frac{\varepsilon}{2}a^2 + \frac{1}{2\varepsilon}b^2 \quad \text{for all} \quad a,b \in \mathbb{R},\, \varepsilon > 0 \tag{Young}$$

If trace inequalities are excluded, then a rule of thumb is: "Estimates valid on infinite dimensional function spaces do not introduce dependencies on mesh properties". An example is given by (CS$_1$).

2.2.1. Anisotropic trace inequalities

Trace (and inverse) estimates introduce dependencies on local mesh properties. These dependencies have to be known, so that methods can be designed appropriately. Subsequently, we present and discuss trace estimates with constants that are separated into a geometric (cell-dependent) component and everything else, for example the dimension of space and polynomial degree k.

For trace inequalities that are valid on infinite dimensional spaces, that is, $H^1(K)$ where $K \in \mathcal{P}$, the constants cannot depend on polynomial degrees. Below we prove such estimates for triangles and parallelograms, we include their proofs as they are not common. Additionally, we point out that the estimates are strict for locally constant functions. The following lemma states a version of Green's formula which we use later in the proof of the trace estimates. We did not find the proof, but it seems to be classical.

Lemma 2.2. *Let ω be a bounded open subset of $\mathbb{R}^d$ with a Lipschitz-continuous boundary $\partial\omega$. Let $\boldsymbol{\phi} \in \mathcal{C}^\infty(\omega)^d$ and $v \in H^1(\omega)$, then*

$$\int_{\partial\omega} v^2(\boldsymbol{\phi}\cdot\boldsymbol{n})\,\mathrm{d}s = \int_\omega v^2 \operatorname{div}\boldsymbol{\phi}\,\mathrm{d}\boldsymbol{x} + 2\int_\omega v(\boldsymbol{\phi}\cdot\nabla v)\,\mathrm{d}\boldsymbol{x}\,. \tag{2.2}$$

Proof. Let $\boldsymbol{\phi} = (\phi_1,\dots,\phi_d)^\top$ and $w_i \coloneqq \phi_i v$ for $i = 1,\dots,d$. We observe that $w_i \in H^1(\omega)$ and Green's formula [GR86, eq. (1.19)] yields

$$\int_{\partial\omega} v w_i n_i\,\mathrm{d}s = \int_\omega w_i(\partial v/\partial x_i)\,\mathrm{d}\boldsymbol{x} + \int_\omega (\partial w_i/\partial x_i) v\,\mathrm{d}\boldsymbol{x}\,.$$

Furthermore, the product rule applies (cf. [Ada75, p. 21, point 1.58]), and gives

$$\partial w_i/\partial x_i = \partial(v\phi_i)/\partial x_i = v(\partial\phi_i/\partial x_i) + \phi_i(\partial v/\partial x_i) \text{ a.e. in } \omega.$$

Inserting this identity into the previous one and rearranging (using $w_i = v\phi_i$), we get

$$\int_{\partial\omega} v^2\phi_i n_i\,\mathrm{d}s = 2\int_\omega v\phi_i(\partial v/\partial x_i)\,\mathrm{d}\boldsymbol{x} + \int_\omega v^2(\partial\phi_i/\partial x_i)\,\mathrm{d}\boldsymbol{x}\,.$$

Now, summing over $i = 1,\dots,d$ gives (2.2) and finishes the proof. □

Lemma 2.3. *Let T be a triangle, e one of its edges, and $\boldsymbol{p}_e$ the node opposite to e. Then, all $v \in H^1(T)$ satisfy*

$$\|v\|_{0,e}^2 \le \frac{|e|}{|T|}\|v\|_{0,T}\Big(\|v\|_{0,T} + \|(\boldsymbol{x}-\boldsymbol{p}_e)\cdot\nabla v\|_{0,T}\Big)\,.$$

Proof. We prepare to apply Lemma 2.2 with $\omega \coloneqq T$ and $\boldsymbol{\phi}_e \coloneqq \boldsymbol{x} - \boldsymbol{p}_e$ and $\boldsymbol{n}$ as the outward unit vector on ∂T. Now, direct evaluation gives $\operatorname{div}\boldsymbol{\phi}_e = 2$ and $\boldsymbol{\phi}_e\cdot\boldsymbol{n} = 0$ on $\partial T\setminus e$, since $\boldsymbol{\phi}_e$ is a tangential vector on this part of the boundary. Furthermore, on e we have $\boldsymbol{\phi}_e\cdot\boldsymbol{n}_e = 2|T||e|^{-1}$, since $\boldsymbol{x}\in e$ is given by

$$\boldsymbol{x} = \boldsymbol{p}_e + 2|T||e|^{-1}\boldsymbol{n}_e + r\boldsymbol{t}_e \quad \text{for some} \quad r\in\mathbb{R},$$

where $\boldsymbol{t}_e$ is a tangential vector of e.

Inserting the obtained values into (2.2) and applying (CS_1) finishes the proof. □

The proof of Lemma 2.3 can also be applied to tetrahedrons, as Lemma 2.2 remains valid in more dimensions. Also, a similar result with a non-explicit constant is given in [Kun00, Lemma 1]. Next we present a result for parallelograms.

Lemma 2.4. *Let K be a parallelogram with edge e and let $\boldsymbol{t}_i$ be a unit tangential vector of an edge i that is incident to e. Then, all $v \in H^1(K)$ satisfy*

$$\|v\|_{0,e}^2 \le \|v\|_{0,K}\left(\frac{|e|}{|K|}\|v\|_{0,K} + \frac{2}{\sin\alpha}\|\boldsymbol{t}_i\cdot\nabla v\|_{0,K}\right) \tag{2.3a}$$

$$= \frac{|e|}{|K|}\|v\|_{0,K}\Big(\|v\|_{0,K} + 2|i|\,\|\boldsymbol{t}_i\cdot\nabla v\|_{0,K}\Big)\,. \tag{2.3b}$$

Proof. Using the notation given by Figure 2.3, we define

$$\boldsymbol{\phi}_e(\boldsymbol{x}) \coloneqq \big(\boldsymbol{n}_e \cdot (\boldsymbol{x} - \boldsymbol{p}_{\bar{\bar{e}}})\big)\boldsymbol{t}_i\,,$$

where $\boldsymbol{n}_e$ is the outer unit normal to edge e, $\boldsymbol{t}_i$ is a tangential unit vector of an incident edge such that $\boldsymbol{t}_i \cdot \boldsymbol{n}_e > 0$ and $\boldsymbol{p}_{\bar{\bar{e}}}$ is any point on the opposite edge $\bar{\bar{e}}$ (parallel to e). It remains to evaluate the terms involving $\boldsymbol{\phi}_e$. We start by observing that

$$\operatorname{div} \boldsymbol{\phi}_e = n_{e1}t_{i1} + n_{e2}t_{i2} = \boldsymbol{n}_e \cdot \boldsymbol{t}_i = \cos(\pi - (\pi/2 + \alpha)) = \sin(\alpha)\,. \tag{2.4}$$

Furthermore, the unit tangential and normal vector of edge e form a basis of $\mathbb{R}^2$, that is, each $\boldsymbol{x} \in K$ is representable as $\boldsymbol{x} = \boldsymbol{p}_{\bar{\bar{e}}} + r_1(\boldsymbol{x})|e|^{-1}|K|\boldsymbol{n}_e + r_2(\boldsymbol{x})\boldsymbol{t}_e$ with $r_1 \in [0,1]$ and $r_2 \in \mathbb{R}$. Therefore, the definition of $\boldsymbol{\phi}_e$ simplifies to

$$\boldsymbol{\phi}_e = r_1(\boldsymbol{x})|e|^{-1}|K|\boldsymbol{t}_i \quad \text{for} \quad r_1 \in [0,1]\,, \tag{2.5}$$

with $r_1 \equiv 0$ on $\bar{\bar{e}}$ and $r_1 \equiv 1$ on e (since K is a parallelogram). Therefore, $\boldsymbol{\phi}_e \cdot \boldsymbol{n} = 0$ on $\partial K \setminus e$ and

$$\int_{\partial K} (\boldsymbol{\phi}_e \cdot \boldsymbol{n}) v^2 \,\mathrm{d}s = \int_e (\boldsymbol{\phi}_e \cdot \boldsymbol{n}_e) v^2 \,\mathrm{d}s = \frac{|K|}{|e|}(\boldsymbol{n}_e \cdot \boldsymbol{t}_i) \int_e v^2 \,\mathrm{d}s = \frac{|K|}{|e|}\sin(\alpha) \int_e v^2 \,\mathrm{d}s\,. \tag{2.6}$$

Then, inserting (2.4), (2.5) and (2.6) into (2.2) we arrive at

$$\sin(\alpha)\frac{|K|}{|e|}\int_e v^2 \,\mathrm{d}s = \sin(\alpha)\int_K v^2 \,\mathrm{d}\boldsymbol{x} + \frac{|K|}{|e|}\int_K r_1(\boldsymbol{x}) 2v(\boldsymbol{t}_i \cdot \nabla v)\,\mathrm{d}\boldsymbol{x}$$

which, after recalling $\max_{\boldsymbol{x}\in K} r_1(\boldsymbol{x}) = 1$ and applying (CS_1) gives

$$\begin{aligned}\|v\|_{0,e}^2 &\le \|v\|_{0,K}\Big(\frac{|e|}{|K|}\|v\|_{0,K} + \frac{2}{\sin\alpha}\|\boldsymbol{t}_i \cdot \nabla v\|_{0,K}\Big) \\ &= \frac{|e|}{|K|}\|v\|_{0,K}\Big(\|v\|_{0,K} + 2|i|\,\|\boldsymbol{t}_i \cdot \nabla v\|_{0,K}\Big)\end{aligned}$$

and finishes the proof. □

For rectangles, incident tangential vectors are also normal vectors of edge e and Lemma 2.4 implies the following result which is similar to, e. g. [Geo03, Lemma A.1].

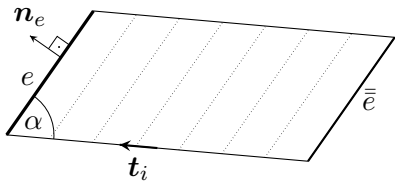

Fig. 2.3. Parallelogram K with notation and level-sets of $\boldsymbol{\phi}_e$.

Corollary 2.5. *Let K be a rectangle and let $u \in H^1(K)$. Then*

$$\|u\|_{0,e}^2 \leq \frac{|e|}{|K|}\|u\|_{0,K}^2 + 2\|u\|_{0,K}\|\partial_{n_e} u\|_{0,K}\,,$$

for each edge e of K with $\boldsymbol{n}_e$ denoting a unit normal vector of e.

By analogy the proof of Corollary 2.5 can also be applied on rectangular cuboids. The proof of Lemma 2.4 works on parallelepipeds (affine cubes) if the incident tangential vector is chosen as follows. Let e_i be an incident edge shared by two incident faces and let $\boldsymbol{t}_i$ be its tangential vector such that $\boldsymbol{n}_e \cdot \boldsymbol{t}_i > 0$. This tangential vector is orthogonal to the normal vectors of all incident faces.

2.2.2. Anisotropic discrete trace inequalities

Here we recall some optimal results on triangles and tetrahedrons.

Lemma 2.6 (trace-inverse estimates). *Let T be a triangle with an edge e and let K be a tetrahedron with a face F. Then, all $u \in \mathbb{P}_p(T), v \in \mathbb{P}_p(K)$ satisfy*

$$\frac{|T|}{|e|}\|u\|_{0,e}^2 \leq \frac{1}{2}(p+1)(p+2)\|u\|_{0,T}^2\,,$$

$$\frac{|K|}{|F|}\|v\|_{0,F}^2 \leq \frac{1}{3}(p+1)(p+3)\|v\|_{0,K}^2\,.$$

Proof. See proofs of Theorem 3 and 4 in [WH03]. □

In what follows we present similar but more detailed results for intervals and parallelograms. In this case we include the proofs, as they allow the construction of special polynomials whose L^2-norm behaves as the inverse of the trace constant. Later in Chapter 3 this property is invaluable for the optimal convergence of the designed methods.

Estimates on intervals and parallelograms

In the proofs of the estimates we use the following properties of Legendre polynomials. A detailed reference for all properties mentioned here is for instance [Riv81, pp. 62f].

Let $j \in \mathbb{N}$, $k \in \mathbb{N}_+$, and P_j be the *Legendre polynomial* of degree j. Then, the set $\{P_j\}_{j=0}^{k-1}$ forms a basis of $\mathbb{P}_{k-1}([-1,1])$, and satisfies the recurrence relation: $P_0(s) = 1$, $P_1(s) = s$ and

$$mP_m(s) = (2m-1)sP_{m-1}(s) - (m-1)P_{m-2}(s) \quad \text{for} \quad m = 2,\ldots,k-1\,. \tag{2.7}$$

Additionally, we have $P_j(1) = 1$, $P_j(-1) = (-1)^j$ and

$$\int_{-1}^{1} P_m(s)P_j(s)\mathrm{d}s = C_{L,j}\delta_{jm} \quad \text{where} \quad C_{L,j} = \frac{2}{2j+1}\,, \tag{2.8}$$

where δ_{jm} is the Kronecker delta.

Later in this section we prove trace estimates of optimal order in polynomial degree. The following result is used to show their optimality.

Corollary 2.7. *Let $j \in \mathbb{N}_+$. Then, $P_j(0) = 0$ for odd j and*

$$(j+1)P_j(0)^2 \in \left(\frac{2}{\pi}, \frac{3}{4}\right] \quad \textit{for even} \quad j \geq 2\,. \tag{2.9}$$

Proof. First, the recurrence relation (2.7) gives $P_j(0) = -\frac{j-1}{j}P_{j-2}(0)$ for $j \geq 2$. Therefore, $P_j(0) = 0$ for odd j and $P_j(0) = \prod_{m=1}^{j/2}\left(-\frac{2m-1}{2m}\right)$ for even j. For even $j \geq 2$, this last identity implies

$$(j+1)P_j(0)^2 = (j+1)\prod_{m=1}^{j/2}\left(\frac{2m-1}{2m}\right)^2 = \prod_{m=1}^{j/2}\frac{(2m+1)(2m-1)}{4m^2}\,.$$

Evaluating this product for $j = 2$ gives the upper bound. The lower bound follows from Wallis' product, that is, $\prod_{m=1}^{\infty}\frac{(2m+1)(2m-1)}{4m^2} = \frac{2}{\pi}$ (see [BB98, p. 338]). □

We next present an estimate of the mid-point value of a univariate polynomial.

Lemma 2.8. *Let $k \in \mathbb{N}_+$. Then, for all $q \in \mathbb{P}_{k-1}([a,b])$ the following bound holds*

$$\left|q\left(\frac{a+b}{2}\right)\right|^2 \leq \frac{3k+1}{4}\,\frac{1}{b-a}\|q\|^2_{0,[a,b]}\,. \tag{2.10}$$

Proof. We first prove (2.10) on the interval $[-1,1]$. To this end, let $\{P_j\}_{j=0}^{k-1}$ denote the basis of $\mathbb{P}_{k-1}([-1,1])$ consisting of Legendre polynomials. Let $f \in \mathbb{P}_{k-1}([-1,1])$. Hence $f = \sum_{j=0}^{k-1} f_j P_j$, and (2.8) yields $\|f\|^2_{0,[-1,1]} = \sum_{j=0}^{k-1} f_j^2 \frac{2}{2j+1}$. Now, using ($\mathrm{CS}_2$) we obtain

$$|f(0)|^2 \leq \left(\sum_{j=0}^{k-1}\frac{2j+1}{2}P_j(0)^2\right)\left(\sum_{j=0}^{k-1}\frac{2}{2j+1}f_j^2\right) = \Sigma_{k,01}\frac{1}{2}\|f\|^2_{0,[-1,1]}\,. \tag{2.11}$$

where $\Sigma_{k,01} \coloneqq \sum_{j=0}^{k-1}(2j+1)P_j(0)^2$. Our next aim is to show that $\Sigma_{k,01} \leq (3k+1)/4$.

Using Corollary 2.7 we bound each even summand from below and above. Let $j \geq 2$ be even, then

$$(2j+1)P_j(0)^2 \in \frac{2j+1}{j+1}\cdot\left(\frac{2}{\pi}, \frac{3}{4}\right] \subset \left(1, \frac{3}{2}\right), \tag{2.12}$$

since the j-dependent ratio belongs to $[5/3, 2)$ for $j \geq 2$, and $10/(3\pi) > 1$. Therefore, recalling $P_j(0) = 0$ for odd j and $P_0 = 1$, we get

$$\Sigma_{k,01} = \sum_{j=0}^{k-1} (2j+1) P_j(0)^2 \leq 1 + \frac{3}{2} \left\lfloor \frac{k-1}{2} \right\rfloor \leq 1 + \frac{3}{4}(k-1) = \frac{3k+1}{4},$$

where $\lfloor r \rfloor \leq r$ is the integer part of $r \geq 0$. This completes (2.11). Then, inserting $f(s) = q\big(\frac{a+b}{2} + s\frac{b-a}{2}\big)$, where $q \in \mathbb{P}_{k-1}([a,b])$, gives (2.10). □

The following two lemmas contain trace estimates and show the existence of special polynomials $\ell_{k-1} \in \mathbb{P}_{k-1}(K)$ for rectangles. In Chapter 3 we use the affine version of these polynomials.

Lemma 2.9. *Let $k \in \mathbb{N}_+$. Then, there exists $\ell_{k-1} \in \mathbb{P}_{k-1}([-1,1]^2)$ such that $\ell_{k-1}(1,0) = 1$ and*

$$\int_{-1}^{1}\int_{-1}^{1} \ell_{k-1}(x,y)^2 \mathrm{d}x\mathrm{d}y = \frac{4}{\Sigma_k} = \int_{-1}^{1}\int_{-1}^{1} \ell_{k-1}(x,y) \mathrm{d}x\mathrm{d}y\,, \tag{2.13}$$

where Σ_k is a constant that only depends on the polynomial degree. For a parallelogram K, let $x_e \in \partial K$ be the midpoint of an edge $e \subset \partial K$. Then, for all $q \in \mathbb{P}_{k-1}(K)$ the following bound holds

$$q(x_e)^2 \leq \frac{\Sigma_k}{|K|} \|q\|_{0,K}^2 \quad \textit{with} \quad \frac{1}{6}k^3 < \Sigma_k \leq k^3\,. \tag{2.14}$$

Proof. Let $\hat{\kappa} = [-1,1] \times [-1,1]$, $f \in \mathbb{P}_{k-1}(\hat{\kappa})$ and write

$$f(x,y) = \sum_{i=0}^{k-1} \sum_{j=0}^{k-1-i} f_{ij} P_j(x) P_i(y)\,,$$

where P_j denotes the Legendre polynomial of degree j. Then, (2.7)–(2.8) yield $P_j(1) = 1$ and $\int_{\hat{\kappa}} f^2 \mathrm{d}\boldsymbol{x} = \sum_{i=0}^{k-1} \sum_{j=0}^{k-1-i} f_{ij}^2 C_{L,j} C_{L,i}$. Therefore, applying ($\mathrm{CS}_2$) gives

$$f(1,0)^2 = \left(\sum_{i=0}^{k-1} \sum_{j=0}^{k-1-i} f_{ij} P_i(0) \right)^2 \leq \left(4 \sum_{i=0}^{k-1} \sum_{j=0}^{k-1-i} \frac{P_i(0)^2}{C_{L,j} C_{L,i}} \right) \frac{1}{4} \int_{\hat{\kappa}} f^2 \mathrm{d}\boldsymbol{x}\,.$$

We define a shortcut, i. e., let $\Sigma_k \coloneqq 4 \sum_{i=0}^{k-1} \sum_{j=0}^{k-1-i} P_i(0)^2 C_{L,j}^{-1} C_{L,i}^{-1}$. At this point, inserting the polynomial ℓ_{k-1} with the coefficients $\ell_{ij} \coloneqq \frac{4}{\Sigma_k} P_i(0) C_{L,j}^{-1} C_{L,i}^{-1}$, for i, j, gives an equality, $\ell_{k-1}(1,0) = 1$ and $\int_{\hat{\kappa}} \ell_{k-1}(\boldsymbol{x}) \mathrm{d}\boldsymbol{x} = \frac{4}{\Sigma_k} = \int_{\hat{\kappa}} \ell_{k-1}(\boldsymbol{x})^2 \mathrm{d}\boldsymbol{x}$.

Now, (2.14) follows by a change of variables, once we bound the (k-dependent) con-

stant Σ_k, i. e., show that $k^{-3}\Sigma_k \in (1/6, 1]$. We sum up ($\sum_{i=1}^{0} \coloneqq 0$) to obtain

$$\begin{aligned}\Sigma_k = 4\sum_{i=0}^{k-1} \frac{P_i(0)^2}{C_{L,i}} \sum_{j=0}^{k-1-i} \frac{1}{C_{L,j}} &= 4\sum_{i=0}^{k-1} \frac{P_i(0)^2}{C_{L,i}} \frac{(k-i)^2}{2} \\ &= k^2 + 4 \sum_{i=1}^{\lfloor (k-1)/2 \rfloor} \frac{P_{2i}(0)^2}{C_{L,2i}} \frac{(k-2i)^2}{2} \\ &= k^2 + \sum_{i=1}^{\lfloor (k-1)/2 \rfloor} 2\frac{P_{2i}(0)^2}{C_{L,2i}} (k-2i)^2 \,.\end{aligned}$$

By means of (2.12), we get $2P_{2j}(0)^2/C_{L,2j} = (2(2j)+1)P_{2j}(0)^2 \in (1, 3/2)$. Additionally, we evaluate $\sum_{i=1}^{\lfloor (k-1)/2 \rfloor} (k-2i)^2 = k(k-1)(k-2)/6$, which holds for even and odd $k \in \mathbb{N}$. Hence, we get the bounds

$$\frac{1}{6}k^3 < k^2 + \frac{1}{6}k(k-1)(k-2) \leq \Sigma_k \leq k^2 + \frac{1}{4}k(k-1)(k-2) \leq k^3 \,,$$

which finishes the proof. □

Lemma 2.10. *Let $H, h > 0$ and $k-1 \in \mathbb{N}$. Then, there exists a univariate polynomial ℓ_{k-1} of degree $k-1$ such that*

$$\ell_{k-1}(1) = 1 \quad \textit{and} \quad \int_{-1}^{1} \ell_{k-1}(s)^2 \,\mathrm{d}s = \frac{2}{k^2} = \int_{-1}^{1} \ell_{k-1}(s) \,\mathrm{d}s \,. \tag{2.15}$$

Moreover, for all $q \in \mathbb{P}_{k-1}((0,H) \times (0,h))$ the following, optimal bound holds

$$\frac{1}{h} \int_0^h q(0,y)^2 \mathrm{d}y \leq \frac{1}{Hh}\, k^2 \int_0^h \int_0^H q(x,y)^2 \mathrm{d}x\mathrm{d}y \,. \tag{2.16}$$

Proof. Let P_j denote the Legendre polynomial of degree j. We recall the identities $P_0 = 1$, $P_j(+1) = 1$, $P_j(-1) = (-1)^j$ and (2.8). Let $f \in \mathbb{P}_{k-1}([-1,1])$, and write $f = \sum_{j=0}^{k-1} f_j P_j$. Then, the properties above, the triangle inequality and (CS_2) show

$$|f(\pm 1)|^2 \leq \left(\sum_{j=0}^{k-1} |f_j| \right)^2 \leq \left(\sum_{j=0}^{k-1} \frac{2j+1}{2} \right) \left(\sum_{j=0}^{k-1} \frac{2}{2j+1} f_j^2 \right) = \Sigma_k \int_{-1}^{1} f(s)^2 \,\mathrm{d}s \,, \tag{2.17}$$

where $\Sigma_k \coloneqq \sum_{j=0}^{k-1} (2j+1)/2 = k^2/2$.

The first result is obtained by choosing $\ell_{k-1}(s) = \sum_{j \in J} f_j P_j(s)$ with coefficients $f_j \coloneqq \Sigma_k^{-1}(2j+1)/2$, $j \in \{0, \dots, k-1\}$ and from the fact that only P_0 has non-vanishing average. Bound (2.17) is then sharp, as equality is attained for $f = \ell_{k-1}$.

Finally, let $q \in \mathbb{P}_{k-1}([0,H] \times [0,h])$ and let $y \in [0,h]$ be fixed. Then, we insert $f(s) = q((1+s)H/2, y)$, $s \in (-1,1)$ into inequality (2.17). Integrating the resulting inequality over $y \in [0,h]$ gives the second result. □

2.2.3. Interpolation on anisotropic meshes

Later in the thesis, we will restrict ourselves to the proof of a priori estimates with respect to the best approximation on a given mesh. This is done to avoid the usual discussion whether the anisotropic mesh is aligned with the "anisotropic" behaviour of the solution which is a related but different issue. If not known a priori, then a posteriori information may be used to refine and/or realign the mesh, but this is not within the scope of this thesis.

Many authors prefer a final estimate containing only explicit quantities. Such an estimate is obtained by replacing the best-approximation by an interpolant whose error can be bounded explicitly. In this section we show two interpolation error estimates on anisotropic meshes, so that we gain an idea of how the error behaves in some cases. We restrict the presentation to interpolants defined explicitly on each cell, since known results for averaging interpolants, like the one of Clément, or Scott–Zhang, restrict anisotropies in the neighbourhood of each cell, for example the meshes shown in Figures 1.1, 2.1c, and 2.2 are ruled out by [MPP03, eq. (2.1)] and [Ape99, p. 100, eq. (3.4)], or in [Bla08, AKL08].

First, we state an estimate for the L^2-projection into (globally discontinuous) piecewise constant polynomials.

Lemma 2.11. *Let $p \in H^1(K)$ and let K be an axis-aligned rectangle of width h_x and height h_y. Furthermore, let $\Pi_0 p \in \mathbb{P}_0(K)$ be the L^2-projection given by $\Pi_0 p = |K|^{-1} \int_K p \,\mathrm{d}\boldsymbol{x}$. Then, there exists $C > 0$, independent of K, such that*

$$C\|p - \Pi_0 p\|_{0,K} \leq h_x \|\partial_x p\|_{0,K} + h_y \|\partial_y p\|_{0,K} .$$

Proof. See [AMR03]. □

In order to define a continuous function more regularity is required. The following lemma is an example.

Lemma 2.12. *Let K be an axis-aligned rectangle with edges of lengths h_1 and h_2. Let $u \in H^\ell(K)$ for some $\ell \geq 2$. Then, there exists an interpolant $I_h u \in \mathbb{Q}_k(K)$, such that*

$$\|u - I_h u\|_{0,K} \leq C \sum_{|\alpha| \leq s} h_1^{\alpha_1} h_2^{\alpha_2} \|D^\alpha u\|_{0,K} ,$$

and

$$|u - I_h u|_{1,K} \leq C \sum_{|\alpha| \leq s-1} h_1^{\alpha_1} h_2^{\alpha_2} |D^\alpha u|_{1,K}$$

where $s \coloneqq \min\{k+1, \ell\}$, $\alpha \in \mathbb{N}^2$ with $|\alpha| \coloneqq \alpha_1 + \alpha_2$ and $D^\alpha \coloneqq \partial_{x_2}^{\alpha_2} \partial_{x_1}^{\alpha_1}$. The constants C are independent of K.

Proof. In [AADL08, Thm. 3] the proof is carried out for an interpolant defined by moments and nodal values (see [GR86] where this operator seems to be defined for the first time), which extends previous estimates from [ST08, Ape99, GR86, MS09]. Earlier, the estimates were proven for the Lagrange interpolant in [Ape99, Thm. 2.7]. □

A result similar to Lemma 2.12 can be proven for triangles, tetrahedrons, parallelograms, parallelepipeds and some non-affine elements, see [AADL08]. On general elements, the constants may depend on angles of the cell. Such dependencies are discussed for example in [AD99, Ape99, BA76].

Hereafter the capital letter C (without subscripts) denotes a constant independent of the polynomial degree k and of properties of the mesh (except angles). It will be explicitly pointed out when such a C is independent of angles. In a sequence of estimates, the value of C may be different at every occurrence.

2.3. Operators and conventions

In the subsequent chapters we frequently use the following definitions and conventions. For $\ell \in \mathbb{N}_+$ and a given $v\colon \omega \to \mathbb{R}^\ell$, we define $\operatorname{supp} v \coloneqq \overline{\{\boldsymbol{x} \in \omega\colon v(\boldsymbol{x}) \neq \mathbf{0} \in \mathbb{R}^\ell\}}$ to be the *support* of v. The operator $\langle\cdot\rangle_\omega\colon L^2(\omega) \to \mathbb{R}$ returns the average given by

$$\langle v\rangle_\omega \coloneqq \frac{1}{|\omega|}\int_\omega v \,\mathrm{d}\boldsymbol{x}\,,$$

where ω is a cell K, or an edge e or another subdomain of $\overline{\Omega}$.

Let $e \in \mathcal{E}_\mathcal{P}$ be an edge, such that $e = K \cap K'$. Given a function v belonging to the set $H^1(\mathcal{P}) = \left\{v \in L^2(\Omega)\colon\ v|_K \in H^1(K) \text{ for } K \in \mathcal{P}\right\}$ we define its *jump* across edge e by

$$[\![v]\!]_e \coloneqq\ v|_K|_e - \ v|_{K'}|_e$$

where $v|_K|_e$ denotes the restriction of v first to K and then to e.

For a linear functional $L\colon V \to \mathbb{R}$ and a norm $\|\cdot\|_V$ on V, we use the short form

$$\sup_{v\in V}\frac{L(v)}{\|v\|_V} \quad \text{instead of} \quad \sup_{v\in V\setminus\{0\}}\frac{L(v)}{\|v\|_V} \quad \text{or} \quad \sup_{v\in V,\|v\|_V=1} L(v)\,.$$

The same applies to infima.

Chapter 3

Minimal stabilisation for arbitrary order

In this and the next chapter, the main concern of our study is to solve the Stokes flow problem by a finite element method on anisotropic meshes. Our approach is motivated by meshes containing corner patches that possess arbitrary high aspect ratios. We start with the finite element pair $\boldsymbol{Q}^c_{k+1} \times \mathbb{P}_{k-1}$. This pair is known to be inf-sup stable, but the inf-sup constant depends on geometrical properties of corner patches, cf. [AC00] or Table 1.1 (3rd. row). Within this chapter we generalise some results from [AC00] which enables us to identify the minimal number of spurious (responsible) pressure modes. With this knowledge, we identify uniformly inf-sup stable subspaces. Then, it is possible to define two new finite element methods; a mixed FEM (using a minimally reduced pressure space) and a stabilised FEM, which adds the minimal number of constraints in form of stabilisation terms. These terms take the form of (almost) consistent jumps and identify the spurious modes automatically. Additionally, the stabilisation parameters are completely local and optimal in terms of mesh properties and polynomial degree k.

This chapter is organised as follows. The next section deals with the model problem and notation. In Section 3.2 we restrict the set of considered partitions to allow certain anisotropies. This allows us to identify a subspace G of the pressure space, such that $\boldsymbol{V}_{\mathcal{P}} \times G$ is uniformly inf-sup stable and G is of maximal dimension. For readability, the proof of these results is located in Section 3.5. In Section 3.2.2 an inf-sup deficiency is proven which motivates the definition of the stabilised method in Section 3.3. Afterwards, well-posedness and approximation qualities are discussed. Then, in Section 3.4, numerical experiments confirm that our stabilisation removes the dependency on the mesh properties and that the space G is of maximal dimension. The ideas and results contained in Sections 3.2–3.5 have been modified and published in [ABW15]. In Section 3.6 the published results are listed.

In Section 3.7 we conclude and show possible extensions which lead naturally into the subsequent chapters.

3.1. The problem of interest and notations

Hereafter, we deal with the Stokes equations in a bounded, polygonal domain $\Omega \subset \mathbb{R}^2$. We recall the problem, existence results and define used finite element spaces.

For $\boldsymbol{f} \in L^2(\Omega)^2$, find a velocity $\boldsymbol{u}\colon \Omega \to \mathbb{R}^2$ and a pressure $p\colon \Omega \to \mathbb{R}$, such that

$$-\Delta \boldsymbol{u} + \operatorname{grad} p = \boldsymbol{f} \quad \text{and} \quad \operatorname{div} \boldsymbol{u} = 0 \quad \text{in} \quad \Omega\,, \tag{3.1}$$

where $\boldsymbol{u} = \boldsymbol{0}$ on $\partial\Omega$ and $\langle p \rangle_\Omega = 0$.

We recall the notation for Sobolev spaces and that $\langle p \rangle_\omega$ denotes the mean value of p on $\omega \subset \overline{\Omega}$. Furthermore, we recall the variational formulation of Problem (3.1).

Find $(\boldsymbol{u}, p) \in \boldsymbol{V} \times M \coloneqq \boldsymbol{H}^1_0(\Omega) \times L^2_0(\Omega)$ such that

$$\mathfrak{B}(\boldsymbol{u}, p; \boldsymbol{v}, q) = (\boldsymbol{f}, \boldsymbol{v})_\Omega \quad \text{for all} \quad (\boldsymbol{v}, q) \in \boldsymbol{V} \times M \tag{3.2a}$$

where

$$\mathfrak{B}(\boldsymbol{u}, p; \boldsymbol{v}, q) \coloneqq (\operatorname{grad} \boldsymbol{u}, \operatorname{grad} \boldsymbol{v})_\Omega - (p, \operatorname{div} \boldsymbol{v})_\Omega - (q, \operatorname{div} \boldsymbol{u})_\Omega\,. \tag{3.2b}$$

Problem (3.2a) is a well studied saddle-point problem. Its well-posedness is a consequence of the inf-sup condition [GR86, pp. 58–61] or [Gal94, Lemma III.3.1]:

$$\inf_{q \in M} \sup_{\boldsymbol{v} \in \boldsymbol{V}} \frac{(\operatorname{div} \boldsymbol{v}, q)_\Omega}{|\boldsymbol{v}|_{1,\Omega} \|q\|_{0,\Omega}} \geq \beta_\Omega > 0\,. \tag{3.3}$$

For the finite element approximation, we suppose the domain Ω is covered by a conforming partition $\mathcal{P}$ consisting of closed parallelograms K, more properties of $\mathcal{P}$ are defined in the next section. We aim to approximate the solution of (3.2a) within the spaces

$$\boldsymbol{V}_\mathcal{P} \coloneqq \left\{ \boldsymbol{v} \in \boldsymbol{V}\colon \boldsymbol{v}|_K \in \mathbb{Q}_{k+1}(K)^2 \quad \text{for} \quad K \in \mathcal{P} \right\},$$

and

$$M_\mathcal{P} \coloneqq \{ q \in M\colon q|_K \in \mathbb{P}_{k-1}(K) \quad \text{for} \quad K \in \mathcal{P} \}\,.$$

For our results, later on, we also require local subspaces. For $\omega \subseteq \overline{\Omega}$ we define the restrictions

$$\boldsymbol{V}_\mathcal{P}(\omega) \coloneqq \{ \boldsymbol{v} \in \boldsymbol{V}_\mathcal{P}\colon \operatorname{supp} \boldsymbol{v} \subseteq \overline{\omega} \}\,,$$
$$M_\mathcal{P}(\omega) \coloneqq \{ q \in M_\mathcal{P}\colon \operatorname{supp} q \subseteq \overline{\omega} \}\,.$$

We observe that a function $\boldsymbol{v} \in \boldsymbol{V}_\mathcal{P}(\omega)$ belongs to $\boldsymbol{H}^1_0(\omega)$, since $\boldsymbol{v} \in \mathcal{C}^0(\Omega)$. Similarly, $q \in M_\mathcal{P}(\omega)$ belongs to $L^2_0(\omega)$, since $0 = \langle q \rangle_\Omega = \langle q \rangle_{(\operatorname{supp} q)}$.

As mentioned in the introduction, the pair $\boldsymbol{V}_{\mathcal{P}} \times M_{\mathcal{P}}$ does satisfy a discrete version of (3.3). However, the discrete inf-sup constant degenerates as the aspect ratio tends to zero. In the next section, we first state that certain spurious pressure modes cause this behaviour. Then, we generalise some results from [AC00] and introduce a maximal subspace $G \subset M_{\mathcal{P}}$, such that the pair $\boldsymbol{V}_{\mathcal{P}} \times G$ is *uniformly inf-sup stable*, that is, $\boldsymbol{V}_{\mathcal{P}} \times G$ satisfies an inf-sup condition with a constant β_G independent of the aspect ratio. Using this information we derive an inf-sup deficiency caused by the spurious modes.

3.2. A decomposition of the pressure space

We restrict our attention to conforming partitions $\mathcal{P}$ consisting of parallelograms, and allow them to contain highly stretched (also anisotropic) cells, as shown in Figure 3.1. In what follows, we require some notation and properties related to partition $\mathcal{P}$. Most importantly, we require that $\mathcal{P}$ is the anisotropic refinement of an initial shape regular partition, say $\mathcal{P}_{sr}$. During this refinement we select a few nodes $\boldsymbol{c} \in \mathcal{C}$ of $\mathcal{P}_{sr}$. For $\boldsymbol{c} \in \mathcal{C}$, the subdomains $\Omega_{\boldsymbol{c}} \coloneqq \bigcup\{K \in \mathcal{P}_{sr} \colon \boldsymbol{c} \in K\}$ should be disjoint (which requires $\mathcal{P}_{sr}$ to be sufficiently fine). Then the anisotropic refinement towards each node $\boldsymbol{c} \in \mathcal{C}$ inserts one of the corner patches shown in Figure 3.2. Once this is done, edge patches are fitted as required, to ensure the conformity of the resulting mesh $\mathcal{P}$.

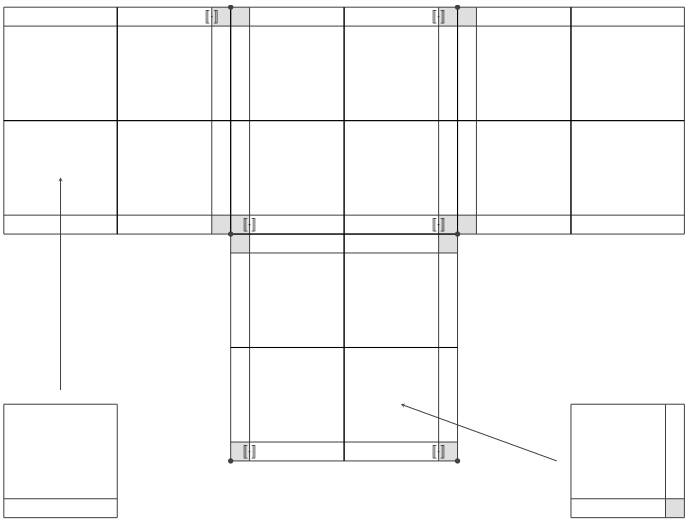

(a) Edge patch (b) single corner patch

Fig. 3.1. An affine, anisotropic mesh (from [AC00]) consisting of edge and corner patches.

It is convenient to associate each node $\boldsymbol{c} \in \mathcal{C}$ with a corner patch and with the subdomains $\Omega_{\boldsymbol{c}}$ and $\omega_{\boldsymbol{c}} \coloneqq \bigcup\{K \in \mathcal{P} \colon \boldsymbol{c} \in K\}$. By construction, the part of $\mathcal{P}$ covering the subdomains $\omega_{\boldsymbol{c}}$ only contains (extremely) small and shape-regular cells (shaded in

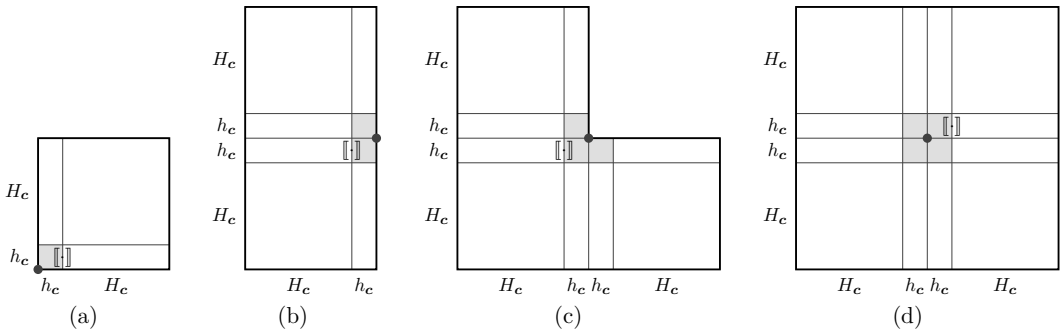

Fig. 3.2. Corner patches with $\varrho_{\boldsymbol{c}} = h_{\boldsymbol{c}}/H_{\boldsymbol{c}}$.

Figures 3.1–3.2). Furthermore, for $\boldsymbol{c} \in \mathcal{C}$ let $\gamma_{\boldsymbol{c}} \subset \partial\omega_{\boldsymbol{c}} \cap \partial(\Omega_{\boldsymbol{c}} \setminus \omega_{\boldsymbol{c}})$ be an edge in $\mathcal{E}_{\mathcal{P}}$, for instance, the edges enclosed by the jump symbol $[\![\cdot]\!]$ in Figures 3.1–3.2.

At this point, we realise that each subdomain $\Omega_{\boldsymbol{c}}$ contains anisotropic cells $K \in \mathcal{P}$ with *aspect ratio* $\varrho_{\boldsymbol{c}} \coloneqq h_{\boldsymbol{c}}/H_{\boldsymbol{c}} \ll 1$. This is desirable to resolve local features of solutions, but has a drawback: the discrete inf-sup constant depends on the aspect ratio ϱ. More precisely, a detailed analysis in [AC00] (see Lemma 3.1 below) proves

$$\inf_{q \in M_{\mathcal{P}}} \sup_{\boldsymbol{v} \in \boldsymbol{V}_{\mathcal{P}}} \frac{(\operatorname{div} \boldsymbol{v}, q)_{\Omega}}{|\boldsymbol{v}|_{1,\Omega} \|q\|_{0,\Omega}} =: \beta_{\mathcal{P}} \geq C k^{-1/2} \min\{1, k\sqrt{\varrho}\}, \tag{3.4}$$

with $\varrho = \min\{\varrho_{\boldsymbol{c}} \colon \boldsymbol{c} \in \mathcal{C}\}$.

The proof of (3.4) is decomposed into local inf-sup conditions. In the following lemma we restate these conditions for a *single corner patch* (Figure 3.1b), as more insight is given.

Lemma 3.1. *Let $\Omega_{\boldsymbol{c}}$ denote a single corner patch (cf. Figure 3.1b), and let $q \in M_{\mathcal{P}}(\Omega_{\boldsymbol{c}})$. Then, there exists $\boldsymbol{v} \in \boldsymbol{V}_{\mathcal{P}}$, such that*

$$(\operatorname{div} \boldsymbol{v}, q)_{\Omega_{\boldsymbol{c}}} = \|q\|^2_{0,\Omega_{\boldsymbol{c}}} \quad \textit{and} \quad |\boldsymbol{v}|_{1,\Omega_{\boldsymbol{c}}} \leq C k^{1/2} \min\{1, k\sqrt{\varrho_{\boldsymbol{c}}}\}^{-1} \|q\|_{0,\Omega_{\boldsymbol{c}}}\,. \tag{3.5}$$

Furthermore, if $\langle q \rangle_{\omega_{\boldsymbol{c}}} = 0$, then

$$(\operatorname{div} \boldsymbol{v}, q)_{\Omega_{\boldsymbol{c}}} = \|q\|^2_{0,\Omega_{\boldsymbol{c}}} \quad \textit{and} \quad |\boldsymbol{v}|_{1,\Omega_{\boldsymbol{c}}} \leq C k^{1/2} \|q\|_{0,\Omega_{\boldsymbol{c}}}\,. \tag{3.6}$$

Both constants C are independent of partition and polynomial degree k.

Proof. Condition (3.6) is proven in [AC00, Lemma 4.3]. Condition (3.5) is a consequence of [AC00, Lemma 4.6]. □

One consequence of (3.6) is that spurious pressure modes belong to a one-dimensional subspace, say $M_{\mathcal{P}}(\Omega_{\boldsymbol{c}}) \setminus \big\{q \in M_{\mathcal{P}}(\Omega_{\boldsymbol{c}}) \colon \langle q \rangle_{\omega_{\boldsymbol{c}}} = 0\big\}$. Another, more important, consequence is elaborated in the following remark.

Remark 3.2. *The dependency of $\beta_{\mathcal{P}}$ on $\sqrt{\varrho}$ is caused by the presence of a function in $M_{\mathcal{P}}$ that "connects" $M_{\mathcal{P}}(\omega_{\boldsymbol{c}})$ and $M_{\mathcal{P}}(\Omega_{\boldsymbol{c}} \setminus \omega_{\boldsymbol{c}})$. This function's support is non-local and may cover the whole of $\Omega_{\boldsymbol{c}}$. Then, the inf-sup degeneracy is not caused only by local aspect ratios ϱ (or grading factors κ), but rather by the topology of the mesh $\mathcal{P}$. To stress this fact, we notice that for a mesh that consists of edge patches only, the inf-sup constant does not depend on the aspect ratio, or the grading factor. Then, the culprit of the inf-sup deficiency is not the aspect ratio (or grading factor)* per se*, but the presence of corner patches.*

In order to avoid the repetition of this discussion and, since for corner patches (as in Figure 2.2) $\beta_{\mathcal{P}}$ decays like $\sqrt{\varrho}$, we will abuse the language and say "$\beta_{\mathcal{P}}$ depends on aspect ratios", instead of the less precise term "$\beta_{\mathcal{P}}$ depends on topological properties".

In [AC00], the equivalent of (3.5) is used in a macro-element technique to obtain the global inf-sup condition (3.4). These arguments seem to suggest that there are as many spurious pressure modes as there are single corner patches in the partition $\mathcal{P}$, for example twelve on the T-mesh of Figure 3.1 and one, two, three or four on the corner patches shown in Figure 3.2.

A closer inspection (located in Section 3.5) shows that whenever single corner patches are neighbours and the small corners form a small connected domain $\omega_{\boldsymbol{c}}$ (shaded in Figures 3.1–3.2), then there is only one spurious pressure mode per each of these domains. That is, there is only one spurious mode per $\boldsymbol{c} \in \mathcal{C}$. That means, six spurious modes in the T-mesh of Figure 3.1 and one spurious mode on each of the partitions shown in Figure 3.2. Additionally, the spurious subspace of $M_{\mathcal{P}}$ is not unique, an advantage that allows us to construct a subspace $G \subset M_{\mathcal{P}}$ (of maximal dimension), such that $\boldsymbol{V}_{\mathcal{P}} \times G$ satisfies a uniform inf-sup condition. The next section is devoted to make this statement precise.

3.2.1. A uniformly inf-sup stable subspace

The following result characterises a subspace $G \subset M_{\mathcal{P}}$, such that $\boldsymbol{V}_{\mathcal{P}} \times G$ is uniformly inf-sup stable. The theorem and its proof are considered as key results of this chapter, since they motivate every method we propose in this thesis.

Theorem 3.3 (A uniformly inf-sup stable subspace). *Let Ω and $\mathcal{P}$ be as defined in Section 3.2. Suppose $\mathcal{P}$ contains corner patches and for $\boldsymbol{c} \in \mathcal{C}$, let $\boldsymbol{x}_{\boldsymbol{c}}$ be the midpoint of the previously selected edge $\gamma_{\boldsymbol{c}}$. Finally, let G be defined as*

$$G \coloneqq \left\{ q \in M_{\mathcal{P}} \colon [\![q(\boldsymbol{x}_{\boldsymbol{c}})]\!]_{\gamma_{\boldsymbol{c}}} = 0 \quad \textit{for} \quad \boldsymbol{c} \in \mathcal{C} \right\}. \tag{3.7}$$

Then,

$$\sup_{\boldsymbol{v}\in\boldsymbol{V}_{\mathcal{P}}} \frac{(\operatorname{div}\boldsymbol{v}, q)_\Omega}{|\boldsymbol{v}|_{1,\Omega}} \geq \beta_G \|q\|_{0,\Omega} \quad \textit{for all} \quad q \in G\,. \tag{3.8}$$

with a constant $\beta_G \geq \max\{\beta_{\mathcal{P}}, Ck^{-2}\} > 0$ *and* C *independent of* ϱ *and* k*.*

The proof of Theorem 3.3 is postponed to the end of Section 3.5.

Remark 3.4. *We realise that for each selected edge* $\gamma_{\boldsymbol{c}}$ *(*$\boldsymbol{c} \in \mathcal{C}$*), definition* (3.7) *imposes a continuity in one point. Considering uniform inf-sup condition* (3.8) *we conclude that spurious pressure modes belong to, say* $B \coloneqq M_{\mathcal{P}} \setminus G$*, and that*

$$\dim(B) = \dim(M_{\mathcal{P}}) - \dim(G) = \operatorname{card}(\mathcal{C}) > 0\,.$$

So, the number of spurious pressure modes is smaller than, or equal to, the number of corner patches. Later in the numerical experiments, we confirm that there exists one spurious mode for each of the corner patches shown in Figure 3.2.

3.2.2. Inf-sup deficiency

In this section, we first characterise the inf-sup deficiency of the space $\boldsymbol{V}_{\mathcal{P}} \times M_{\mathcal{P}}$ in terms of the space G. Then, we prove an equivalence between the deficient part and a few jumps which motivates the stabilisation term used later.

In the following lemma we show that any surjective projection Π_G onto G implies a deficiency equivalent to the inf-sup condition of $\boldsymbol{V}_{\mathcal{P}} \times G$. After that, we choose Π_G conveniently and prove the desired equivalence.

Lemma 3.5 (general inf-sup deficiency).
Let $\Pi_G \colon M_{\mathcal{P}} \to G$ *be any projection. Then, for all* $q \in M_{\mathcal{P}}$ *the following holds*

$$\sup_{\boldsymbol{v}\in\boldsymbol{V}_{\mathcal{P}}} \frac{(\operatorname{div}\boldsymbol{v}, q)_\Omega}{|\boldsymbol{v}|_{1,\Omega}} \geq \beta_G \|\Pi_G q\|_{0,\Omega} - \|q - \Pi_G q\|_{0,\Omega}\,, \tag{3.9}$$

where β_G *is the constant from Theorem 3.3, which is independent of aspect ratios* ϱ*. Furthermore, if* Π *is surjective, then* (3.9) *implies* (3.8)*.*

Proof. Let $q \in M_{\mathcal{P}}$, then $\Pi_G q \in G$ and by Theorem 3.3 there exists a non-zero $\boldsymbol{v} \in \boldsymbol{V}_{\mathcal{P}}$, such that

$$\begin{aligned}\beta_G |\boldsymbol{v}|_{1,\Omega} \|\Pi_G q\|_{0,\Omega} \leq (\operatorname{div}\boldsymbol{v}, \Pi_G q)_\Omega &= -(\operatorname{div}\boldsymbol{v}, q - \Pi_G q)_\Omega + (\operatorname{div}\boldsymbol{v}, q)_\Omega \\ &\leq |\boldsymbol{v}|_{1,\Omega} \|q - \Pi_G q\|_{0,\Omega} + (\operatorname{div}\boldsymbol{v}, q)_\Omega\,.\end{aligned}$$

Now, dividing by $|\boldsymbol{v}|_{1,\Omega}$ and taking the supremum over $\boldsymbol{v} \in \boldsymbol{V}_{\mathcal{P}}$ proves (3.9). The reverse follows since $q = \Pi q$ for $q \in G$, which finishes the proof. □

Our next aim, is to define a suitable projection onto G. Since the different regions $\Omega_{\boldsymbol{c}}$ are disjoint (cf. Section 3.2) we start locally. For $\boldsymbol{c} \in \mathcal{C}$, we require a function, say $\phi_{\boldsymbol{c}}$, that jumps in $\boldsymbol{x}_{\boldsymbol{c}}$. The following lemma fixes $\phi_{\boldsymbol{c}}$ and provides useful properties.

Lemma 3.6. *Let $B_{\boldsymbol{c}} \coloneqq \{q \in M_{\mathcal{P}}(\Omega_{\boldsymbol{c}}) \colon [\![q(\boldsymbol{x}_{\boldsymbol{c}})]\!]_{\gamma_{\boldsymbol{c}}} \neq 0\}$ with $\gamma_{\boldsymbol{c}} = K \cap K'$. Then, there exists $\phi_{\boldsymbol{c}} \in B_{\boldsymbol{c}}$, such that $\langle \phi_{\boldsymbol{c}} \rangle_{\Omega_{\boldsymbol{c}}} = 0$ and*

$$[\![\phi_{\boldsymbol{c}}(\boldsymbol{x}_{\boldsymbol{c}})]\!]_{\gamma_{\boldsymbol{c}}} = \frac{1}{|K|} + \frac{1}{|K'|} \quad \text{and} \quad \|\phi_{\boldsymbol{c}}\|^2_{0,\Omega_{\boldsymbol{c}}} = \frac{1}{\Sigma_k}\left(\frac{1}{|K|} + \frac{1}{|K'|}\right),$$

where Σ_k is the (k-dependent) constant in the trace inverse estimate in Lemma 2.9.

Proof. Let $\widehat{\kappa} \coloneqq [-1,1] \times [-1,1]$ and let $F_K \colon \widehat{\kappa} \to K$ be an affine, invertible transformation, such that $\ell^K_{k-1}(\boldsymbol{x}_{\boldsymbol{c}}) = 1$, where $\ell^K_{k-1} \coloneqq \ell_{k-1} \circ F_K^{-1}$ is the image of the polynomial ℓ_{k-1} defined in Lemma 2.9. Similarly, let $\ell^{K'}_{k-1}$ such that $\ell^{K'}_{k-1}(\boldsymbol{x}_{\boldsymbol{c}}) = 1$. Then, we define

$$\phi_{\boldsymbol{c}} \coloneqq \begin{cases} \frac{1}{|K|}\ell^K_{k-1} & \text{, in } K, \\ -\frac{1}{|K'|}\ell^{K'}_{k-1} & \text{, in } K', \\ 0 & \text{elsewhere.} \end{cases}$$

The jump condition follows directly. The average freeness of $\phi_{\boldsymbol{c}}$ follows using the properties of affine transformations and ℓ_{k-1} on the reference cell, that is,

$$\int_{\Omega_{\boldsymbol{c}}} \phi_{\boldsymbol{c}} = \left\langle \ell^K_{k-1} \right\rangle_K - \left\langle \ell^{K'}_{k-1} \right\rangle_{K'} = \langle \ell_{k-1} \rangle_{\widehat{\kappa}} - \langle \ell_{k-1} \rangle_{\widehat{\kappa}} = 0.$$

Similarly, again using properties of ℓ_{k-1}, the norm satisfies

$$\begin{aligned} \|\phi_{\boldsymbol{c}}\|^2_{0,\Omega_{\boldsymbol{c}}} &= \frac{1}{|K|^2}\left\|\ell^K_{k-1}\right\|^2_{0,K} + \frac{1}{|K'|^2}\left\|\ell^{K'}_{k-1}\right\|^2_{0,K'} \\ &= \frac{1}{4|K|}\|\ell_{k-1}\|^2_{0,\widehat{\kappa}} + \frac{1}{4|K'|}\|\ell_{k-1}\|^2_{0,\widehat{\kappa}} = \frac{1}{\Sigma_k}\left(\frac{1}{|K|} + \frac{1}{|K'|}\right), \end{aligned}$$

where Σ_k is the (k-dependent) trace constant from Lemma 2.9. □

In order to remove the jumps across $\gamma_{\boldsymbol{c}}\,(\boldsymbol{c} \in \mathcal{C})$, we define $\Pi_G \colon M_{\mathcal{P}} \to G$ by

$$\Pi_G q \coloneqq q - \sum_{\boldsymbol{c} \in \mathcal{C}} \frac{[\![q(\boldsymbol{x}_{\boldsymbol{c}})]\!]_{\gamma_{\boldsymbol{c}}}}{[\![\phi_{\boldsymbol{c}}(\boldsymbol{x}_{\boldsymbol{c}})]\!]_{\gamma_{\boldsymbol{c}}}} \phi_{\boldsymbol{c}}\,, \tag{3.10}$$

where $\phi_{\boldsymbol{c}}$ (for $\boldsymbol{c} \in \mathcal{C}$) is the function constructed in Lemma 3.6. Using this definition we are now in the position to formulate the equivalence that motivates the stabilisation term and allows us to propose a new stabilised method.

Lemma 3.7. *Let Π_G be the projection defined by* (3.10)*. Then, all $q \in M_{\mathcal{P}}$ satisfy*

$$\frac{1}{6}\|q - \Pi_G q\|^2_{0,\Omega} < \frac{1}{k^3} \sum_{\boldsymbol{c} \in \mathcal{C}} \frac{|K||K'|}{|K \cup K'|} [\![q(\boldsymbol{x}_{\boldsymbol{c}})]\!]^2_{\gamma_{\boldsymbol{c}}} \leq \|q - \Pi_G q\|^2_{0,\Omega}\,. \tag{3.11}$$

Proof. Our mesh assumptions imply that different sets $\Omega_{\boldsymbol{c}}$ ($\boldsymbol{c} \in \mathcal{C}$) are disjoint. Then, since $\operatorname{supp} \phi_{\boldsymbol{c}} \subseteq \Omega_{\boldsymbol{c}}$, definition (3.10) and the properties of $\phi_{\boldsymbol{c}}$ imply

$$\|q - \Pi_G q\|_{0,\Omega}^2 = \sum_{\boldsymbol{c}\in\mathcal{C}} \frac{[\![q(\boldsymbol{x}_{\boldsymbol{c}})]\!]_{\gamma_{\boldsymbol{c}}}^2}{[\![\phi_{\boldsymbol{c}}(\boldsymbol{x}_{\boldsymbol{c}})]\!]_{\gamma_{\boldsymbol{c}}}^2} \|\phi_{\boldsymbol{c}}\|_{0,\Omega_{\boldsymbol{c}}}^2 = \frac{1}{\Sigma_k} \sum_{\boldsymbol{c}\in\mathcal{C}} \frac{|K||K'|}{|K \cup K'|} [\![q(\boldsymbol{x}_{\boldsymbol{c}})]\!]_{\gamma_{\boldsymbol{c}}}^2 . \tag{3.12}$$

Then, multiplying (3.12) through by Σ_k/k^3, which by Lemma 2.9 belongs to the interval $(1/6, 1]$, finishes the proof. □

Remark 3.8. *The number of jumps is* $\operatorname{card}(\mathcal{C})$ *for both Theorem 3.3 and Lemma 3.7. This is the minimal dimension we have to remove from* $M_{\mathcal{P}}$ *to be uniformly stable. On the other hand, since* Π_G *is not the* $L^2(\Omega)$ *projection onto* G*, we have* $\|p - \Pi_G p\|_{0,\Omega} \neq \inf_{q\in G} \|p - q\|_{0,\Omega}$*. Nevertheless, the pair* $\boldsymbol{V}_{\mathcal{P}} \times G$ *has optimal approximation properties, both in terms of geometry and polynomial degree* k*, as we will see later. Additionally, applying trace inequality Lemma 2.9 and* (CS_2) *to* (3.12) *we obtain the continuity property* $\|q - \Pi_G q\|_{0,\Omega} \leq \|q\|_{0,\Omega}$ *for all* $q \in M_{\mathcal{P}}$*.*

3.3. The stabilised method

We start this section by presenting a new stabilised method. It is motivated by Lemma 3.5 and Lemma 3.7.

Seek $(\boldsymbol{u}_{\mathcal{P}}, p_{\mathcal{P}}) \in \boldsymbol{V}_{\mathcal{P}} \times M_{\mathcal{P}}$ *such that*

$$\mathfrak{B}_s(\boldsymbol{u}_{\mathcal{P}}, p_{\mathcal{P}}; \boldsymbol{v}, q) = (\boldsymbol{f}, q)_\Omega \quad \text{for all} \quad (\boldsymbol{v}, q) \in \boldsymbol{V}_{\mathcal{P}} \times M_{\mathcal{P}} \tag{3.13a}$$

where

$$\mathfrak{B}_s(\boldsymbol{u}, p; \boldsymbol{v}, q) \coloneqq \mathfrak{B}(\boldsymbol{u}, p; \boldsymbol{v}, q) - s_p(p, q) \tag{3.13b}$$

with bilinear form $\mathfrak{B}$ *from* (3.2b) *and*

$$s_p(p, q) \coloneqq \frac{1}{k^3} \sum_{\boldsymbol{c}\in\mathcal{C}} \frac{|K||K'|}{|K \cup K'|} [\![p(\boldsymbol{x}_{\boldsymbol{c}})]\!]_{\gamma_{\boldsymbol{c}}} [\![q(\boldsymbol{x}_{\boldsymbol{c}})]\!]_{\gamma_{\boldsymbol{c}}} . \tag{3.13c}$$

For each corner patch we recall that the edge $\gamma_{\boldsymbol{c}}$ separates a small from a large cell.

Remark 3.9. *Alternatively to method* (3.13a) *we may impose the constraints strongly and approximate in* $\boldsymbol{V}_{\mathcal{P}} \times G$*. In terms of pressure accuracy, the mixed method using* $\boldsymbol{V}_{\mathcal{P}} \times G$ *would converge at least as fast as the stabilised method for* $\boldsymbol{V}_{\mathcal{P}} \times M_{\mathcal{P}}$*, which*

follows from Π_G *being surjective,* (3.13c) *and* (3.11)*. More precisely, we get*

$$\begin{aligned}\inf_{q_G\in G}\|p-q_G\|_{0,\Omega} &= \inf_{q\in M_\mathcal{P}}\|p-\Pi_G q\|_{0,\Omega}\\ &\le \inf_{q\in M_\mathcal{P}}\|p-q\|_{0,\Omega}+\|q-\Pi_G q\|_{0,\Omega}\\ &\le \inf_{q\in M_\mathcal{P}}\|p-q\|_{0,\Omega}+\sqrt{6s_p(q,q)}\,.\end{aligned}$$

Remark 3.10. *From the implementation point of view, the bilinear form* s_p*, defined in* (3.13c)*, can be seen as an one-point quadrature approximation of the more usual jump term* $(\llbracket p_\mathcal{P}\rrbracket,\llbracket q_\mathcal{P}\rrbracket)_{\gamma_\boldsymbol{c}}$*. This approximation is exact for locally constant functions, that is, for* $k=1$ *we may write the stabilisation term as*

$$s_p(p,q)=\sum_{\boldsymbol{c}\in\mathcal{C}}\frac{|K||K'|}{|K\cup K'|}\frac{1}{|\gamma_\boldsymbol{c}|}\int_{\gamma_\boldsymbol{c}}\llbracket p\rrbracket\llbracket q\rrbracket\,\mathrm{d}s\,.$$

Remark 3.11. *It is worth mentioning that the knowledge of the geometry of the mesh fully suffices to define* $G\subset M_\mathcal{P}$ *and the stabilisation term* s_p (3.13c)*. Therefore, after selecting edges as described in Section 3.2, penalising certain jumps is easy to implement and automatically identifies spurious pressure modes within the basis of* $M_\mathcal{P}$*.*

3.3.1. Stability and a priori estimates

This section is devoted to study the existence, uniqueness and convergence of discrete solutions $(\boldsymbol{u}_\mathcal{P},p_\mathcal{P})\in\boldsymbol{V}_\mathcal{P}\times M_\mathcal{P}$. We state stability and a priori estimates for method (3.13a) with respect to the norm given by

$$|||(\boldsymbol{v},q)|||^2 \coloneqq |\boldsymbol{v}|_{1,\Omega}^2+\|q\|_{0,\Omega}^2\,. \tag{3.14}$$

The proof of the following stability result is fairly similar to, for instance, the one of [BDG06, Theorem 4.1].

Theorem 3.12. *There exists* $\mu_s=C\beta_G^2>0$*, with* $C>0$ *independent of mesh properties and polynomial degree, such that all* $(\boldsymbol{w},r)\in\boldsymbol{V}_\mathcal{P}\times M_\mathcal{P}$ *satisfy*

$$\sup_{(\boldsymbol{v},q)\in\boldsymbol{V}_\mathcal{P}\times M_\mathcal{P}\setminus\{0\}}\frac{\mathfrak{B}_s(\boldsymbol{w},r;\boldsymbol{v},q)}{|||(\boldsymbol{v},q)|||}\ge\mu_s|||(\boldsymbol{w},r)|||\,. \tag{3.15}$$

Consequently, Problem (3.13a) *has a unique solution* $(\boldsymbol{u}_\mathcal{P},p_\mathcal{P})\in\boldsymbol{V}_\mathcal{P}\times M_\mathcal{P}$*.*

Proof. Let $(\boldsymbol{w},r)\in\boldsymbol{V}_\mathcal{P}\times M_\mathcal{P}$ be given. In terms of this pair we construct a suitable pair $(\boldsymbol{v},q)\in\boldsymbol{V}_\mathcal{P}\times M_\mathcal{P}$. First, the definition of $\mathfrak{B}_s$ by (3.13b) gives

$$\mathfrak{B}_s(\boldsymbol{w},r;\boldsymbol{w},-r)=|\boldsymbol{w}|_{1,\Omega}^2+s_p(r,r)\,. \tag{3.16}$$

Additionally, using (CS_1) and (Young) with $\varepsilon \coloneqq 2/(1+\beta_G^2)$ all $\boldsymbol{w}_\delta \in \boldsymbol{V}_{\mathcal{P}}$ satisfy

$$\begin{aligned}\mathfrak{B}_s(\boldsymbol{w}, r; -\boldsymbol{w}_\delta, 0) &= -(\nabla \boldsymbol{w}, \nabla \boldsymbol{w}_\delta)_\Omega + (\operatorname{div} \boldsymbol{w}_\delta, r)_\Omega \\ &\geq -\frac{1}{1+\beta_G^2}|\boldsymbol{w}|_{1,\Omega}^2 - \frac{1+\beta_G^2}{4}|\boldsymbol{w}_\delta|_{1,\Omega}^2 + (\operatorname{div} \boldsymbol{w}_\delta, r)_\Omega. \end{aligned} \tag{3.17}$$

Next, we choose a particular $\boldsymbol{w}_\delta$. By Lemma 3.5 there exists $\boldsymbol{z} \in \boldsymbol{V}_{\mathcal{P}}$ with $|\boldsymbol{z}|_{1,\Omega} = 1$, such that

$$(\operatorname{div} \boldsymbol{z}, r)_\Omega \geq \beta_G \|\Pi_G r\|_{0,\Omega} - \|r - \Pi_G r\|_{0,\Omega} \geq \beta_G \|r\|_{0,\Omega} - (1+\beta_G)\|r - \Pi_G r\|_{0,\Omega}.$$

Hence, inserting $\boldsymbol{w}_\delta \coloneqq \delta \|r\|_{0,\Omega} \boldsymbol{z}$, with $\delta > 0$ to be chosen, followed by applying (3.11), (3.13c), and $ab \leq a^2/4 + b^2$ gives

$$\begin{aligned}(\operatorname{div} \boldsymbol{w}_\delta, r) &\geq \delta\beta_G \|r\|_{0,\Omega}^2 - (1+\beta_G)\delta \|r\|_{0,\Omega} C_1^{-1/2} s_p(r,r)^{1/2} \\ &\geq \delta\beta_G \|r\|_{0,\Omega}^2 - \frac{(1+\beta_G)^2\delta^2}{4C_1}\|r\|_{0,\Omega}^2 - s_p(r,r)\,, \end{aligned}$$

where $C_1 = 1/6$. Now, let $(\boldsymbol{v}, q) \coloneqq (\boldsymbol{w} - \boldsymbol{w}_\delta, r)$. Then, $|\boldsymbol{w}_\delta|_{1,\Omega} = \delta\|r\|_{0,\Omega}$, (3.16), (3.17), and this lower bound yield

$$\begin{aligned}\mathfrak{B}_s(\boldsymbol{w}, r; \boldsymbol{v}, q) &\geq \frac{\beta_G^2}{1+\beta_G^2}|\boldsymbol{w}|_{1,\Omega}^2 + \left(\delta\beta_G - \frac{(1+\beta_G)^2\delta^2}{4C_1}\right)\|r\|_{0,\Omega}^2 - \frac{1+\beta_G^2}{4}\delta^2\|r\|_{0,\Omega}^2 \\ &\geq \frac{\beta_G^2}{1+\beta_G^2}|\boldsymbol{w}|_{1,\Omega}^2 + \left(\delta\beta_G - \delta^2\frac{1}{\min\{1, C_1\}}\frac{1+\beta_G+\beta_G^2}{2}\right)\|r\|_{0,\Omega}^2 \\ &\geq \frac{\delta\beta_G}{2}\Big(|\boldsymbol{w}|_{1,\Omega}^2 + \|r\|_{0,\Omega}^2\Big) = \frac{\delta\beta_G}{2}|||(\boldsymbol{w}, r)|||^2 \end{aligned}$$

where we chose $\delta \coloneqq \min\{1, C_1\}\beta_G/(1+\beta_G+\beta_G^2)$ to obtain the last estimate.

Finally, using the definition of $\boldsymbol{w}_\delta$, (3.14) and the triangle inequality we get

$$|||(\boldsymbol{v}, q)||| \leq |||(\boldsymbol{w}, r)||| + |\boldsymbol{w}_\delta|_{1,\Omega} \leq |||(\boldsymbol{w}, r)||| + \delta\|r\|_{0,\Omega} \leq (1+\delta)|||(\boldsymbol{w}, r)|||\,,$$

which proves (3.15) with $\mu_s \geq \delta\beta_G/(2+2\delta) = C\beta_G^2$. □

The following bounds will simplify the a priori estimate later on.

Lemma 3.13. *Let $q_{\mathcal{P}} \in M_{\mathcal{P}}$ and $p \in H^1(\Omega)$. Then, the stabilisation term is bounded as follows*

$$s_p(q_{\mathcal{P}}, q_{\mathcal{P}}) \leq \begin{cases} \|q_{\mathcal{P}}\|_{0,\Omega}^2\,, \\ Ck^{-2}\sum_{\boldsymbol{c}\in\mathcal{C}}\left(\|p - q_{\mathcal{P}}\|_{0,K\cup K'}^2 + |\gamma_{\boldsymbol{c}}|^2\big\|\partial(p-q_{\mathcal{P}})/\partial\tilde{t}_{\boldsymbol{c}}\big\|_{0,K\cup K'}^2\right), \end{cases} \tag{3.18}$$

where $\tilde{\boldsymbol{t}}_{\boldsymbol{c}}$ is evaluated element-wise as the tangential vector of the neighbouring edge of $\gamma_{\boldsymbol{c}}$ inside K and K', respectively, and C is a constant independent of mesh properties and polynomial degree k.

Proof. We first note that $\gamma_{\boldsymbol{c}} = K \cap K'$ for all $\boldsymbol{c} \in \mathcal{C}$. Then, using definition (3.13c), the trace estimate (2.14), and (CS_2), we get

$$s_p(q_{\mathcal{P}}, q_{\mathcal{P}}) = \frac{1}{k^3} \sum_{\boldsymbol{c}\in\mathcal{C}} \frac{|K||K'|}{|K \cup K'|} \left| q_{\mathcal{P}}|_K(\boldsymbol{x}_{\boldsymbol{c}}) - q_{\mathcal{P}}|_{K'}(\boldsymbol{x}_{\boldsymbol{c}}) \right|^2 \\ \leq \sum_{\boldsymbol{c}\in\mathcal{C}} \frac{|K||K'|}{|K \cup K'|} \left(\frac{1}{|K|} + \frac{1}{|K'|} \right) \|q_{\mathcal{P}}\|^2_{0,K\cup K'} \leq \|q_{\mathcal{P}}\|^2_{0,\Omega} \,,$$

where the last estimate follows using that the corner patches are non-overlapping. This proves $(3.18)_1$. Similarly, since $[\![q_{\mathcal{P}}]\!]_{\gamma_{\boldsymbol{c}}} \in \mathbb{P}_{k-1}(\gamma_{\boldsymbol{c}})$, we apply (2.10) to get

$$s_p(q_{\mathcal{P}}, q_{\mathcal{P}}) = \frac{1}{k^3} \sum_{\boldsymbol{c}\in\mathcal{C}} \frac{|K||K'|}{|K \cup K'|} [\![q_{\mathcal{P}}(\boldsymbol{x}_{\boldsymbol{c}})]\!]^2_{\gamma_{\boldsymbol{c}}} \leq \frac{1}{k^2} \sum_{\boldsymbol{c}\in\mathcal{C}} \frac{|K||K'|}{|K \cup K'|} |\gamma_{\boldsymbol{c}}|^{-1} \|[\![q_{\mathcal{P}}]\!]\|^2_{0,\gamma_{\boldsymbol{c}}} \,.$$

Using the regularity of $p \in H^1(\Omega)$, that is, $[\![p]\!]_e = 0$ a.e. in Ω, we insert p, apply trace estimate (2.3a) and $\frac{|K||K'|}{|K\cup K'|} \leq \min\{|K|, |K'|\} \leq C|\gamma_{\boldsymbol{c}}|^2$, to obtain

$$\begin{aligned} s_p(q_{\mathcal{P}}, q_{\mathcal{P}}) &\leq k^{-2} \sum_{\boldsymbol{c}\in\mathcal{C}} \frac{\min\{|K|, |K'|\}}{|\gamma_{\boldsymbol{c}}|} \|[\![p - q_{\mathcal{P}}]\!]\|^2_{0,\gamma_{\boldsymbol{c}}} \\ &\leq Ck^{-2} \sum_{\boldsymbol{c}\in\mathcal{C}} \sum_{\omega\in\{K,K'\}} \left(\|p - q_{\mathcal{P}}\|^2_{0,\omega} + |\gamma_{\boldsymbol{c}}| \, \|p - q_{\mathcal{P}}\|_{0,\omega} \big\|\partial(p - q_{\mathcal{P}})/\partial\tilde{t}_{\boldsymbol{c}}\big\|_{0,\omega} \right) \\ &\leq Ck^{-2} \sum_{\boldsymbol{c}\in\mathcal{C}} \|p - q_{\mathcal{P}}\|^2_{0,K\cup K'} + |\gamma_{\boldsymbol{c}}|^2 \big\|\partial(p - q_{\mathcal{P}})/\partial\tilde{t}_{\boldsymbol{c}}\big\|^2_{0,K\cup K'} \,, \end{aligned}$$

which finishes the proof. □

We end this section with the main a priori error bound for the method.

Theorem 3.14. *Let $(\boldsymbol{u}, p) \in \boldsymbol{V} \times M$ be the solution of Problem* (3.2a) *with $p \in H^1(\Omega)$, and $(\boldsymbol{u}_{\mathcal{P}}, p_{\mathcal{P}}) \in \boldsymbol{V}_{\mathcal{P}} \times M_{\mathcal{P}}$ be the solution of* (3.13a)*. Then*

$$|\boldsymbol{u} - \boldsymbol{u}_{\mathcal{P}}|_{1,\Omega} + \|p - p_{\mathcal{P}}\|_{0,\Omega} \leq \frac{C}{\mu_s} \inf_{(\boldsymbol{v}_{\mathcal{P}}, q_{\mathcal{P}})\in\boldsymbol{V}_{\mathcal{P}}\times M_{\mathcal{P}}} \Big\{ |\boldsymbol{u} - \boldsymbol{v}_{\mathcal{P}}|_{1,\Omega} + \|p - q_{\mathcal{P}}\|_{0,\Omega} \\ + \Big(k^{-2} \sum_{\boldsymbol{c}\in\mathcal{C}} |\gamma_{\boldsymbol{c}}|^2 \big\|\partial(p - q_{\mathcal{P}})/\partial\tilde{t}_{\boldsymbol{c}}\big\|^2_{0,K\cup K'} \Big)^{1/2} \Big\} \,,$$

where C is a constant independent of mesh properties and the polynomial degree, and $\tilde{\boldsymbol{t}}_{\boldsymbol{c}}$ is defined in Lemma 3.13.

Proof. We use standard arguments. For an arbitrary pair $(\boldsymbol{v}_{\mathcal{P}}, q_{\mathcal{P}}) \in \boldsymbol{V}_{\mathcal{P}} \times M_{\mathcal{P}}$ the triangle inequality gives

$$|||(\boldsymbol{u} - \boldsymbol{u}_{\mathcal{P}}, p - p_{\mathcal{P}})||| \leq |||(\boldsymbol{u} - \boldsymbol{v}_{\mathcal{P}}, p - q_{\mathcal{P}})||| + |||(\boldsymbol{\xi}_v, \xi_p)||| \,, \tag{3.19}$$

where $\boldsymbol{\xi}_v \coloneqq \boldsymbol{u}_\mathcal{P} - \boldsymbol{v}_\mathcal{P}$ and $\xi_p \coloneqq p_\mathcal{P} - q_\mathcal{P}$ are discrete errors. Our aim is to bound them. To do so, we prepare a useful identity. A direct computation using $\boldsymbol{V}_\mathcal{P} \subset \boldsymbol{V}$, and the definitions of methods (3.2a) and (3.13a), shows

$$\mathfrak{B}(\boldsymbol{u}, p; \boldsymbol{w}_\mathcal{P}, r_\mathcal{P}) = \mathfrak{B}_s(\boldsymbol{u}_\mathcal{P}, p_\mathcal{P}; \boldsymbol{w}_\mathcal{P}, r_\mathcal{P}) \quad \text{for all} \quad (\boldsymbol{w}_\mathcal{P}, r_\mathcal{P}) \in \boldsymbol{V}_\mathcal{P} \times M_\mathcal{P}\,,$$

which together with the linearity of $\mathfrak{B}_s$ and $\mathfrak{B}$ implies

$$\begin{aligned}\mathfrak{B}_s(\boldsymbol{\xi}_v, \xi_p; \boldsymbol{w}_\mathcal{P}, r_\mathcal{P}) &= \mathfrak{B}_s(\boldsymbol{u}_\mathcal{P}, p_\mathcal{P}; \boldsymbol{w}_\mathcal{P}, r_\mathcal{P}) - \mathfrak{B}(\boldsymbol{v}_\mathcal{P}, q_\mathcal{P}; \boldsymbol{w}_\mathcal{P}, r_\mathcal{P}) + s_p(q_\mathcal{P}, r_\mathcal{P}) \\ &= \mathfrak{B}(\boldsymbol{u} - \boldsymbol{v}_\mathcal{P}, p - q_\mathcal{P}; \boldsymbol{w}_\mathcal{P}, r_\mathcal{P}) + s_p(q_\mathcal{P}, r_\mathcal{P})\,,\end{aligned}$$

for all $(\boldsymbol{w}_\mathcal{P}, r_\mathcal{P}) \in \boldsymbol{V}_\mathcal{P} \times M_\mathcal{P}$.

Now, by Theorem 3.12, there exists a pair $(\tilde{\boldsymbol{w}}_\mathcal{P}, \tilde{r}_\mathcal{P}) \in \boldsymbol{V}_\mathcal{P} \times M_\mathcal{P}$ with $|||(\tilde{\boldsymbol{w}}_\mathcal{P}, \tilde{r}_\mathcal{P})||| = 1$, such that

$$\begin{aligned}\mu_s |||(\boldsymbol{\xi}_v, \xi_p)||| &\le \mathfrak{B}_s(\boldsymbol{\xi}_v, \xi_p; \tilde{\boldsymbol{w}}_\mathcal{P}, \tilde{r}_\mathcal{P}) \\ &= \mathfrak{B}(\boldsymbol{u} - \boldsymbol{v}_\mathcal{P}, p - q_\mathcal{P}; \tilde{\boldsymbol{w}}_\mathcal{P}, \tilde{r}_\mathcal{P}) + s_p(q_\mathcal{P}, \tilde{r}_\mathcal{P}) \\ &\le C|||(\boldsymbol{u} - \boldsymbol{v}_\mathcal{P}, p - q_\mathcal{P})||| + \sqrt{s_p(q_\mathcal{P}, q_\mathcal{P})}\sqrt{s_p(\tilde{r}_\mathcal{P}, \tilde{r}_\mathcal{P})}\,, \qquad (3.20)\end{aligned}$$

where we have used the continuity of $\mathfrak{B}$ with respect to $|||\cdot|||$, and (CS_1) to bound s_p. Now, inserting (3.20) into (3.19) and applying $(3.18)_1$ and $\|\tilde{r}_\mathcal{P}\|_{0,\Omega} \le 1$, we get

$$|||(\boldsymbol{u} - \boldsymbol{u}_\mathcal{P}, p - p_\mathcal{P})||| \le (1 + \mu_s^{-1} C)\Big(|||(\boldsymbol{u} - \boldsymbol{v}_\mathcal{P}, p - q_\mathcal{P})||| + \sqrt{s_p(q_\mathcal{P}, q_\mathcal{P})}\Big)\,.$$

Finally, applying the equivalence of $|\boldsymbol{v}|_{1,\Omega} + \|q\|_{0,\Omega}$ and $|||(\boldsymbol{v}, q)|||$, as well as, part two of (3.18) gives

$$\begin{aligned}|\boldsymbol{u} - \boldsymbol{u}_\mathcal{P}|_{1,\Omega} + \|p - p_\mathcal{P}\|_{0,\Omega} \le C\mu_s^{-1}\Big\{&|\boldsymbol{u} - \boldsymbol{v}_\mathcal{P}|_{1,\Omega} + \|p - q_\mathcal{P}\|_{0,\Omega} \\ &+ \Big(\frac{1}{k^2}\sum_{\boldsymbol{c}\in\mathcal{C}} |\gamma_{\boldsymbol{c}}|^2 \big\|\partial(p - q_\mathcal{P})/\partial\tilde{t}_{\boldsymbol{c}}\big\|^2_{0,K\cup K'}\Big)^{1/2}\Big\}\,,\end{aligned}$$

which finishes the proof, as the pair $(\boldsymbol{v}_\mathcal{P}, q_\mathcal{P})$ was arbitrary. □

3.4. Numerical evidence

In this section we present numerical evidence that confirms the theoretical results obtained so far. For this, we recall the (aspect) ratio $\varrho \coloneqq \min_{\boldsymbol{c}\in\mathcal{C}} h_{\boldsymbol{c}}/H_{\boldsymbol{c}}$, and for quick reference, the LBB constants $\beta_\mathcal{P}$ from (3.4) and β_G from Theorem 3.3, as well as the stability constant μ_s from (3.15). All experiments are performed on meshes shown in Figures 3.1 and 3.2 with $h_{\boldsymbol{c}} + H_{\boldsymbol{c}} = 1$. The edges embraced by the jump symbol $[\![\cdot]\!]$ were chosen as $\gamma_{\boldsymbol{c}}\,(\boldsymbol{c} \in \mathcal{C})$.

The implementation of the finite element methods was done in MatLab. And, eigenvalue problems posed in Corollary 4.7 and Lemma 4.8 (see Chapter 4) were used to calculate the stability constant μ_s and to compute $\beta_{\mathcal{P}}$ and β_G, respectively.

The numerical evidence confirms the following points.

- One (appropriate) constraint suffices to obtain an LBB constant β_G independent of ϱ on either of the corner patches shown in Figure 3.2. On the T-mesh (Figure 3.1), six constraints are sufficient. All this is confirmed by Figure 3.3, which depicts β_G and $\beta_{\mathcal{P}}$ for $k = 1$ (left) and $k = 4$ (right).

- Figure 3.4 shows the behaviour of the squared LBB constants $\beta_{\mathcal{P}}$ and β_G, as well as the stability constant μ_s on the T-mesh for various ϱ and k. This confirms that the stability constant μ_s in (3.15) behaves like β_G^2.

- Another confirmation that $\mu_s = C\beta_G^2$ is shown in Figure 3.5 for a fixed aspect ratio $\varrho = 10^{-5}$ and various polynomial degrees k. This also confirms that both μ_s and the error constant in Theorem 3.14 are independent of the (aspect) ratio $h_{\boldsymbol{c}}/H_{\boldsymbol{c}}$.

- It is necessary to choose an edge $\gamma_{\boldsymbol{c}} \subset \partial\omega_{\boldsymbol{c}} \cap \partial(\Omega_{\boldsymbol{c}} \setminus \omega_{\boldsymbol{c}})$. If this is not done, then there is virtually no improvement of β_G over $\beta_{\mathcal{P}}$. To illustrate, we have chosen the edge labelled in Figure 3.6 (left, $e \not\subset \partial\omega_{\boldsymbol{c}} \cap \partial(\Omega_{\boldsymbol{c}} \setminus \omega_{\boldsymbol{c}})$), and then Figure 3.6 (right) compares the obtained "β_G" to the possible improvement.

In summary, we have observed that $\beta_{\mathcal{P}}$ behaves as predicted by (3.4) and [AC00, Lemma 4.6], respectively. That is, $\beta_{\mathcal{P}} \to 0$ as $\varrho \to 0$, and $\beta_{\mathcal{P}}$ grows with k until $k\sqrt{\varrho} \approx 1$. More importantly, our β_G is, as predicted, independent of ϱ and mostly (despite a decay in k) much larger than $\beta_{\mathcal{P}}$.

$\mathcal{P}$	$k=1$	$k=4$
Figure 3.2a	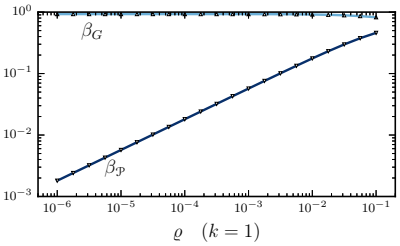	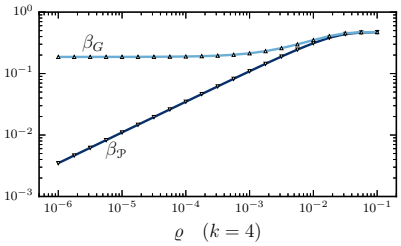
Figure 3.2b	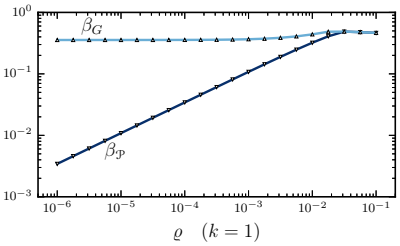	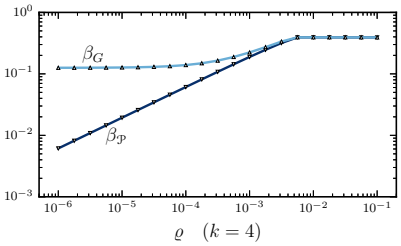
Figure 3.2c	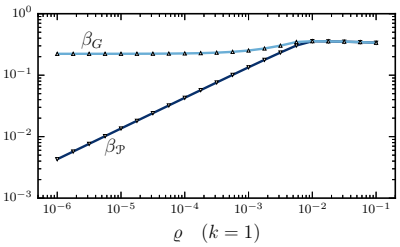	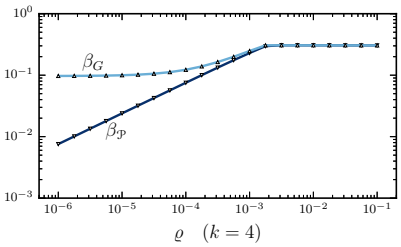
Figure 3.2d	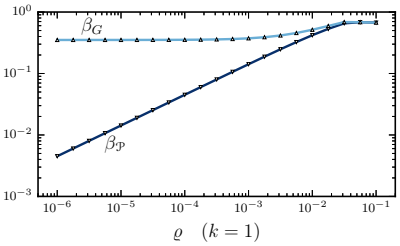	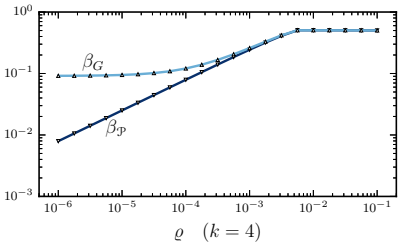
T-mesh of Figure 3.1	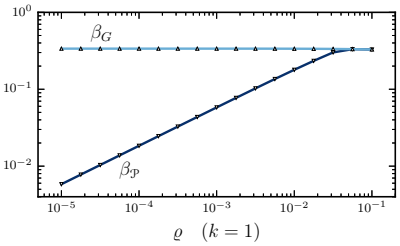	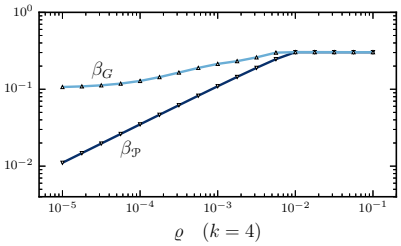

Fig. 3.3. LBB constants $\beta_{\mathcal{P}}$ and β_G vs ϱ on corner patches and the T-mesh.

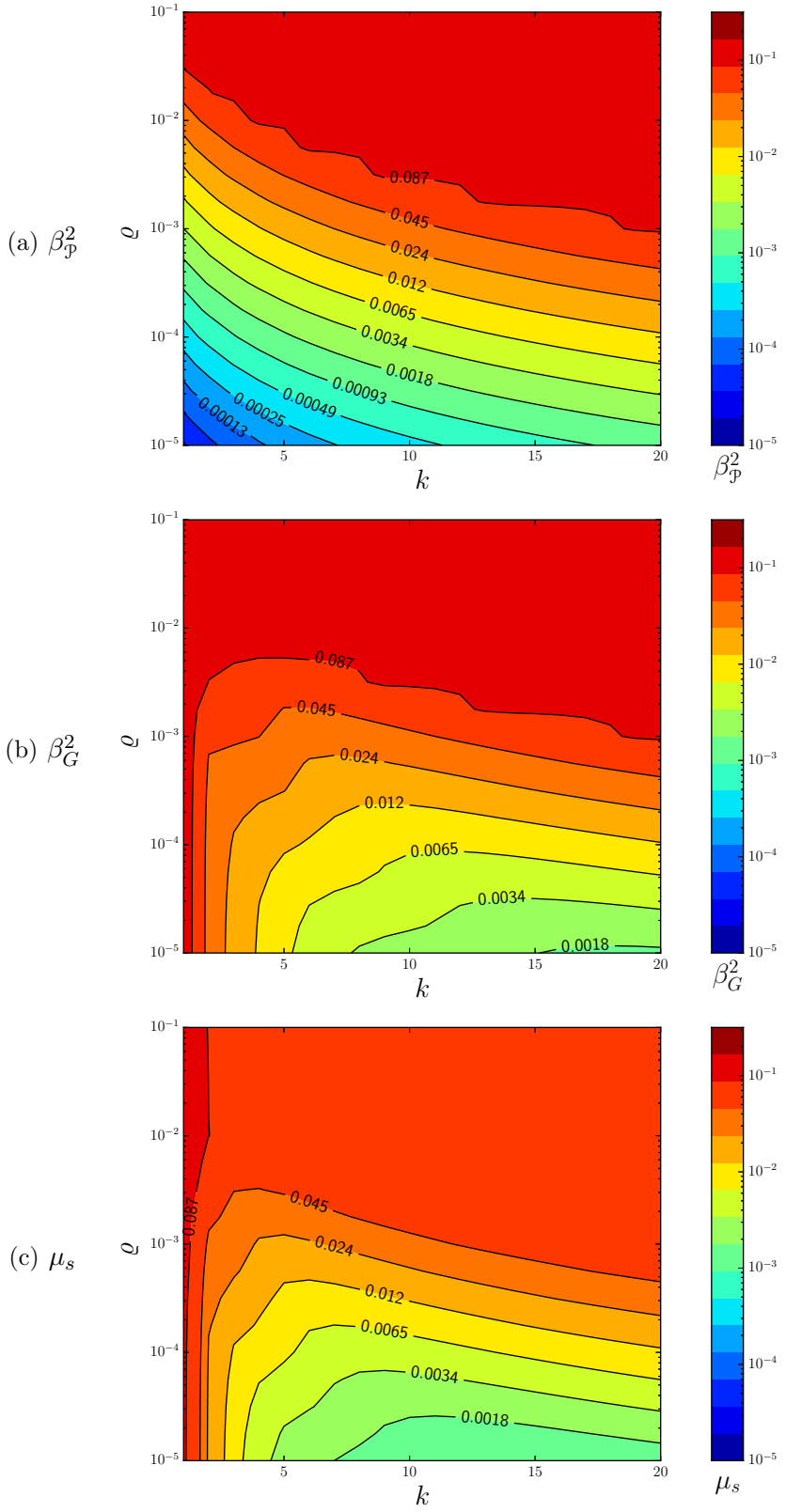

Fig. 3.4. LBB consants $\beta^2_{\mathcal{P}}$, β^2_G and stability constant μ_s vs. ϱ and k on T-mesh.

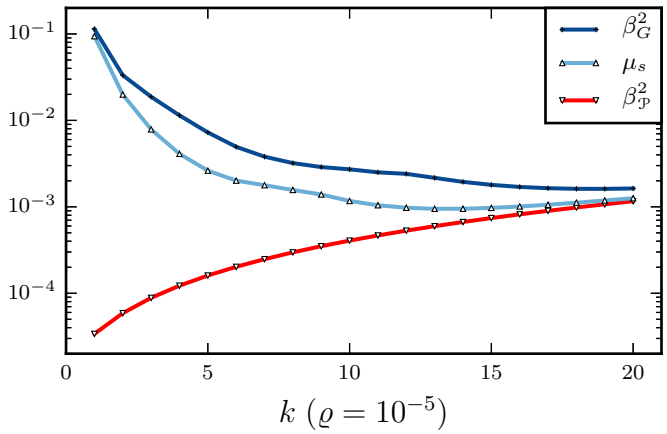

Fig. 3.5. Stability constant $\mu_s = C\beta_G^2$ (Theorem 3.12) on T-Mesh (Figure 3.1).

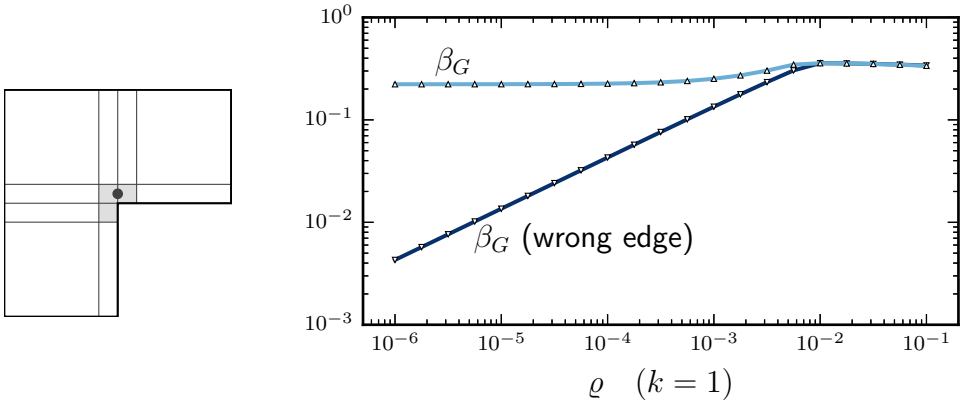

Fig. 3.6. LBB constant β_G is independent of ϱ, only for edges $e \subset \partial\omega_{\boldsymbol{c}} \cap \partial(\Omega_{\boldsymbol{c}} \setminus \omega_{\boldsymbol{c}})$.

3.5. Uniformly inf-sup stable sub-spaces

This section contains the theoretical justification of Theorem 3.3 in Section 3.2.1. That is, we prove that the pair $\boldsymbol{V}_{\mathcal{P}} \times G$ is uniformly inf-sup stable. The proof is split into the following parts. We first present known LBB conditions for partitions consisting of shape-regular parts and edge patches. These allow us to prove local uniform inf-sup conditions by constraining averages, in particular, Corollary 3.15 which generalises inf-sup condition (3.6) and [AC00, Lemma 4.3], respectively. This corollary also confirms the reduced number of spurious pressure modes. After that, we replace the average constraints by jump constraints, to prove a local inf-sup condition for the pair $\boldsymbol{V}_{\mathcal{P}} \times G$. We end this section with the proof of Theorem 3.3.

Let $\mathcal{P}_{sr}$ be a shape-regular partition of ω. Then, the pair $\boldsymbol{Q}_k^c \times \mathbb{P}_{k-1} (\subset \boldsymbol{V}_{\mathcal{P}_{sr}} \times M_{\mathcal{P}_{sr}})$ is inf-sup stable on shape-regular meshes, see [BM99, Proposition 4.1]. Hence, for all $q \in M_{\mathcal{P}_{sr}}$ there exists $\boldsymbol{v} \in \boldsymbol{V}_{\mathcal{P}_{sr}}$ such that

$$(\operatorname{div} \boldsymbol{v}, q)_\omega = \|q\|_{0,\omega}^2 \quad \text{and} \quad |\boldsymbol{v}|_{1,\omega} \leq C \|q\|_{0,\omega} \,, \tag{3.21}$$

with a constant C independent of mesh properties and polynomial degree k.

Let $\mathcal{P}_E$ be a partition of ω containing shape-regular parts and edge patches. Then, by [AC00, Theorem 4.7] the pair $\boldsymbol{V}_{\mathcal{P}_E} \times M_{\mathcal{P}_E}$ is uniformly inf-sup stable, that is, for all $q \in M_{\mathcal{P}_E}$ there exists a $\boldsymbol{v} \in \boldsymbol{V}_{\mathcal{P}_E}$ such that

$$(\operatorname{div} \boldsymbol{v}, q)_\omega = \|q\|_{0,\omega}^2 \quad \text{and} \quad |\boldsymbol{v}|_{1,\omega} \leq C k^{1/2} \|q\|_{0,\omega} \,, \tag{3.22}$$

with a constant C independent of mesh properties and polynomial degree k.

In particular, if edge patches are overlapping without creating a finely resolved corner, then (3.22) holds; for instance, in [AC00, Lemma 4.2] the uniform inf-sup condition (3.22) is proved for a single overlapping edge patch, that is, the mesh in Figure 3.7(centre). Then, by [AC00, Theorem 4.7] condition (3.22) holds on the unshaded parts of Figures 3.1 and 3.2.

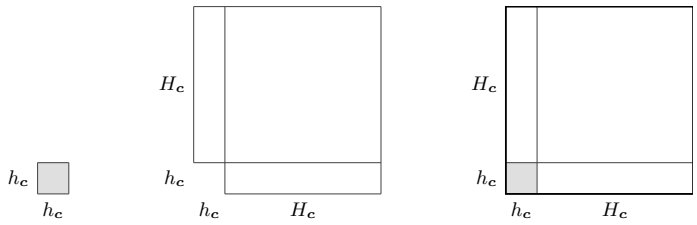

Fig. 3.7. A corner patch decomposed into its regular part and (overlapped) edge patches.

3.5.1. A uniformly inf-sup stable space by average constraints

Hereafter, we derive an orthogonal decomposition of the local pressure space on corner patches. The arguments require local notation. We recall the localized finite element spaces $\boldsymbol{V}_{\mathcal{P}}(\omega)$ and $M_{\mathcal{P}}(\omega)$, defined in Section 3.1.

The following corollary generalises Lemma 3.1 (see also [AC00, Lemma 4.3]). The proof follows the same lines, but is valid for all corner patches shown in Figure 3.2. We include it in an abstract form. The main idea of the proof is to connect uniform inf-sup conditions of the involved finite element spaces on subdomains $\omega_{\boldsymbol{c}}$ and $\Omega_{\boldsymbol{c}} \setminus \omega_{\boldsymbol{c}}$, which are covered by partitions consisting of shape-regular parts and edge patches. Later in this thesis, we will apply this idea to more general situations.

Corollary 3.15. *Let $\Omega_{\boldsymbol{c}} \subseteq \overline{\Omega}$ be one of the corner patches shown in Figure 3.2 with $\omega_{\boldsymbol{c}}$ being the small shaded set. Let*

$$M^{\star}_{\mathcal{P}}(\Omega_{\boldsymbol{c}}) \coloneqq \left\{ q \in M_{\mathcal{P}} \colon \operatorname{supp} q \subseteq \Omega_{\boldsymbol{c}} \text{ and } \langle q \rangle_{\omega_{\boldsymbol{c}}} = 0 \right\}.$$

Then, for all $q \in M^{\star}_{\mathcal{P}}(\Omega_{\boldsymbol{c}})$ there exists $\boldsymbol{v} \in \boldsymbol{V}_{\mathcal{P}}(\Omega_{\boldsymbol{c}})$ such that $\boldsymbol{v}|_{\omega_{\boldsymbol{c}}} \in \boldsymbol{H}^1_0(\omega_{\boldsymbol{c}})$ and

$$(\operatorname{div} \boldsymbol{v}, q)_{\Omega_{\boldsymbol{c}}} = \|q\|^2_{0,\Omega_{\boldsymbol{c}}} \quad \text{and} \quad |\boldsymbol{v}|_{1,\Omega_{\boldsymbol{c}}} \leq C k^{1/2} \|q\|_{0,\Omega_{\boldsymbol{c}}}, \tag{3.23}$$

with a constant C independent of mesh properties and polynomial degree.

Proof. Let $q \in M^{\star}_{\mathcal{P}}(\Omega_{\boldsymbol{c}})$. Then, since $q \in L^2_0(\Omega_{\boldsymbol{c}})$, we have $0 = (q,1)_{\omega_{\boldsymbol{c}}} = -(q,1)_{\Omega_{\boldsymbol{c}} \setminus \omega_{\boldsymbol{c}}}$. Therefore, we may write $q = q_{\boldsymbol{c}} + q_I$ with $q_{\boldsymbol{c}} \in M_{\mathcal{P}}(\omega_{\boldsymbol{c}})$ and $q_I \in M_{\mathcal{P}}(\Omega_{\boldsymbol{c}} \setminus \omega_{\boldsymbol{c}})$. We remark that the partition $\mathcal{P}$ on $\omega_{\boldsymbol{c}}$ consists of a small number of shape-regular cells. Hence, by (3.21) there exists $\boldsymbol{v}_c \in \boldsymbol{V}_{\mathcal{P}}(\omega_{\boldsymbol{c}})$ such that

$$(\operatorname{div} \boldsymbol{v}_{\boldsymbol{c}}, q_{\boldsymbol{c}})_{\omega_{\boldsymbol{c}}} = \|q_{\boldsymbol{c}}\|^2_{0,\omega_{\boldsymbol{c}}} \quad \text{and} \quad |\boldsymbol{v}_{\boldsymbol{c}}|_{1,\omega_{\boldsymbol{c}}} \leq C \|q_{\boldsymbol{c}}\|_{0,\omega_{\boldsymbol{c}}}.$$

Similarly, the partition on $\Omega_{\boldsymbol{c}} \setminus \omega_{\boldsymbol{c}}$ consists of (overlapped) edge patches only and hence, by (3.22), there exists $\boldsymbol{v}_I \in \boldsymbol{V}_{\mathcal{P}}(\Omega_{\boldsymbol{c}} \setminus \omega_{\boldsymbol{c}})$ such that

$$(\operatorname{div} \boldsymbol{v}_I, q_I)_{\Omega_{\boldsymbol{c}} \setminus \omega_{\boldsymbol{c}}} = \|q_I\|^2_{0,\Omega_{\boldsymbol{c}} \setminus \omega_{\boldsymbol{c}}} \quad \text{and} \quad |\boldsymbol{v}_I|_{1,\Omega_{\boldsymbol{c}} \setminus \omega_{\boldsymbol{c}}} \leq C k^{1/2} \|q_I\|_{0,\Omega_{\boldsymbol{c}} \setminus \omega_{\boldsymbol{c}}}.$$

Together, we let $\boldsymbol{v} \coloneqq \boldsymbol{v}_{\boldsymbol{c}} + \boldsymbol{v}_I$ and realise because of disjoint supports that

$$(\operatorname{div} \boldsymbol{v}, q)_{\Omega_{\boldsymbol{c}}} = (\operatorname{div} \boldsymbol{v}_{\boldsymbol{c}}, q_{\boldsymbol{c}})_{\omega_{\boldsymbol{c}}} + (\operatorname{div} \boldsymbol{v}_I, q_I)_{\Omega_{\boldsymbol{c}} \setminus \omega_{\boldsymbol{c}}} = \|q_{\boldsymbol{c}}\|^2_{0,\omega_{\boldsymbol{c}}} + \|q_I\|^2_{0,\Omega_{\boldsymbol{c}} \setminus \omega_{\boldsymbol{c}}} = \|q\|^2_{0,\Omega_{\boldsymbol{c}}},$$

and

$$|\boldsymbol{v}|^2_{1,\Omega_{\boldsymbol{c}}} = |\boldsymbol{v}_{\boldsymbol{c}}|^2_{1,\omega_{\boldsymbol{c}}} + |\boldsymbol{v}_I|^2_{1,\Omega_{\boldsymbol{c}} \setminus \omega_{\boldsymbol{c}}} \leq C \|q_{\boldsymbol{c}}\|^2_{0,\omega_{\boldsymbol{c}}} + C k \|q_I\|^2_{0,\Omega_{\boldsymbol{c}} \setminus \omega_{\boldsymbol{c}}} \leq C k \|q\|^2_{0,\Omega_{\boldsymbol{c}}},$$

which proves (3.23). □

Corollary 3.15 proves that the space containing the spurious modes is (at most) one-dimensional on each corner patch shown in Figure 3.2. From the experiments in Section 3.4 we know that there is at least one spurious pressure mode. In conclusion there is exactly one spurious pressure mode on each corner patch.

Remark 3.16. *For the local pressure space we have the decomposition*

$$M_{\mathcal{P}}(\Omega_{\boldsymbol{c}}) = M^{\star}_{\mathcal{P}}(\Omega_{\boldsymbol{c}}) \oplus \operatorname{span}\{q_B\} = M_{\mathcal{P}}(\omega_{\boldsymbol{c}}) \oplus M_{\mathcal{P}}(\Omega_{\boldsymbol{c}} \setminus \omega_{\boldsymbol{c}}) \oplus \operatorname{span}\{q_B\}\,,$$

where $q_B \in M_{\mathcal{P}}(\Omega_{\boldsymbol{c}})$ *is defined by*

$$q_B \coloneqq \begin{cases} \frac{1}{|\omega_{\boldsymbol{c}}|} & \text{in } \omega_{\boldsymbol{c}}\,, \\ -\frac{1}{|\Omega_{\boldsymbol{c}} \setminus \omega_{\boldsymbol{c}}|} & \text{in } \Omega_{\boldsymbol{c}} \setminus \omega_{\boldsymbol{c}}\,. \end{cases}$$

Alternatively, every $q \in M_{\mathcal{P}}(\Omega_{\boldsymbol{c}})$ *can be written as*

$$q = q^{\star} + \Pi_{\boldsymbol{c}} q \quad \text{with} \quad q^{\star} \in M^{\star}_{\mathcal{P}}(\Omega_{\boldsymbol{c}}) \quad \text{and} \quad \Pi_{\boldsymbol{c}} q \coloneqq (q,1)_{\omega_{\boldsymbol{c}}} q_B\,, \tag{3.24}$$

and $(q^{\star}, \Pi_{\boldsymbol{c}} q)_{\Omega_{\boldsymbol{c}}} = 0$.

Moreover, let $(\Omega, \mathcal{P})$ *be a pair of domain and partition as shown in Figure 3.2. Then* $\mathcal{P}$ *consists of one corner patch. Hence, comparing the results Corollary 3.15 and* (3.4)*, we observe that the degeneration of the inf-sup constant appears as a consequence of connecting the pressure spaces on the subdomains* $\omega_{\boldsymbol{c}}$ *and* $\Omega_{\boldsymbol{c}} \setminus \omega_{\boldsymbol{c}}$*, by the average-free function* q_B*. This generalises Remark 3.2 to the meshes shown in Figure 3.2.*

In Corollary 3.15 we impose an average constraint to remove the spurious mode $q_B \in M_{\mathcal{P}}(\Omega_{\boldsymbol{c}})$. The next aim is to show that we alternatively can remove a single degree of freedom by imposing a single jump constraint. The motivation for selecting an edge on $\partial\omega_{\boldsymbol{c}} \cap \partial(\Omega_{\boldsymbol{c}} \setminus \omega_{\boldsymbol{c}})$, is that the pressure spaces $M_{\mathcal{P}}(\omega_{\boldsymbol{c}})$ and $M_{\mathcal{P}}(\Omega_{\boldsymbol{c}} \setminus \omega_{\boldsymbol{c}})$ do not contain spurious modes and that the basis function q_B has the same jump across each of these edges.

In the next section we enforce the continuity of the discrete pressure space in the mid-point $\boldsymbol{x}_{\boldsymbol{c}}$ of an edge $\gamma_{\boldsymbol{c}}$. An abstract implementation concept enabling this idea is described in Appendix A.1.

3.5.2. A uniformly inf-sup stable space by jump constraints

In this section we prove Theorem 3.3; we start with a local result. To this end, let $(\Omega_{\boldsymbol{c}}, \mathcal{P})$ be one of the domains and its associated partition given by Figure 3.2, let $\omega_{\boldsymbol{c}} \subset \Omega_{\boldsymbol{c}}$ be the small shaded subset, and let $\gamma_{\boldsymbol{c}}$ be an edge on $\partial\omega_{\boldsymbol{c}} \cap \partial(\Omega_{\boldsymbol{c}} \setminus \omega_{\boldsymbol{c}})$. Then,

we restrict G, defined in (3.7), to $\Omega_{\boldsymbol{c}}$ by

$$G_{\boldsymbol{c}} \coloneqq \left\{ q \in M_{\mathcal{P}}(\Omega_{\boldsymbol{c}}) \colon [\![q(\boldsymbol{x}_{\boldsymbol{c}})]\!]_{\gamma_{\boldsymbol{c}}} = 0 \quad \text{where } \boldsymbol{x}_{\boldsymbol{c}} \text{ is the midpoint of } \gamma_{\boldsymbol{c}} \right\}. \tag{3.25}$$

The upcoming results are based on the decomposition proposed in Corollary 3.15 and Remark 3.16, respectively. In order to prepare the proof of the local uniform inf-sup condition on $\boldsymbol{V}_{\mathcal{P}}(\Omega_{\boldsymbol{c}}) \times G_{\boldsymbol{c}}$, we give the following auxiliary estimate.

Lemma 3.17. *Let $G_{\boldsymbol{c}}$ be defined by (3.25) and $q \in G_{\boldsymbol{c}}$. Then, $q = q^\star + \Pi_{\boldsymbol{c}} q$ with $q^\star \in M^\star_{\mathcal{P}}(\Omega_{\boldsymbol{c}})$ as defined in Remark 3.16 and*

$$\|q\|_{0,\Omega_{\boldsymbol{c}}} \leq C k^{3/2} \|q^\star\|_{0,\Omega_{\boldsymbol{c}}}, \tag{3.26}$$

with a constant C independent of mesh properties and polynomial degree.

Proof. Let $q \in G_{\boldsymbol{c}}$, and write $q = q^\star + \Pi_{\boldsymbol{c}} q$ with $q^\star \in M^\star_{\mathcal{P}}(\Omega_{\boldsymbol{c}})$. Using the orthogonality of $q^\star$ and $\Pi_{\boldsymbol{c}} q$ we obtain

$$\|q\|^2_{0,\Omega_{\boldsymbol{c}}} = \|q^\star\|^2_{0,\Omega_{\boldsymbol{c}}} + \|\Pi_{\boldsymbol{c}} q\|^2_{0,\Omega_{\boldsymbol{c}}}.$$

Therefore, (3.26) follows once we prove $\|\Pi_{\boldsymbol{c}} q\|_{0,\Omega_{\boldsymbol{c}}} \leq C k^{3/2} \|q^\star\|_{0,\Omega_{\boldsymbol{c}}}$.

We start by observing $\Pi_{\boldsymbol{c}} q = \alpha q_B$ for a coefficient $\alpha \in \mathbb{R}$ and q_B from Remark 3.16. Then, a direct computation shows

$$\|\Pi_{\boldsymbol{c}} q\|^2_{0,\Omega_{\boldsymbol{c}}} = \alpha^2 |[\![q_B(\boldsymbol{x}_{\boldsymbol{c}})]\!]| = \frac{1}{|[\![q_B(\boldsymbol{x}_{\boldsymbol{c}})]\!]|} \alpha^2 [\![q_B(\boldsymbol{x}_{\boldsymbol{c}})]\!]^2 = \frac{|\omega_{\boldsymbol{c}}||\Omega_{\boldsymbol{c}} \setminus \omega_{\boldsymbol{c}}|}{|\Omega_{\boldsymbol{c}}|} [\![\Pi_{\boldsymbol{c}} q(\boldsymbol{x}_{\boldsymbol{c}})]\!]^2.$$

Using $[\![q(\boldsymbol{x}_{\boldsymbol{c}})]\!] = 0$, we get $-[\![\Pi_{\boldsymbol{c}} q(\boldsymbol{x}_{\boldsymbol{c}})]\!] = [\![q^\star(\boldsymbol{x}_{\boldsymbol{c}})]\!]$ and then

$$\|\Pi_{\boldsymbol{c}} q\|^2_{0,\Omega_{\boldsymbol{c}}} = \frac{|\omega_{\boldsymbol{c}}||\Omega_{\boldsymbol{c}} \setminus \omega_{\boldsymbol{c}}|}{|\Omega_{\boldsymbol{c}}|} [\![q^\star(\boldsymbol{x}_{\boldsymbol{c}})]\!]^2. \tag{3.27}$$

Next, we recall $\gamma_{\boldsymbol{c}} = K \cap K'$, and apply trace inequality (2.14) and (CS_2) to get

$$[\![q^\star(\boldsymbol{x}_{\boldsymbol{c}})]\!]^2 \leq k^3 \left(\frac{1}{|K|} + \frac{1}{|K'|} \right) \|q^\star\|^2_{0,K \cup K'}. \tag{3.28}$$

The inverses of the areas need to be compensated. For corner patches with $K \subseteq \omega_{\boldsymbol{c}}$ and $|K| \leq |K'|$ we have $|\omega_{\boldsymbol{c}}| = \delta_{\boldsymbol{c}} |K|$ where $\delta_{\boldsymbol{c}}$ is number of small cells in $\omega_{\boldsymbol{c}}$, cf. Figure 3.2. Therefore, we obtain

$$|\omega_{\boldsymbol{c}}| \big(|K|^{-1} + |K'|^{-1} \big) = \delta_{\boldsymbol{c}} (1 + \varrho_{K'}) \leq 2\, \delta_{\boldsymbol{c}} \leq C. \tag{3.29}$$

Finally, inserting (3.28) into (3.27) and applying (3.29) gives

$$\|\Pi_{\boldsymbol{c}} q\|^2_{0,\Omega_{\boldsymbol{c}}} \leq \frac{|\omega_{\boldsymbol{c}}||\Omega_{\boldsymbol{c}} \setminus \omega_{\boldsymbol{c}}|}{|\Omega_{\boldsymbol{c}}|} k^3 \left(\frac{1}{|K|} + \frac{1}{|K'|} \right) \|q^\star\|^2_{0,K \cup K'} \leq C k^3 \|q^\star\|^2_{0,\Omega_{\boldsymbol{c}}},$$

which finishes the proof. □

Remark 3.18. *The number $\delta_{\boldsymbol{c}}$ in* (3.29) *is uniformly bounded thanks to the maximum angle condition of $\mathcal{P}$ (inherited from $\mathcal{P}_{sr}$).*

Lemma 3.19. *Let $\Omega_{\boldsymbol{c}}$ be one of the domains in Figure 3.2 and let $G_{\boldsymbol{c}}$ be defined by* (3.25)*. Then there exists a positive constant C, independent of mesh properties, such that for all $q \in G_{\boldsymbol{c}}$ there exists $\boldsymbol{v} \in \boldsymbol{V}_{\mathcal{P}}(\Omega_{\boldsymbol{c}})$ satisfying*

$$(\operatorname{div} \boldsymbol{v}, q)_{\Omega_{\boldsymbol{c}}} = \|q\|^2_{0,\Omega_{\boldsymbol{c}}} \quad \textit{and} \quad |\boldsymbol{v}|_{1,\Omega_{\boldsymbol{c}}} \leq Ck^2 \|q\|_{0,\Omega_{\boldsymbol{c}}} \,. \tag{3.30}$$

Proof. Let $q \in G_{\boldsymbol{c}}$, and write $q = q^\star + \Pi_{\boldsymbol{c}} q$ with $q^\star \in M^\star_{\mathcal{P}}(\Omega_{\boldsymbol{c}})$. Then, using Corollary 3.15 there exists $\boldsymbol{v}^\star \in \boldsymbol{V}_{\mathcal{P}}(\Omega_{\boldsymbol{c}})$ such that $\boldsymbol{v}^\star|_{\omega_{\boldsymbol{c}}} \in \boldsymbol{H}^1_0(\omega_{\boldsymbol{c}})$ and

$$(\operatorname{div} \boldsymbol{v}^\star, q^\star)_{\Omega_{\boldsymbol{c}}} = \|q^\star\|^2_{0,\Omega_{\boldsymbol{c}}} \quad \text{and} \quad |\boldsymbol{v}^\star|_{1,\Omega_{\boldsymbol{c}}} \leq Ck^{1/2} \|q^\star\|_{0,\Omega_{\boldsymbol{c}}} \,,$$

and, due to $\Pi_{\boldsymbol{c}} q \in \operatorname{span}\{q_B\}$ and q_B being constant on $\omega_{\boldsymbol{c}}$ and $\Omega_{\boldsymbol{c}} \setminus \omega_{\boldsymbol{c}}$, we have

$$(\operatorname{div} \boldsymbol{v}^\star, \Pi_{\boldsymbol{c}} q)_{\Omega_{\boldsymbol{c}}} = 0 \,.$$

Together, we define $\boldsymbol{v} \coloneqq \|q\|^2_{0,\Omega_{\boldsymbol{c}}} \|q^\star\|^{-2}_{0,\Omega_{\boldsymbol{c}}} \boldsymbol{v}^\star$ and use the equalities above to obtain

$$(\operatorname{div} \boldsymbol{v}, q)_{\Omega_{\boldsymbol{c}}} = \frac{\|q\|^2_{0,\Omega_{\boldsymbol{c}}}}{\|q^\star\|^2_{0,\Omega_{\boldsymbol{c}}}} (\operatorname{div} \boldsymbol{v}^\star, q^\star + \Pi_{\boldsymbol{c}} q)_{\Omega_{\boldsymbol{c}}} = \|q\|^2_{0,\Omega_{\boldsymbol{c}}} \,.$$

Furthermore, using the estimate for $|\boldsymbol{v}^\star|_{1,\Omega_{\boldsymbol{c}}}$ and (3.26), we get

$$|\boldsymbol{v}|_{1,\Omega_{\boldsymbol{c}}} = \frac{\|q\|^2_{0,\Omega_{\boldsymbol{c}}}}{\|q^\star\|^2_{0,\Omega_{\boldsymbol{c}}}} |\boldsymbol{v}^\star|_{1,\Omega_{\boldsymbol{c}}} \leq Ck^{1/2} \frac{\|q\|^2_{0,\Omega_{\boldsymbol{c}}}}{\|q^\star\|_{0,\Omega_{\boldsymbol{c}}}} \leq Ck^{1/2} k^{3/2} \|q\|_{0,\Omega_{\boldsymbol{c}}} \,,$$

which proves (3.30). □

We conclude this section with the proof of the main result, cf. Section 3.2.1.

Proof of Theorem 3.3. We collect the ingredients such that a proof using a macro-element technique can be applied. To this end, we recall that $\mathcal{P}$ arose as an anisotropic refinement of a shape-regular partition $\mathcal{P}_{sr}$. At first we notice that on $\mathcal{P}_{sr}$ the pair $\boldsymbol{Q}_2 \times \mathbb{P}_0$ is inf-sup stable, and hence $\boldsymbol{V}_{\mathcal{P}_{sr}} \times \overline{M_{\mathcal{P}_{sr}}}$ is inf-sup stable, where

$$\overline{M_{\mathcal{P}_{sr}}} \coloneqq \{q\colon q|_K = \textit{const.} \text{ for } K \in \mathcal{P}_{sr}\} \cap \left\{q\colon q|_{\Omega_{\boldsymbol{c}}} = \textit{const.} \text{ for } \boldsymbol{c} \in \mathcal{C}\right\} .$$

Then, on shape-regular parts, edge patches and corner patches of partition $\mathcal{P}$ we have the local inf-sup conditions (3.21), (3.22) and (3.30). Therefore, performing a macro-element technique, as in [AC00, Section 4.4] or [GR86] we conclude β_G in Theorem 3.3 satisfies $\beta_G \geq Ck^{-2}$. Furthermore, since $G \subset M_{\mathcal{P}}$ we get $\beta_G \geq \beta_{\mathcal{P}}$ which finishes the proof. □

3.6. Published results

In collaboration with Prof. Mark Ainsworth results based this on chapter were published in [ABW15]. The purpose of this section is to list the published results.

In [ABW15] we replaced $G \subset M_{\mathcal{P}}$ by the subspace $\widetilde{M}_{\mathcal{P}} \subset M_{\mathcal{P}}$ defined by

$$\widetilde{M}_{\mathcal{P}} \coloneqq \left\{ q \in M_{\mathcal{P}} \colon \int_{\gamma_{\boldsymbol{c}}} [\![q]\!] \, \mathrm{d}s = 0 \text{ for } \boldsymbol{c} \in \mathcal{C} \right\}, \tag{3.31}$$

where $[\![q]\!]$ is the jump of the pressure $q \in M_{\mathcal{P}}$ across the edge $\gamma_{\boldsymbol{c}}$.

Then, the following properties are proven in [ABW15]:

- The pair $\boldsymbol{V}_{\mathcal{P}} \times \widetilde{M}_{\mathcal{P}}$ is uniformly inf-sup stable with an LBB constant $\tilde{\beta}_{\mathcal{P}}$ satisfying $\tilde{\beta}_{\mathcal{P}} \geq \max\{\beta_{\mathcal{P}}, Ck^{-3/2}\}$. This constant may be up to $k^{1/2}$ larger than β_G in Theorem 3.3.

- The constraints in definition (3.31) motivate the stabilisation term:

  $$s_p(p,q) \coloneqq \frac{1}{k^2} \sum_{\boldsymbol{c} \in \mathcal{C}} \int_{\gamma_{\boldsymbol{c}}} [\![p]\!] \, \mathrm{d}s \cdot \int_{\gamma_{\boldsymbol{c}}} [\![q]\!] \, \mathrm{d}s \,.$$

  This term satisfies the equivalence

  $$C_1 \left\| q_{\mathcal{P}} - \widetilde{\Pi}_{\mathcal{P}} q_{\mathcal{P}} \right\|_{0,\Omega}^2 \leq s_p(q_{\mathcal{P}}, q_{\mathcal{P}}) \leq C_2 \left\| q_{\mathcal{P}} - \widetilde{\Pi}_{\mathcal{P}} q_{\mathcal{P}} \right\|_{0,\Omega}^2 ,$$

  where $\widetilde{\Pi}_{\mathcal{P}}$ is an appropriate projection and C_1, C_2 are constants only depending on angles. Additionally, for all $q \in M_{\mathcal{P}}$ and $p \in H^1(\Omega)$ we have

  $$s_p(q_{\mathcal{P}}, q_{\mathcal{P}}) \leq C \begin{cases} \|q_{\mathcal{P}}\|_{0,\Omega}^2 \,, \\ k^{-2} \sum_{\boldsymbol{c} \in \mathcal{C}} \left(\|p - q_{\mathcal{P}}\|_{0,K \cup K'}^2 + |\gamma_{\boldsymbol{c}}|^2 \|\partial (p - q_{\mathcal{P}}) / \partial n_{\boldsymbol{c}}\|_{0,K \cup K'}^2 \right) , \end{cases}$$

  where $n_{\boldsymbol{c}}$ is a unit normal vector of the edge $\gamma_{\boldsymbol{c}}$.

- Using the properties above (similar to Remark 3.9) we get:

  $$\inf_{\tilde{q}_{\mathcal{P}} \in \widetilde{M}_{\mathcal{P}}} \|p - \tilde{q}_{\mathcal{P}}\|_{0,\Omega}^2 \leq C \inf_{q_{\mathcal{P}} \in M_{\mathcal{P}}} \left(\|p - q_{\mathcal{P}}\|_{0,\Omega}^2 + k^{-2} \sum_{\boldsymbol{c} \in \mathcal{C}} |\gamma_{\boldsymbol{c}}|^2 \|\partial (p - q_{\mathcal{P}}) / \partial n_{\boldsymbol{c}}\|_{0,K \cup K'}^2 \right).$$

- Both the mixed method using the pair $\boldsymbol{V}_{\mathcal{P}} \times \widetilde{M}_{\mathcal{P}}$ and the method using $\boldsymbol{V}_{\mathcal{P}} \times M_{\mathcal{P}}$ which has been stabilised by adding the term above are stable, independent of properties of the mesh, and in particular of the properties of the corner patches.

Furthermore, both methods satisfy the a priori estimate

$$|\boldsymbol{u}-\boldsymbol{u}_{\mathcal{P}}|_{1,\Omega}+\|p-p_{\mathcal{P}}\|_{0,\Omega}\leq C\tilde{\beta}_{\mathcal{P}}^{-2}\Big\{\inf_{\boldsymbol{v}_{\mathcal{P}}\in\boldsymbol{V}_{\mathcal{P}}}|\boldsymbol{u}-\boldsymbol{v}_{\mathcal{P}}|_{1,\Omega} + \inf_{q_{\mathcal{P}}\in M_{\mathcal{P}}}\Big(\|p-q_{\mathcal{P}}\|_{0,\Omega}^2+k^{-2}\sum_{\boldsymbol{c}\in\mathcal{C}}|\gamma_{\boldsymbol{c}}|^2\|\partial(p-q_{\mathcal{P}})/\partial n_{\boldsymbol{c}}\|_{0,K\cup K'}^2\Big)^{1/2}\Big\}.$$

3.7. Conclusions

In this chapter, we discussed the stability of the mixed finite element scheme $\boldsymbol{Q}_{k+1}^c\times\mathbb{P}_{k-1}$ on anisotropic meshes. The unconstrained pair satisfies uniform inf-sup conditions on shape-regular meshes [SS96, BM99] and on edge patches [SSS99, AC00, SS98]. Unfortunately, the LBB constant degenerates on partitions containing corner patches with their aspect ratio, cf. (3.4), which is a result proved in [AC00]. Further results in [AC00] give the impression that the degeneration is caused by as many spurious modes as single corner patches (see Figure 3.1b) are present in the partition.

The first achievement of this chapter is Corollary 3.15, which shows that the number of spurious pressure modes is smaller, since the uniformly inf-sup stable part of the space is larger. Then, the inf-sup condition in Corollary 3.15 is the basis for the results Theorem 3.3, and [ABW15, Thm. 1.1], which prove the existence of alternative uniformly inf-sup stable spaces G and $\widetilde{M}_{\mathcal{P}}$. These spaces impose constraints on the pressure space which, similarly to boundary conditions, may be enforced strongly (by using the reduced space) or weakly (by adding a stabilisation term to the formulation). Numerical experiments confirmed that the number of constraints is indeed minimal. It turns out that the schemes using the reduced pressure spaces converge at least as fast as the stabilised alternatives, cf. Remark 3.9 and Theorem 3.14, as well as [ABW15, Theorems 1.1 and 1.2].

In conclusion, the chapter is the basis for four new mixed methods for the Stokes flow problem whose stability is independent of mesh properties, even on meshes that contain corner patches. For the lowest polynomial degree $k=1$ ($\boldsymbol{Q}_2^c\times\mathbb{P}_0$), the reduced spaces G (3.7) and $\widetilde{M}_{\mathcal{P}}$ (3.31) coincide. Similarly, the stabilisation terms, and therefore the stabilised methods, coincide. The methods proposed here represent an easy to implement alternative to the method in [AC00]. Each of the methods circumvents a dependency of $\beta_{\mathcal{P}}$ on the ratio $\min_{\boldsymbol{c}\in\mathcal{C}}h_{\boldsymbol{c}}/H_{\boldsymbol{c}}$, cf. Figure 3.2, which is a non-local quantity, cf. Remark 3.2.

3.7.1. Extensions

The approach presented in this chapter can be extended into various directions. An extension to a balanced-order pair requires more stabilisation terms as a dependency on local aspect ratios arises, see also Table 1.1. The lowest order pair $\boldsymbol{Q}_1^c \times \mathbb{P}_0$ is treated in the next chapter. The results are then extended to the Oseen problem in Chapter 5.

Chapter 4

A note on the stabilised $\boldsymbol{Q}_1^c \times \mathbb{P}_0$ method

In this chapter, we extend results obtained so far to the lowest balanced-order pair for the Stokes problem, that is, we propose a method using bilinear velocities and constant pressures. For this, we extend the method proposed in [LS13] to cover the case in which the mesh contains anisotropically refined corners. This modification consists of adding extra jump terms in selected edges connecting small shape regular with large anisotropic elements. We prove stability and convergence of the proposed method, and provide numerical evidence for the fact that our approach successfully removes the dependence on the anisotropy.

The results contained in this chapter are the basis of the publication [BW15].

4.1. Motivation

As in Chapter 3 we consider the Stokes problem in a bounded, connected, polygonal domain $\Omega \subset \mathbb{R}^2$. We recall the problem to pose the context:

Find a velocity $\boldsymbol{u}$ and a pressure p such that

$$-\Delta \boldsymbol{u} + \operatorname{grad} p = \boldsymbol{f}\,, \quad \operatorname{div} \boldsymbol{u} = 0 \quad \text{in} \quad \Omega \tag{4.1}$$

subject to $\boldsymbol{u} = \boldsymbol{0}$ on $\partial\Omega$ and $p \in L_0^2(\Omega)$, with given source term $\boldsymbol{f} \in L^2(\Omega)^2$.

For the discrete space we choose the $\boldsymbol{Q}_1^c \times \mathbb{P}_0$ pair and allow the mesh to be anisotropic. It is well known that the $\boldsymbol{Q}_1^c \times \mathbb{P}_0$ pair is not inf-sup stable (cf. [GR86]). In the introduction we saw that several stabilised finite element methods have been proposed.

In this chapter, we focus on the case in which the mesh used contains anisotropic elements. This possibility is considered in [LS13], but the method needs to be extended to accommodate the anisotropies we consider in this chapter. In fact, the method considered in [LS13] is an extension of the locally stabilised FEM [KS92]. In order to build the method, the mesh $\mathcal{P}$ used in the discretization has to be a uniform refinement of an initial (*macro element*) partition $\mathcal{P}_0$ (see Figure 4.1). This refinement divides

each macro element $M \in \mathcal{P}_0$ into 4 quadrangles by connecting the mid-points of opposite edges (see Figure 4.1, right). The stability of the locally stabilised method is a consequence of the stability of the $\boldsymbol{Q}_2^c \times \mathbb{P}_0$ space over the initial partition $\mathcal{P}_0$.

Now, from Chapter 3 (or [AC00]) we know that the following fact holds

$$\inf_{q\in\mathbb{P}_0} \sup_{\boldsymbol{v}\in\boldsymbol{Q}_2^c} \frac{(q, \operatorname{div} \boldsymbol{v})_\Omega}{|\boldsymbol{v}|_{1,\Omega}\|q\|_{0,\Omega}} \geq C\sqrt{\varrho}\,, \tag{4.2}$$

where $\varrho = h/H$ is the aspect ratio (recall Remark 3.2 for a more precise statement). Hence, (4.2) leads to a deterioration of the stability constant when ϱ tends to zero, as suggested by Figure 4.1. This dependence is still present in [LS13], since that method only considers jumps inside macro elements $M \in \mathcal{P}_0$, and then, in such a case, a deterioration of stability of the type (4.2) will not be corrected.

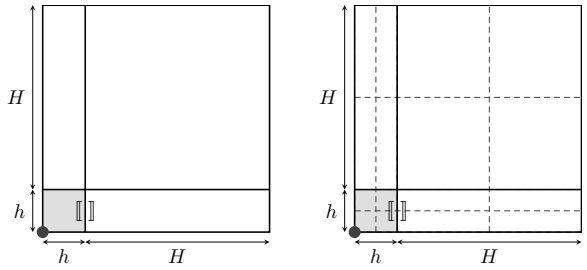

Fig. 4.1. Partition $\mathcal{P}_0$ (left) and $\mathcal{P}$ (right).

In this chapter we propose an extension of the method from [LS13] which remains uniformly stable as ϱ tends to zero. For this, we apply the techniques developed in the previous chapter and augment the method by adding jumps in selected edges of the partition $\mathcal{P}$. More precisely, we add jumps to the formulation that allow to "connect" the small (shaded) corner macro element in $\mathcal{P}_0$ to the rest of the corner patch from Figure 4.1.

We recall the weak formulation of (4.1):
Find $\boldsymbol{u} \in \boldsymbol{V} \coloneqq \boldsymbol{H}_0^1(\Omega)$ and $p \in M \coloneqq L_0^2(\Omega)$ such that

$$\mathfrak{B}(\boldsymbol{u}, p; \boldsymbol{v}, q) = (\boldsymbol{f}, \boldsymbol{v})_\Omega \quad \text{for all} \quad (\boldsymbol{v}, q) \in \boldsymbol{V} \times M \tag{4.3}$$

where

$$\mathfrak{B}(\boldsymbol{u}, p; \boldsymbol{v}, q) \coloneqq (\operatorname{grad} \boldsymbol{u}, \operatorname{grad} \boldsymbol{v})_\Omega - (\operatorname{div} \boldsymbol{v}, p)_\Omega - (\operatorname{div} \boldsymbol{u}, q)_\Omega\,. \tag{4.4}$$

The well-posedness of (4.3) was discussed in Chapter 3.

The rest of this chapter is organised as follows. We define required notation and extend the stabilisation terms of the method in [LS13] by a few jumps. Then, the

stability, a priori estimates and numerical experiments are stated. These experiments confirm the dependency on ϱ and that the additional jumps remove it. Then, the proof of the main results and concluding remarks are given. Finally we justify the numerical experiments made.

4.2. The finite element approximation

In order to construct partition $\mathcal{P}$ we start from an initial *macro element* partition $\mathcal{P}_0$ that consists of closed parallelograms and satisfies a maximal angle condition. We suppose that $\mathcal{P}_0$ is a conforming partition of Ω and allow it to be highly anisotropic and contain corner patches, as in Chapter 3. See for example the shaded cells and their neighbourhoods in Figures 4.1 and 4.3 (later).

We define the partition $\mathcal{P}$ as a uniform refinement of $\mathcal{P}_0$, and state important definitions and properties of $\mathcal{P}$:

- Let $\mathcal{E}_\mathcal{P}$ denote the set of interior edges of $\mathcal{P}$. Throughout we use K to denote elements of $\mathcal{P}$, and M to denote elements of $\mathcal{P}_0$. We refer to M as *macro element*.
- The uniform refinement splits each macro element $M \in \mathcal{P}_0$ into $K_1, K_2, K_3, K_4 \in \mathcal{P}$, such that $|K_i| = |M|/4\,(i = 1, .., 4)$ and each K_i has the same angles as M, see Figure 4.1(right).
- For $M \in \mathcal{P}_0$, let $\mathcal{E}_M \subseteq \mathcal{E}_\mathcal{P}$ collect its interior edges, dashed in Figure 4.1(right).
- Let $\mathcal{C}$ be the set of *corners*, that is, nodes $\boldsymbol{c}$ of the mesh $\mathcal{P}_0$ towards which the mesh is graded, denoted by filled circles in Figures 4.1 and 4.3. Moreover, for $\boldsymbol{c} \in \mathcal{C}$, we select a single edge $\gamma_{\boldsymbol{c}} \in \mathcal{E}_{\mathcal{P}_0}$ that separates an extremely small corner macro element (shaded) from a highly stretched neighbouring macro element, for instance, the embraced edges in Figures 4.1(left) and 4.3. The selected edges $\gamma_{\boldsymbol{c}}$ are collected in the set $\mathcal{E}_\mathcal{C}$.

Finally, we define the finite element spaces

$$\boldsymbol{Q}^c_{\ell,\mathcal{P}} \coloneqq \left\{\boldsymbol{v} \in \boldsymbol{V} \colon \boldsymbol{v}|_K \in \mathbb{Q}_\ell(K)^2 \quad \text{for all} \quad K \in \mathcal{P}\right\}, \quad \ell = 1, 2$$

and

$$M_\mathcal{P} \coloneqq \left\{q \in M \colon q|_K \in \mathbb{P}_0(K) \quad \text{for all} \quad K \in \mathcal{P}\right\},$$

and seek an approximation of the solution $(\boldsymbol{u}, p)$ of Problem (4.3) within the discrete space $\boldsymbol{Q}^c_{1,\mathcal{P}} \times M_\mathcal{P}$. Then, the stabilised method reads:

Find $(\boldsymbol{u}_{\mathcal{P}}^s, p_{\mathcal{P}}^s) \in \boldsymbol{Q}_{1,\mathcal{P}}^c \times M_{\mathcal{P}}$ such that

$$\mathfrak{B}_s(\boldsymbol{u}_{\mathcal{P}}^s, p_{\mathcal{P}}^s; \boldsymbol{v}, q) = (\boldsymbol{f}, \boldsymbol{v})_\Omega \quad \text{for all} \quad (\boldsymbol{v}, q) \in \boldsymbol{Q}_{1,\mathcal{P}}^c \times M_{\mathcal{P}}\,. \tag{4.5}$$

Here,

$$\mathfrak{B}_s(\boldsymbol{u}, p; \boldsymbol{v}, q) \coloneqq \mathfrak{B}(\boldsymbol{u}, p; \boldsymbol{v}, q) - \frac{1}{4} s_p(p, q)\,, \tag{4.6}$$

and the stabilisation terms are

$$s_p(p, q) \coloneqq \sum_{M \in \mathcal{P}_0} S_M(p, q) + \sum_{\gamma_{\boldsymbol{c}} \in \mathcal{E}_{\mathcal{C}}} S_{\gamma_{\boldsymbol{c}}}(p, q) \tag{4.7}$$

where, if $[\![\cdot]\!]_e$ stands for the *jump* of a function across edge $e = K \cap K'$, then

$$S_M(p, q) \coloneqq \sum_{e \in \mathcal{E}_M} \frac{|M|}{4|e|} \int_e [\![p]\!][\![q]\!]\, \mathrm{d}s\,,$$
$$S_{\gamma_{\boldsymbol{c}}}(p, q) \coloneqq \sum_{e \subset \gamma_{\boldsymbol{c}}} \frac{\min\{|K|, |K'|\}}{|e|} \int_e [\![p]\!][\![q]\!]\, \mathrm{d}s\,.$$

Remark 4.1. *The method proposed in [LS13] seeks $(\boldsymbol{u}, p) \in \boldsymbol{Q}_{1,\mathcal{P}}^c \times M_{\mathcal{P}}$, such that*

$$\mathfrak{B}(\boldsymbol{u}, p; \boldsymbol{v}, q) - \frac{1}{4} \sum_{M \in \mathcal{P}_0} S_M(p, q) = (\boldsymbol{f}, \boldsymbol{v})_\Omega \quad \textit{for all} \quad (\boldsymbol{v}, q) \in \boldsymbol{Q}_{1,\mathcal{P}}^c \times M_{\mathcal{P}}\,. \tag{4.8}$$

Then, the difference is given by additional jumps across a few selected edges.

For simplicity, in this chapter, we restrict ourselves to axis-parallel meshes. The results can be easily extended to meshes consisting of parallelograms. We summarise the existence and a priori results here, the proofs are postponed until after the numerical experiments.

Theorem 4.2. *Let $|||(\boldsymbol{v}, q)|||^2 \coloneqq |\boldsymbol{v}|_{1,\Omega}^2 + \|q\|_{0,\Omega}^2$. Then, there exists a constant $\mu_s > 0$ independent of ϱ, such that*

$$\sup_{(\boldsymbol{v},q) \in \boldsymbol{Q}_{1,\mathcal{P}}^c \times M_{\mathcal{P}}} \frac{\mathfrak{B}_s(\boldsymbol{w}, r; \boldsymbol{v}, q)}{|||(\boldsymbol{v}, q)|||} \geq \mu_s\, |||(\boldsymbol{w}, r)||| \quad \textit{for all} \quad (\boldsymbol{w}, r) \in \boldsymbol{Q}_{1,\mathcal{P}}^c \times M_{\mathcal{P}}\,. \tag{4.9}$$

Consequently, Problem (4.5) has a unique solution $(\boldsymbol{u}_{\mathcal{P}}^s, p_{\mathcal{P}}^s) \in \boldsymbol{Q}_{1,\mathcal{P}}^c \times M_{\mathcal{P}}$. Moreover, if $p \in H^1(\Omega)$, then there exists a positive constant C such that

$$|||(\boldsymbol{u} - \boldsymbol{u}_{\mathcal{P}}^s, p - p_{\mathcal{P}}^s)||| \leq (1 + C\mu_s^{-1})$$
$$\left(\inf_{(\boldsymbol{v}_{\mathcal{P}}, q_{\mathcal{P}}) \in \boldsymbol{Q}_{1,\mathcal{P}}^c \times M_{\mathcal{P}}} |||(\boldsymbol{u} - \boldsymbol{v}_{\mathcal{P}}, p - q_{\mathcal{P}})||| + \Big\{ \sum_{K \in \mathcal{P}} \|\mathrm{diag}(h_{K,x},\, h_{K,y}) \nabla p\|_{0,K}^2 \Big\}^{1/2} \right), \tag{4.10}$$

where $h_{K,x}$ and $h_{K,y}$ is the length of cell $K \in \mathcal{P}$ in x- and y-direction, respectively.

4.3. Numerical results

We compare μ_s from (4.9) and the stability constant ξ from [LS13] given by

$$\xi = \inf_{(\boldsymbol{w},r)\in \boldsymbol{Q}^c_{1,\mathcal{P}}\times M_{\mathcal{P}}} \sup_{(\boldsymbol{v},q)\in \boldsymbol{Q}^c_{1,\mathcal{P}}\times M_{\mathcal{P}}} \frac{\mathfrak{B}(\boldsymbol{w},r;\boldsymbol{v},q) - 4^{-1}\sum_{M\in\mathcal{P}_0} S_M(r,q)}{|||(\boldsymbol{v},q)|||\,|||(\boldsymbol{w},r)|||}\,.$$

The experiments in Figure 4.2 were performed on partitions $\mathcal{P}$ shown in Figure 4.1 (right) and Figure 4.3 on the domains $\Omega = (0,1)\times(0,1)$ and $\Omega = (-3,3)\times(0,2) \cup (-1,1)\times(-2,0]$, respectively. The set of additional edges $\mathcal{E}_{\mathfrak{C}}$ was chosen to contain all edges enclosed by a jump symbol $[\![\cdot]\!]$. We observe for $\varrho \to 0$, that while μ_s remains uniformly bounded away from zero, ξ degrades and tends to zero. Hence, the additional jumps correct the dependency of ξ on ϱ. We used Corollary 4.7 (cf. Section 4.6) to calculate the values of ξ and μ_s.

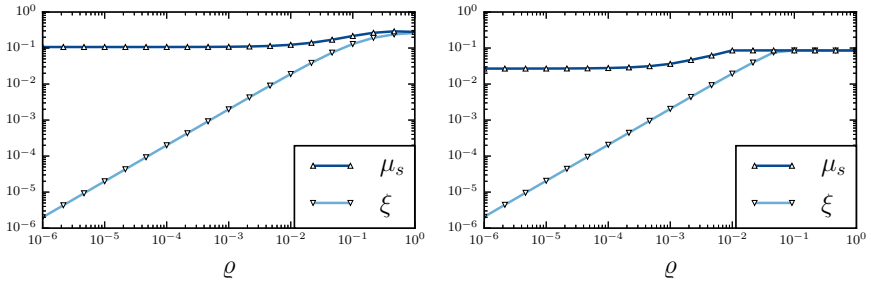

Fig. 4.2. Stability constants μ_s in (4.9) and ξ in [LS13, (3.12)] for various values of ϱ. Left: on the mesh of Figure 4.1, right: on mesh in Figure 4.3.

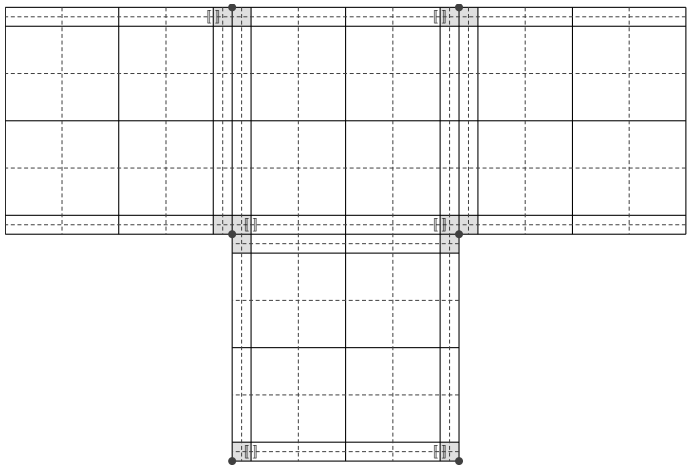

Fig. 4.3. An anisotropic mesh on a T-shaped domain.

4.4. Proof of stability

In this section we prove Theorem 4.2. We start by deriving a uniformly inf-sup-stable subspace $G \subset M_{\mathcal{P}}$ and an inf-sup deficiency. To this end, we recall the definition of $\mathcal{E}_{\mathcal{C}}$ in Section 4.2.

Lemma 4.3. *For the subspace $G \subset M_{\mathcal{P}_0} \subset M_{\mathcal{P}}$, defined by*

$$G \coloneqq \Big\{ q \in M_{\mathcal{P}_0} \colon [\![q]\!]_{\gamma_{\boldsymbol{c}}} = 0 \quad \text{for} \quad \gamma_{\boldsymbol{c}} \in \mathcal{E}_{\mathcal{C}} \Big\}, \tag{4.11}$$

there exists a constant β_G independent of ϱ such that

$$\sup_{\boldsymbol{v}_{\mathcal{P}} \in \boldsymbol{Q}^c_{1,\mathcal{P}}} \frac{(\operatorname{div} \boldsymbol{v}_{\mathcal{P}}, q_{\mathcal{P}})_\Omega}{|\boldsymbol{v}_{\mathcal{P}}|_{1,\Omega}} \geq \beta_G \|q_{\mathcal{P}}\|_{0,\Omega} \quad \text{for all} \quad q \in G\,. \tag{4.12}$$

Proof. We reason by similarity of the velocity spaces $\boldsymbol{Q}^c_{1,\mathcal{P}}$ and $\boldsymbol{Q}^c_{2,\mathcal{P}_0}$. For the pair $\boldsymbol{Q}^c_{2,\mathcal{P}_0} \times G$ the result is a consequence of Theorem 3.3, or [ABW15, Theorem 1.1]. □

The result above induces the following inf-sup deficiency of $\boldsymbol{Q}^c_{1,\mathcal{P}} \times M_{\mathcal{P}}$.

Lemma 4.4. *Let G be defined by* (4.11) *and let $\Pi_G \colon M_{\mathcal{P}} \to G$ be an operator. Then*

$$\sup_{\boldsymbol{v} \in \boldsymbol{Q}^c_{1,\mathcal{P}}} \frac{(\operatorname{div} \boldsymbol{v}, q)_\Omega}{|\boldsymbol{v}|_{1,\Omega}} \geq \beta_G \|\Pi_G q\|_{0,\Omega} - \|q - \Pi_G q\|_{0,\Omega} \quad \text{for all} \quad q \in M_{\mathcal{P}}\,. \tag{4.13}$$

Furthermore, if $\Pi_G q = q$ for all $q \in G$, then (4.13) *implies* (4.12).

Proof. Let $q \in M_{\mathcal{P}}$, then $\Pi_G q \in G$ and by (4.12) there exists a non-zero $\boldsymbol{v} \in \boldsymbol{Q}^c_{1,\mathcal{P}}$ such that

$$\beta_G |\boldsymbol{v}|_{1,\Omega} \|\Pi_G q\|_{0,\Omega} \leq (\operatorname{div} \boldsymbol{v}, \Pi_G q)_\Omega \leq |\boldsymbol{v}|_{1,\Omega} \|q - \Pi_G q\|_{0,\Omega} + (\operatorname{div} \boldsymbol{v}, q)_\Omega\,.$$

Dividing by $|\boldsymbol{v}|_{1,\Omega}$ gives (4.13) for one $\boldsymbol{v} \in \boldsymbol{Q}^c_{1,\mathcal{P}}$. The rest follows easily. □

The last results can be read as follows: The inf-sup deficiency (4.2) is caused by functions whose jumps do not vanish across edges in $\mathcal{E}_{\mathcal{C}}$. Then, in the rest of this section, we show that it is enough to control such jumps to obtain uniform stability.

To this end, we recall that $\mathcal{P}_0$ is conforming and rewrite every selected edge $\gamma_{\boldsymbol{c}} \in \mathcal{E}_{\mathcal{C}}$ as $\gamma_{\boldsymbol{c}} = M \cap M'$ where $M, M' \in \mathcal{P}_0$ and $|M| \leq |M'|$. In order to simplify the proof we define $\omega_{\gamma_{\boldsymbol{c}}} \coloneqq M \cup M'$. Now, let G be defined by (4.11) and let $\Pi_G \colon M_{\mathcal{P}} \to G$ be the L^2-projection into G, which is given by

$$\Pi_G q\big|_M = \begin{cases} \langle q \rangle_{\omega_{\gamma_{\boldsymbol{c}}}} & \text{if } M \subset \omega_{\gamma_{\boldsymbol{c}}}\,, \\ \langle q \rangle_M & \text{otherwise.} \end{cases} \tag{4.14}$$

Now, Lemma 4.5 proves properties of the stabilisation terms (4.7). The proof uses the characteristic function on subdomains $\omega \subseteq \overline{\Omega}$ given by

$$\chi_\omega(\boldsymbol{x}) \coloneqq \begin{cases} 1 & \text{if } \boldsymbol{x} \in \omega\,, \\ 0 & \text{otherwise.} \end{cases}$$

Lemma 4.5. *Let $q_\mathcal{P} \in M_\mathcal{P}$. On $M \in \mathcal{P}_0$ with $M \not\subset \omega_{\gamma_\mathcal{C}}$ we have the equivalence*

$$2\|q_\mathcal{P} - \Pi_G q_\mathcal{P}\|_{0,M}^2 \leq S_M(q_\mathcal{P}, q_\mathcal{P}) \leq 4\|q_\mathcal{P} - \Pi_G q_\mathcal{P}\|_{0,M}^2\,, \tag{4.15a}$$

on $\omega_{\gamma_\mathcal{C}} = M \cup M'$ we have

$$\frac{1}{4}\|q_\mathcal{P} - \Pi_G q_\mathcal{P}\|_{0,\omega_{\gamma_\mathcal{C}}}^2 \leq \big(S_M + S_{M'} + S_{\gamma_\mathcal{C}}\big)(q_\mathcal{P}, q_\mathcal{P}) \leq 6\|q_\mathcal{P} - \Pi_G q_\mathcal{P}\|_{0,\omega_{\gamma_\mathcal{C}}}^2\,. \tag{4.15b}$$

Furthermore, let $s_p|_M \coloneqq S_M$ and $s_p|_{\omega_{\gamma_\mathcal{C}}} \coloneqq S_M + S_{M'} + S_{\gamma_\mathcal{C}}$, then

$$s_p(q_\mathcal{P}, q_\mathcal{P})|_\omega \leq C \begin{cases} \|q_\mathcal{P}\|_{0,\omega}^2 \\ \sum_{K\subset\omega}\Big(\|p - q_\mathcal{P}\|_{0,K}^2 + h_{K,x}^2\|\partial_x p\|_{0,K}^2 + h_{k,y}^2\|\partial_y p\|_{0,K}^2\Big) \end{cases} \tag{4.16}$$

for all $p \in H^1(\Omega)$, where $\omega = M \in \mathcal{P}_0$ or $\omega = \omega_{\gamma_\mathcal{C}}$.

Proof. Equivalence (4.15a) has been proven in [LS13, Lemma 3.2]. We include here an alternative proof which supplies us with notation and arguments for (4.15b). Let $M \in \mathcal{P}_0$ be a (2-by-2) macro element such that $M \not\subset \omega_{\gamma_\mathcal{C}}$, $\gamma_\mathcal{C} \in \mathcal{E}_\mathcal{C}$. Since, all cells $K \subset M$ have the same area, an orthogonal (with respect to the inner product in L^2) basis of $M_\mathcal{P}(M) \coloneqq \{q \in M_\mathcal{P} \colon \operatorname{supp} q \subseteq M\} \subset L_0^2(M)$ is given by (cf. Figure 4.4, left)

$$\begin{aligned} \phi_{1,M} &\coloneqq \chi_{K_1} - \chi_{K_2}\,, \\ \phi_{2,M} &\coloneqq \chi_{K_1\cup K_2} - \chi_{K_3\cup K_4}\,, \\ \phi_{3,M} &\coloneqq \chi_{K_3} - \chi_{K_4}\,. \end{aligned} \tag{4.17}$$

Below, we omit the subscript M when it is clear from the context.

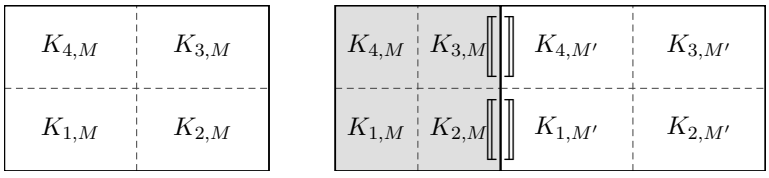

Fig. 4.4. A macro element $M \in \mathcal{P}_0$ (left) and set $\omega_{\gamma_\mathcal{C}}$ (right) with cells $K_{i,M} \in \mathcal{P}$.

We define $r_a \coloneqq (q_\mathcal{P} - \langle q_\mathcal{P}\rangle_M)|_M$ and realise $r_a \in M_\mathcal{P}(M)$. Therefore, from (4.17) we get $r_a = \sum_{i=1}^3 \alpha_i \phi_{i,M}$ with appropriate coefficients α_i $(i = 1, 2, 3)$. Then, using

$|K_i| = |M|/4$, $(i = 1, \dots, 4)$, the definition of S_M, $[\![r_a]\!]_e \in \mathbb{P}_0(e)$ and orthogonalities of the basis we get

$$\begin{aligned} S_M(q_{\mathcal{P}}, q_{\mathcal{P}}) &= \frac{|M|}{4} \sum_{e \in \mathcal{E}_M} \frac{1}{|e|} \int_e [\![q_{\mathcal{P}}]\!]^2 = \frac{|M|}{4} \sum_{e \in \mathcal{E}_M} \frac{1}{|e|} \int_e [\![r_a]\!]^2 = \frac{|M|}{4} \sum_{e \in \mathcal{E}_M} [\![r_a]\!]_e^2 \\ &= \frac{|M|}{4} \big[(2\alpha_1)^2 + (2\alpha_2 - \alpha_1 - \alpha_3)^2 + (2\alpha_3)^2 + (-2\alpha_2 - \alpha_3 - \alpha_1)^2 \big] \\ &= \frac{|M|}{4} \big[4\alpha_1^2 + 4\alpha_3^2 + 8\alpha_2^2 + 2(\alpha_1 + \alpha_3)^2 \big] \\ &= 2\|\alpha_1 \phi_1\|_{0,M}^2 + 2\|\alpha_3 \phi_3\|_{0,M}^2 + 2\|\alpha_2 \phi_2\|_{0,M}^2 + \frac{|M|}{2}(\alpha_1 + \alpha_3)^2 \\ &= 2\|r_a\|_{0,M}^2 + \frac{|M|}{2}(\alpha_1 + \alpha_3)^2 , \end{aligned} \tag{4.18}$$

which proves the lower bound of (4.15a). Applying $(\alpha_1 + \alpha_3)^2 |M|/2 \le 2\|r_a\|_{0,M}^2$ proves the upper bound.

To prove (4.15b), we fix an edge $\gamma_{\boldsymbol{c}} \in \mathcal{E}_{\mathcal{C}}$ and let $r_b \coloneqq (q_{\mathcal{P}} - \langle q_{\mathcal{P}} \rangle_{\omega_{\gamma_{\boldsymbol{c}}}})\big|_{\omega_{\gamma_{\boldsymbol{c}}}}$. Then

$$r_b = \alpha_0 \phi_0 + r_a + r_a' ,$$

where $\phi_0 = |M|^{-1} \chi_M - |M'|^{-1} \chi_{M'}$, $r_a = \sum_{i=1}^3 \alpha_i \phi_{i,M}$ and $r_a' = \sum_{i=1}^3 \alpha_i' \phi_{i,M'}$. Using (4.18), the definition of ϕ_0 and $|K| \le |K'|$ (since $|M| \le |M'|$), the stabilisation terms (4.7) inside $\omega_{\gamma_{\boldsymbol{c}}}$ satisfy

$$\big(S_M + S_{M'} + S_{\gamma_{\boldsymbol{c}}}\big)(q_{\mathcal{P}}, q_{\mathcal{P}}) \ge 2\|r_a\|_{0,M}^2 + 2\big\|r_a'\big\|_{0,M'}^2 + \sum_{e \subset \gamma_{\boldsymbol{c}}} \frac{|K|}{|e|} \int_e [\![r_b]\!]^2 \tag{4.19}$$

where the additional edges $e \subset \gamma_{\boldsymbol{c}}$ satisfy $e \subset M \cap M'$. We need a lower bound for the last term. Using $[\![r_b]\!]_e, [\![\phi_0]\!]_e \in \mathbb{P}_0(e)$, the linearity of the jump, followed by the inequality, $2ab \le \frac{1}{2}a^2 + 2b^2$, we obtain

$$\begin{aligned} \sum_{e \subset \gamma_{\boldsymbol{c}}} \int_e \frac{[\![r_b]\!]^2}{|e|} &= \Big([\![\alpha_0 \phi_0]\!]_{\gamma_{\boldsymbol{c}}} - \alpha_2 + \alpha_2' - \alpha_3 - \alpha_3' \Big)^2 + \Big([\![\alpha_0 \phi_0]\!]_{\gamma_{\boldsymbol{c}}} + \alpha_2 - \alpha_2' - \alpha_1 - \alpha_1' \Big)^2 \\ &= 2[\![\alpha_0 \phi_0]\!]_{\gamma_{\boldsymbol{c}}}^2 + 2(\alpha_2 - \alpha_2')^2 + (\alpha_1 + \alpha_1')^2 + (\alpha_3 + \alpha_3')^2 \\ &\quad - 2([\![\alpha_0 \phi_0]\!]_{\gamma_{\boldsymbol{c}}} + \alpha_2 - \alpha_2')(\alpha_1 + \alpha_1') - 2([\![\alpha_0 \phi_0]\!]_{\gamma_{\boldsymbol{c}}} - \alpha_2 + \alpha_2')(\alpha_3 + \alpha_3') \\ &\ge [\![\alpha_0 \phi_0]\!]_{\gamma_{\boldsymbol{c}}}^2 + (\alpha_2 - \alpha_2')^2 - (\alpha_1 + \alpha_1')^2 - (\alpha_3 + \alpha_3')^2 , \end{aligned}$$

and conclude, multiplying through by $|K| = |M|/4 \le |M'|/4$, that

$$\sum_{e \subset \gamma_{\boldsymbol{c}}} \frac{|K|}{|e|} \int_e [\![r_b]\!]^2 \ge |K| [\![\alpha_0 \phi_0]\!]_{\gamma_{\boldsymbol{c}}}^2 - 2|K|(\alpha_1^2 + \alpha_1'^2 + \alpha_3^2 + \alpha_3'^2) . \tag{4.20}$$

Now, the definition of ϕ_0 and $|K| = |M|/4$ imply

$$|K| [\![\alpha_0 \phi_0]\!]_{\gamma_{\boldsymbol{c}}}^2 = \alpha_0^2 \frac{|M|}{4} \left(\frac{1}{|M|} + \frac{1}{|M'|} \right)^2 \ge \frac{1}{4} \alpha_0^2 \left(\frac{1}{|M|} + \frac{1}{|M'|} \right) = \frac{1}{4} \|\alpha_0 \phi_0\|_{0,\omega_{\gamma_{\boldsymbol{c}}}}^2$$

and $|M| \leq |M'|$ shows

$$2|K|\big(\alpha_1^2 + \alpha_1'^2 + \alpha_3^2 + \alpha_3'^2\big) \leq \frac{|M|}{2}(\alpha_1^2 + \alpha_3^2) + \frac{|M'|}{2}(\alpha_1'^2 + \alpha_3'^2)$$
$$\leq \|r_a\|_{0,M}^2 + \big\|r_a'\big\|_{0,M}^2 .$$

Gathering (4.19), (4.20), the last two estimates and using the fact that ϕ_0 is orthogonal to r_a and r_a' yields the lower bound

$$\big(S_M + S_{M'} + S_{\gamma_c}\big)(q_{\mathcal{P}}, q_{\mathcal{P}}) \geq \|r_a\|_{0,M}^2 + \big\|r_a'\big\|_{0,M}^2 + \frac{1}{4}\|\alpha_0\phi_0\|_{0,\omega_{\gamma_c}}^2 \geq \frac{1}{4}\|r_b\|_{0,\omega_{\gamma_c}}^2 . \quad (4.21)$$

The upper bound follows using that r_b is constant on each $K \subset \omega_{\gamma_c}$ with value r_K and that jumps across at most three edges $e \subset \partial K$ are penalised, i. e.

$$\big(S_M + S_{M'} + S_{\gamma_c}\big)(q_{\mathcal{P}}, q_{\mathcal{P}}) = \big(S_M + S_{M'} + S_{\gamma_c}\big)(r_b, r_b)$$
$$\leq \sum_{e \in \mathcal{E}_M \cup \mathcal{E}_{M'} \cup \{e\colon\, e \subset \gamma_c\}} 2\frac{|K|}{|e|}\int_e (r_K^2 + r_{K'}^2) \leq 6 \sum_{K \subset \omega_{\gamma_c}} |K| r_K^2 = 6\|r_b\|_{0,\omega_{\gamma_c}}^2 .$$

Now, equivalence (4.15b) follows from estimate (4.21) and this upper bound.

Bound $(4.16)_1$ is a consequence of (4.15) and $\|q_{\mathcal{P}} - \Pi_G q_{\mathcal{P}}\|_{0,\omega}^2 + \|\Pi_G q_{\mathcal{P}}\|_{0,\omega}^2 = \|q_{\mathcal{P}}\|_{0,\omega}^2$ for $\omega = M \in \mathcal{P}_0$ or $\omega = \omega_{\gamma_c}$. Finally, estimate $(4.16)_2$ follows using $p \in H^1(M)$ and the arguments used to prove [LS13, estimate (3.24)]. □

Proof of Theorem 4.2. First, by Lemma 4.3 we notice that the pressure space $M_{\mathcal{P}}$ contains a uniformly inf-sup stable subspace G. Then, thanks to (4.15), the stabilisation terms control the non-stable part of $M_{\mathcal{P}}$. Then, (4.9) follows by standard arguments, as in Theorem 3.12 or in [BDG06, LS13, ABW15]. Using (4.16) the a priori estimate also follows known arguments, cf. Theorem 3.14 or [BDG06, LS13, ABW15]. □

4.5. Conclusions

In this chapter we have extended the method from [LS13] to cover the case in which the meshes contain anisotropically refined corners. We have enhanced the aforementioned method with selected, appropriately weighted jumps that improve the stability constant by curing its dependency on $\varrho = h/H$. Finally, it is worth mentioning that the refinement strategy proposed in [LS13] leads to meshes for which the method is as stable as it was on the initial mesh. This explains some numerical results in that reference, since the original mesh used was shape-regular.

4.6. Verifying discrete LBB and stability conditions

For completeness we include the standard result Lemma 4.6. A proof for a special case is given, for instance, in [Mal81, Section 3.B]. However, before we found this result, we proved the general case presented here. Corollary 4.7 is a direct consequence of Lemma 4.6 and justifies our numerical experiments.

Lemma 4.6. *Let $\mathcal{A}, \mathcal{B} \in \mathbb{R}^{n\times n}$ be symmetric matrices and let $\mathcal{B}$ be positive definite. Then, the* generalised eigenvalue problem

$$\mathcal{A}\boldsymbol{v} = \xi\,\mathcal{B}\boldsymbol{v}\,, \tag{4.22}$$

has n real eigenvalues $\{\xi_i\}_i$, and an $\mathcal{A},\mathcal{B}$-orthogonal basis of eigenvectors of $\mathbb{R}^n$, $\{\boldsymbol{v}_i\}_i$, such that

$$\langle \boldsymbol{v}_j, \mathcal{A}\boldsymbol{v}_i\rangle = \xi_i\,\delta_{ij} \quad \textit{and} \quad \langle \boldsymbol{v}_j, \mathcal{B}\boldsymbol{v}_i\rangle = \delta_{ij}\,. \tag{4.23}$$

Moreover, we have the (sharp) discrete inf-sup condition:

$$\sup_{\boldsymbol{v}\in\mathbb{R}^n} \frac{\boldsymbol{v}^\top\mathcal{A}\boldsymbol{u}}{\sqrt{\boldsymbol{v}^\top\mathcal{B}\boldsymbol{v}}} \geq |\xi_1|\sqrt{\boldsymbol{u}^\top\mathcal{B}\boldsymbol{u}} \quad \textit{for all} \quad \boldsymbol{u}\in\mathbb{R}^n \tag{4.24}$$

where ξ_1 is an eigenvalue of Problem (4.22) *of smallest magnitude.*

Proof. Since $\mathcal{B}$ is positive definite, there exists a regular matrix $L \in \mathbb{R}^{n\times n}$, such that $\mathcal{B} = L\,L^\top$. Then, Problem (4.22) is equivalent to a standard eigenvalue problem with a symmetric matrix, i.e.

$$\begin{aligned}\mathcal{A}\boldsymbol{v} = \xi\,\mathcal{B}\boldsymbol{v} &\iff L^{-1}\mathcal{A}L^{-\top}L^\top\boldsymbol{v} = \xi\,L^\top\boldsymbol{v}\\ &\iff \widetilde{\mathcal{A}}\boldsymbol{w} = \xi\,\boldsymbol{w} \qquad\qquad \text{with} \quad \widetilde{\mathcal{A}} = L^{-1}\mathcal{A}L^{-\top}\,.\end{aligned}$$

The equivalent problem is symmetric and has n real eigenvalues $\{\xi_i\}_i$ and a basis of eigenvectors $\{\boldsymbol{w}_i\}_i$ of $\mathbb{R}^n$, such that

$$\widetilde{\mathcal{A}}\boldsymbol{w}_i = \xi_i\,\boldsymbol{w}_i\,, \quad \langle \boldsymbol{w}_j, \boldsymbol{w}_i\rangle = \delta_{ij} \quad \text{and} \quad \left\langle \boldsymbol{w}_j, \widetilde{\mathcal{A}}\boldsymbol{w}_i\right\rangle = \xi_i\,\delta_{ij}\,.$$

Using the regularity of L we define $\boldsymbol{v}_i \coloneqq L^{-T}\boldsymbol{w}_i\,, (i = 1,\dots n)$ and note that $\{\boldsymbol{v}_i\}_i$, is a basis of $\mathbb{R}^n$. Following the equivalence of the eigenvalue problems we realise that each $\boldsymbol{v}_i$ is an eigenvector of (4.22). And, from the equalities above, we obtain

$$\begin{aligned}\langle \boldsymbol{v}_j, \mathcal{B}\boldsymbol{v}_i\rangle &= \left\langle L^\top\boldsymbol{v}_j, L^\top\boldsymbol{v}_i\right\rangle = \langle \boldsymbol{w}_j, \boldsymbol{w}_i\rangle = \delta_{ij}\,,\\ \langle \boldsymbol{v}_j, \mathcal{A}\boldsymbol{v}_i\rangle &= \left\langle L^{-\top}\boldsymbol{w}_j, \mathcal{A}L^{-\top}\boldsymbol{w}_i\right\rangle = \left\langle \boldsymbol{w}_j, \widetilde{\mathcal{A}}\boldsymbol{w}_i\right\rangle = \xi_i\,\delta_{ij}\,,\end{aligned}$$

which proves (4.23).

In order to prove (4.24), let $\boldsymbol{u} \in \mathbb{R}^n$ be given. Using the basis property of $\{\boldsymbol{v}_i\}_{i=1}^n$ we have $\boldsymbol{u} = \sum_{i=1}^n \alpha_i \boldsymbol{v}_i$ and define $\boldsymbol{v} \coloneqq \sum_{i=1}^n \tilde{\alpha}_i \boldsymbol{v}_i$ with $\tilde{\alpha}_i \coloneqq sign(\xi_i)\alpha_i \, (i = 1, \dots, n)$. Now, using (4.23) shows

$$\boldsymbol{v}^\top \mathcal{B} \boldsymbol{v} = \sum_{i=1}^n \tilde{\alpha}_i \Big(\sum_{j=1}^n \tilde{\alpha}_j \langle \boldsymbol{v}_j, \mathcal{B} \boldsymbol{v}_i \rangle \Big) = \sum_{i=1}^n \tilde{\alpha}_i \Big(\sum_{j=1}^n \tilde{\alpha}_j \delta_{ij} \Big) = \sum_{i=1}^n \alpha_i^2 = \boldsymbol{u}^\top \mathcal{B} \boldsymbol{u} \,,$$

and $\sqrt{\boldsymbol{u}^\top \mathcal{B} \boldsymbol{u}} = \sqrt{\boldsymbol{v}^\top \mathcal{B} \boldsymbol{v}}$, respectively. Using this identity and again (4.23), we get

$$\begin{aligned} \boldsymbol{v}^\top \mathcal{A} \boldsymbol{u} = \sum_{i=1}^n \alpha_i \Big(\sum_{j=1}^n \tilde{\alpha}_j \langle \boldsymbol{v}_j, \mathcal{A} \boldsymbol{v}_i \rangle \Big) &= \sum_{i=1}^n \alpha_i \Big(\sum_{j=1}^n \alpha_j sign(\xi_j) \xi_i \delta_{ij} \Big) \\ &= \sum_{i=1}^n \alpha_i^2 \, |\xi_i| \geq |\xi_1| \sum_{i=1}^n \alpha_i^2 = |\xi_1| \sqrt{\boldsymbol{u}^\top \mathcal{B} \boldsymbol{u}} \, \sqrt{\boldsymbol{v}^\top \mathcal{B} \boldsymbol{v}} \,, \end{aligned}$$

which proves (4.24) and its sharpness. □

Corollary 4.7. *Let $\mathfrak{B}$ be as in (4.4) and let $s \colon M_{\mathcal{P}} \times M_{\mathcal{P}} \to \mathbb{R}$ be an arbitrary symmetric non-negative bilinear form. Then*

$$\inf_{(\boldsymbol{u},p) \in \boldsymbol{Q}^c_{1,\mathcal{P}} \times M_{\mathcal{P}}} \sup_{(\boldsymbol{v},q) \in \boldsymbol{Q}^c_{1,\mathcal{P}} \times M_{\mathcal{P}}} \frac{\mathfrak{B}(\boldsymbol{u},p;\boldsymbol{v},q) - s(p,q)}{|||(\boldsymbol{v},q)||| \, |||(\boldsymbol{u},p)|||} = |\xi_1|$$

where ξ_1 is an eigenvalue of smallest magnitude of the problem

$$\begin{pmatrix} A & B \\ B^\top & -S \end{pmatrix} \mathcal{U} = \xi \begin{pmatrix} A & 0 \\ 0 & M \end{pmatrix} \mathcal{U} \tag{4.25}$$

with matrices A, B and S defined as usual from $\mathfrak{B}$ and s, the mass-matrix M on the pressure space $M_{\mathcal{P}}$ and $\mathcal{U} \in \mathbb{R}^n$, $n = \dim(\boldsymbol{Q}^c_{1,\mathcal{P}} \times M_{\mathcal{P}})$.

Proof. We first realise that A and M are symmetric and positive definite. The matrix S is symmetric as its form s. We define

$$\mathcal{A} \coloneqq \begin{pmatrix} A & B \\ B^\top & -S \end{pmatrix}, \quad \mathcal{B} \coloneqq \begin{pmatrix} A & 0 \\ 0 & M \end{pmatrix} \quad \text{and} \quad \mathcal{V} \coloneqq \begin{pmatrix} \boldsymbol{v}^c \\ \boldsymbol{q}^c \end{pmatrix}.$$

Using $\mathcal{V}$ as coefficient vector of $(\boldsymbol{v}, q) \in \boldsymbol{Q}^c_{1,\mathcal{P}} \times M_{\mathcal{P}}$ we obtain

$$\mathcal{V}^\top \mathcal{B} \, \mathcal{V} = |\boldsymbol{v}|^2_{1,\Omega} + \|q\|^2_{0,\Omega} = |||(\boldsymbol{v},q)|||^2 \,,$$

and, using Lemma 4.6 we get

$$\inf_{(\boldsymbol{u},p) \in \boldsymbol{Q}^c_{1,\mathcal{P}} \times M_{\mathcal{P}}} \sup_{(\boldsymbol{v},q) \in \boldsymbol{Q}^c_{1,\mathcal{P}} \times M_{\mathcal{P}}} \frac{\mathfrak{B}(\boldsymbol{u},p;\boldsymbol{v},q) - s(p,q)}{|||(\boldsymbol{v},q)||| \, |||(\boldsymbol{u},p)|||} = \inf_{\mathcal{U} \in \mathbb{R}^n} \sup_{\mathcal{V} \in \mathbb{R}^n} \frac{\mathcal{V}^\top \mathcal{A} \mathcal{U}}{\sqrt{\mathcal{V}^\top \mathcal{B} \, \mathcal{V}} \sqrt{\mathcal{U}^\top \mathcal{B} \mathcal{U}}} = |\xi_1|$$

where ξ_1 is an eigenvalue of smallest magnitude of Problem (4.25). □

Lemma 4.8. *The inf-sup constant defined by*

$$\beta_{\mathcal{P}} \coloneqq \inf_{q \in M_{\mathcal{P}}} \sup_{\boldsymbol{v} \in \boldsymbol{V}_{\mathcal{P}}} \frac{(\operatorname{div} \boldsymbol{v}, q)_\Omega}{|\boldsymbol{v}|_{1,\Omega} \|q\|_{0,\Omega}}$$

satisfies $\beta_{\mathcal{P}}^2 = \xi_1$*, where* ξ_1 *is an eigenvalue of smallest magnitude of the generalised eigenvalue problem*

$$\begin{pmatrix} A & B \\ B^\top & 0 \end{pmatrix} \begin{pmatrix} \boldsymbol{u} \\ p \end{pmatrix} = -\xi \begin{pmatrix} 0 & 0 \\ 0 & M \end{pmatrix} \begin{pmatrix} \boldsymbol{u} \\ p \end{pmatrix}$$

where A, B, M *are the matrices induced by the bilinear forms* $(\operatorname{grad} \boldsymbol{u}, \operatorname{grad} \boldsymbol{v})_\Omega$, $(\operatorname{div} \boldsymbol{v}, p)_\Omega$ *and* $(p, q)_\Omega$.

Proof. See [HSV12, Lemma 9.1]. □

Chapter 5

Low order methods for the Oseen problem

In this chapter, we mix and extend the approaches from Chapter 3, 4 and from [MT15, Bra08] to propose low-order methods for the Oseen equation on meshes containing refined corner patches. To solve this problem we now have to treat two sources of instability. So far we only have dealt with the inf-sup condition. Now, we also allow the case known as the convection-dominated case, in which the instabilities may result in the appearance of spurious (non-physical) oscillations.

Starting with the lowest order $\boldsymbol{Q}_1^c \times \mathbb{P}_0$ pair, we again identify the pressure components that cause this finite element pair to be non-inf-sup stable. We then propose a way to penalise them, both strongly (by directly removing them from the space), and weakly, by adding a stabilisation term based on jumps of the pressure across selected edges. Concerning the velocity stabilisation, we propose an enhanced grad-div term and give a new choice for stabilisation parameters with convincing results for convection-dominated problems. Some of the proofs presented here follow the very general approach given in [MT15].

The presentation is organised as follows. Section 5.1 first recalls the Oseen problem and its weak formulation. Then, the assumptions associated to the mesh are given. After that, results for the Stokes problem are extended to the meshes defined. In particular, we prove the existence of a subspace $G \subset \mathbb{P}_0$ such that the pair $\boldsymbol{Q}_1^c \times G$ satisfies a uniform LBB condition. This is confirmed numerically. Additionally, the existence of the divergence preserving interpolant is stated. In Section 5.2 we then give the general framework for the methods proposed. In Sections 5.2.1 and 5.2.2 stability and a priori estimates are derived. The definition and analysis of the methods leaves the choice of stabilisation terms and parameters flexible. Section 5.3 fixes the latter for the numerical experiments in Section 5.4.

5.1. Notation and preliminary results

As before, constants with capital C are independent of data, but now constants with a lower case c may depend on data. Both the instances of C and c will be independent of all geometric properties of the mesh. We recall the notation for Sobolev spaces and associated norms from Chapter 1.

5.1.1. The problem of interest

Let $\Omega \subset \mathbb{R}^2$ be a polygonal, bounded and connected domain. Then, given a source term $\boldsymbol{f} \in L^2(\Omega)^2$, we consider the following Oseen problem

$$\begin{aligned} -\nu\Delta\boldsymbol{u} + \boldsymbol{b}\cdot\nabla\boldsymbol{u} + \sigma\boldsymbol{u} + \nabla p &= \boldsymbol{f} \quad \text{in } \Omega\,, \\ \operatorname{div}\boldsymbol{u} &= 0 \quad \text{in } \Omega\,, \\ \boldsymbol{u} &= 0 \quad \text{on } \partial\Omega\,, \end{aligned} \tag{5.1}$$

subject to $\langle p\rangle_\Omega = 0$, where $\langle q\rangle_\omega$ denotes the mean value of q over $\omega \subset \Omega$. For simplicity we suppose ν is a positive viscosity constant, σ is a non-negative constant and $\boldsymbol{b} \in \boldsymbol{H}(\operatorname{div},\Omega)\cap L^\infty(\Omega)$, with $\operatorname{div}\boldsymbol{b} = 0$, is a given velocity field.

We let $\boldsymbol{V} \coloneqq \boldsymbol{H}^1_0(\Omega)$, $M \coloneqq L^2_0(\Omega)$ and state a weak formulation of Problem (5.1):

Find $(\boldsymbol{u}, p) \in \boldsymbol{V}\times M$ such that

$$\mathfrak{B}(\boldsymbol{u}, p; \boldsymbol{v}, q) = (\boldsymbol{f}, \boldsymbol{v})_\Omega \quad \text{for all} \quad (\boldsymbol{v}, q) \in \boldsymbol{V}\times M\,, \tag{5.2}$$

where

$$\mathfrak{B}(\boldsymbol{u}, p; \boldsymbol{v}, q) \coloneqq a(\boldsymbol{u}, \boldsymbol{v}) - (\operatorname{div}\boldsymbol{v}, p)_\Omega - (\operatorname{div}\boldsymbol{u}, q)_\Omega\,, \tag{5.3}$$

$$a(\boldsymbol{u}, \boldsymbol{v}) \coloneqq \nu(\nabla\boldsymbol{u}, \nabla\boldsymbol{v})_\Omega + (\boldsymbol{b}\cdot\nabla\boldsymbol{u}, \boldsymbol{v})_\Omega + \sigma(\boldsymbol{u}, \boldsymbol{v})_\Omega\,. \tag{5.4}$$

Using integration by parts and $\operatorname{div}\boldsymbol{b} = 0$ the bilinear form a induces the norm

$$\|\boldsymbol{v}\|_a^2 \coloneqq a(\boldsymbol{v}, \boldsymbol{v}) = \nu|\boldsymbol{v}|_{1,\Omega}^2 + \sigma\|\boldsymbol{v}\|_{0,\Omega}^2 \quad \text{for all} \quad \boldsymbol{v} \in \boldsymbol{V}\,. \tag{5.5}$$

If $\sigma = 0$, then thanks to the *Poincaré inequality*

$$\exists C_\Omega > 0\, \forall \boldsymbol{v} \in \boldsymbol{V}\colon \|\boldsymbol{v}\|_{0,\Omega} \le C_\Omega|\boldsymbol{v}|_{1,\Omega}\,, \tag{5.6}$$

$\|\cdot\|_a$ remains a norm. The *Poincaré constant* C_Ω will be of constant use throughout. Again, the inf-sup condition (1.6) holds, cf. Chapter 1. From (5.5) and (1.6) it follows that the Oseen problem (5.2) has a unique solution, see for instance [GR86]. Finally, the following continuity estimates will be of use in the stability and convergence analysis.

Lemma 5.1. *For all $\boldsymbol{w}, \boldsymbol{v} \in \boldsymbol{V}$ the following inequalities hold*

$$\|\boldsymbol{v}\|_{0,\Omega}^2 \leq \frac{C_\Omega^2}{\nu + \sigma C_\Omega^2} \|\boldsymbol{v}\|_a^2 \,, \tag{5.7}$$

and

$$a(\boldsymbol{w}, \boldsymbol{v}) \leq c_a \|\boldsymbol{w}\|_a |\boldsymbol{v}|_{1,\Omega} \quad \textit{where} \quad c_a \coloneqq \frac{\nu + \sigma C_\Omega^2 + b_{\infty,\Omega}\, C_\Omega}{\left(\nu + \sigma C_\Omega^2\right)^{1/2}} \tag{5.8}$$

with C_Ω from (5.6) *and $b_{\infty,\omega} \coloneqq \|\boldsymbol{b}\|_{\infty,\omega}$ for $\omega \subseteq \overline{\Omega}$.*

Proof. Using the Poincaré inequality (5.6) and a basic computation, we get

$$\|\boldsymbol{v}\|_{0,\Omega}^2 \leq \min_{t\in[0,1]} \left(\frac{(1-t)^2}{\sigma} + \frac{t^2 C_\Omega^2}{\nu} \right) \|\boldsymbol{v}\|_a^2 = \frac{C_\Omega^2}{\nu + \sigma C_\Omega^2} \|\boldsymbol{v}\|_a^2 \,.$$

To prove (5.8), we consider (5.4), (5.5) and estimate each term. First, we obtain

$$\begin{aligned} \nu(\nabla \boldsymbol{w}, \nabla \boldsymbol{z})_\Omega + \sigma(\boldsymbol{w}, \boldsymbol{z})_\Omega &\leq \left(\nu |\boldsymbol{z}|_{1,\Omega}^2 + \sigma \|\boldsymbol{z}\|_{0,\Omega}^2 \right)^{1/2} \|\boldsymbol{w}\|_a \\ &\leq \left(\nu + \sigma C_\Omega^2\right)^{1/2} |\boldsymbol{z}|_{1,\Omega} \|\boldsymbol{w}\|_a . \end{aligned}$$

Now, integrating by parts, using $\operatorname{div} \boldsymbol{b} = 0$, and (5.7) we get

$$|(\boldsymbol{b}\cdot\nabla \boldsymbol{w}, \boldsymbol{z})_\Omega| = |(\boldsymbol{b}\cdot\nabla \boldsymbol{z}, \boldsymbol{w})_\Omega| \leq b_{\infty,\Omega} |\boldsymbol{z}|_{1,\Omega} \|\boldsymbol{w}\|_{0,\Omega} \leq \frac{b_{\infty,\Omega}\, C_\Omega}{\left(\nu + \sigma C_\Omega^2\right)^{1/2}} |\boldsymbol{z}|_{1,\Omega} \|\boldsymbol{w}\|_a . \tag{5.9}$$

Adding these estimates proves the claim. □

5.1.2. Partition and finite elements

Within this chapter, we assume the partition $\mathcal{P}$ to satisfy assumptions very similar to those of Chapter 4, but with a small change concerning the notation associated with the corners. This allows us to generalise some results.

In particular, we assume $\mathcal{P}$ has been obtained by a uniform refinement from a macro element partition $\mathcal{P}_0$. Where $\mathcal{P}_0$ is a conforming partition of Ω consisting of closed parallelograms, and satisfying a maximal angle condition. Again, $\mathcal{P}_0$ is allowed to be highly anisotropic and contain corner patches, for instance, as in Chapter 3 and 4. See for example the shaded cells and their neighbourhoods in Figures 5.1–5.3. Similar to Chapter 4:

- K is an element of $\mathcal{P}$,
- M belongs to $\mathcal{P}_0$ and will be called *macro element*,
- M is split into four elements of $\mathcal{P}$ possessing the same angles and area $|M|/4$,

- $\mathcal{E}_{\mathcal{P}}$ is the set of interior edges, and
- for $M \in \mathcal{P}_0$, let $\mathcal{E}_M$ be the set of edges inside M, dashed in Figures 5.1–5.3.

One of the interests in this chapter is to extend the previous results to refined corner patches. That is why the nodes $\mathcal{C}$, edges $\gamma_{\boldsymbol{c}}$ and subdomains $\omega_{\boldsymbol{c}}$ are re-defined as follows:

- Let $\mathcal{C}$ be the set of *corners*, that is, nodes $\boldsymbol{c}$ of the mesh $\mathcal{P}_0$ towards which the mesh is graded, denoted by filled circles in Figures 5.1–5.3. For $\boldsymbol{c} \in \mathcal{C}$, we denote by $\omega_{\boldsymbol{c}}$ the area around $\boldsymbol{c}$ that is partitioned in a shape-regular way (shaded in Figures 5.1–5.3). Moreover, for $\boldsymbol{c} \in \mathcal{C}$, we select a single edge $\gamma_{\boldsymbol{c}} \in \mathcal{E}_{\mathcal{P}}$ that separates an extremely small corner macro element (shaded) from a highly stretched neighbouring macro element, for example, the embraced edges in Figures 5.1–5.3. The selected edges $\gamma_{\boldsymbol{c}}$ are collected in the set $\mathcal{E}_{\mathcal{C}}$.

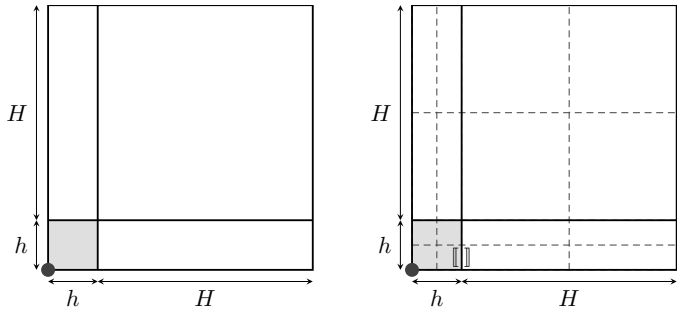

Fig. 5.1. Partition $\mathcal{P}_0$ (left) and $\mathcal{P}$ (right)

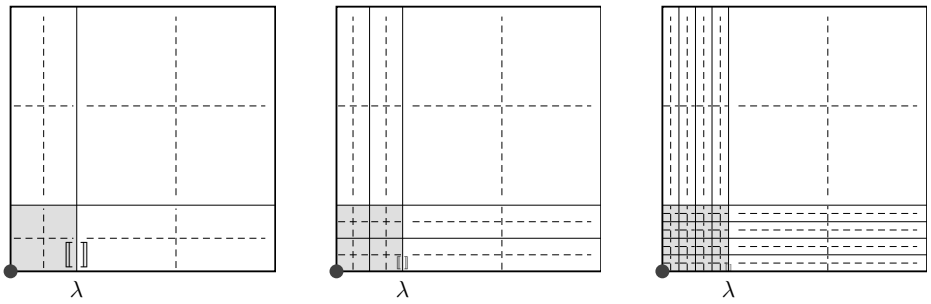

Fig. 5.2. Corner patches on $[0, \lambda + H]^2$ whose corners were refined r times ($r = 0, 1, 2$).

We point out that the condition "$\mathcal{P}$ arises from a uniform refinement of $\mathcal{P}_0$" still allows local (macro-element based) refinements as described in [LS13]. These may produce further anisotropies. In particular, instead of $\mathcal{P}_0$, an initial partition $\mathcal{P}_r$, that contains corner patches that have been refined uniformly r-times, may be used as a macro-element mesh for $\mathcal{P}$, cf. Figure 5.2.

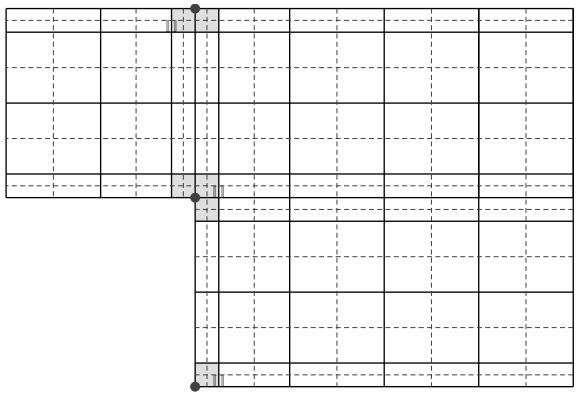

Fig. 5.3. Jumps on an anisotropic mesh for a flow over step problem.

Finally, we define the finite element spaces

$$\boldsymbol{Q}^c_{\ell,\mathcal{P}} \coloneqq \left\{\boldsymbol{v} \in \boldsymbol{V} \colon \boldsymbol{v}|_K \in \mathbb{Q}_\ell(K)^2 \quad \text{for all} \quad K \in \mathcal{P}\right\},\ \ell = 1, 2\,, \tag{5.10}$$

and

$$M_{\mathcal{P}} \coloneqq \{q \in M \colon q|_K \in \mathbb{P}_0(K) \quad \text{for all} \quad K \in \mathcal{P}\}\,, \tag{5.11}$$

and seek an approximation of the solution $(\boldsymbol{u}, p)$ of Problem (5.1) within the discrete space $\boldsymbol{Q}^c_{1,\mathcal{P}} \times M_{\mathcal{P}}$.

5.1.3. Preliminary results

It is well known that $\boldsymbol{Q}^c_{1,\mathcal{P}} \times M_{\mathcal{P}}$ is not inf-sup stable. On the other hand, since $\boldsymbol{Q}^c_{1,\mathcal{P}}$ and $\boldsymbol{Q}^c_{2,\mathcal{P}_0}$ share the same degrees of freedom, $\boldsymbol{Q}^c_{1,\mathcal{P}} \times M_{\mathcal{P}_0}$ is inf-sup stable. Now, the inf-sup constant of the latter pair is affected by geometrical properties of $\mathcal{P}_0$, since $\mathcal{P}_0$ contains corner patches, cf. Chapter 4, condition (4.2). We realised (Remark 3.2) that the deficiency is caused by non-local geometric quantities, which is again indicated by Remark 5.3 below. However, we solve the issue in the next result where we impose a minimal set of additional constraints to obtain a uniformly inf-sup stable subspace G of $M_{\mathcal{P}_0}$.

Lemma 5.2. *Let $G \subset M_{\mathcal{P}_0} \subset M_{\mathcal{P}}$ be the space defined by*

$$G \coloneqq \left\{q \in M_{\mathcal{P}_0} \colon [\![q]\!]_{\gamma_{\boldsymbol{c}}} = 0 \quad \textit{for} \quad \gamma_{\boldsymbol{c}} \in \mathcal{E}_{\mathcal{C}}\right\}. \tag{5.12}$$

Then, the following inf-sup condition holds

$$\sup_{\boldsymbol{v} \in \boldsymbol{Q}^c_{1,\mathcal{P}}} \frac{(\operatorname{div} \boldsymbol{v}, q)_\Omega}{|\boldsymbol{v}|_{1,\Omega}} \geq \beta_G \|q\|_{0,\Omega} \quad \textit{for all} \quad q \in G\,, \tag{5.13}$$

with a constant $\beta_G \geq \max\{\beta_{\mathcal{P}_0}, C/2^r\}$*, where* C *is independent of the mesh and data. Equivalently, the following inf-sup deficiency holds*

$$\sup_{\boldsymbol{v}\in\boldsymbol{Q}^c_{1,\mathcal{P}}} \frac{(\operatorname{div}\boldsymbol{v}, q)_\Omega}{|\boldsymbol{v}|_{1,\Omega}} \geq \beta_G \|\Pi_G q\|_{0,\Omega} - \|q - \Pi_G q\|_{0,\Omega} \quad \textit{for all} \quad q \in M_{\mathcal{P}}\,, \tag{5.14}$$

where $\Pi_G\colon M_{\mathcal{P}} \to G$ *stands for the* L^2*-projection onto* G*.*

Proof. The proof follows a similar path as in [ABW15] allowing the extension to refined corner patches. For completeness we include an abridged version here. We first prove (5.13). Since $G \subset M_{\mathcal{P}_0}$, we have $\beta_G \geq \beta_{\mathcal{P}_0}$. For the alternative $\beta_G \geq C/2^r$, we proceed as in [ABW15]. First, we define

$$M^*_{\mathcal{P}_0} \coloneqq \big\{q \in M_{\mathcal{P}_0}\colon \langle q\rangle_{\omega_{\boldsymbol{c}}} = 0 \text{ for } \boldsymbol{c} \in \mathcal{C}\big\}.$$

Analogously to [ABW15, Corollary 3.1], for all $q^* \in M^*_{\mathcal{P}_0}$ there exists $\boldsymbol{v}^* \in \boldsymbol{Q}^c_{1,\mathcal{P}}$ such that $\boldsymbol{v}^*|_{\omega_{\boldsymbol{c}}} \in \boldsymbol{H}^1_0(\omega_{\boldsymbol{c}})$ for every $\boldsymbol{c} \in \mathcal{C}$, and

$$(\operatorname{div}\boldsymbol{v}^*, q^*)_\Omega = \|q^*\|_{0,\Omega} \quad \text{and} \quad |\boldsymbol{v}^*|_{1,\Omega} \leq C\|q^*\|_{0,\Omega}\,, \tag{5.15}$$

where $C > 0$ depends only on Ω. Now, as in [ABW15, Lemma 3.2], we decompose $q \in G$ into $q = \Pi_{\mathcal{C}} q + q^*$ where $\Pi_{\mathcal{C}} q|_{\omega_{\boldsymbol{c}}}$ (for $\boldsymbol{c} \in \mathcal{C}$) and $\Pi_{\mathcal{C}} q|_{\Omega\setminus(\cup_{\boldsymbol{c}\in\mathcal{C}}\omega_{\boldsymbol{c}})}$ are constants and $q^* \in M^*_{\mathcal{P}_0}$. Then, since $(\operatorname{div}\boldsymbol{v}^*, \Pi_{\mathcal{C}} q)_\Omega = 0$ we get $(\operatorname{div}\boldsymbol{v}^*, q) = \|q^*\|^2_{0,\Omega}$. Therefore, (5.15) implies (5.13), once the following is proved

$$\|q\|_{0,\Omega} \leq C2^r\|q^*\|_{0,\Omega}\,. \tag{5.16}$$

Following analogous steps to those from [ABW15, Lemma 3.2] we conclude that $\|\Pi_{\mathcal{C}} q\|^2_{0,\Omega} \leq C\sum_{\boldsymbol{c}\in\mathcal{C}}|\omega_{\boldsymbol{c}}|\langle[\![q^*]\!]\rangle^2_{\gamma_{\boldsymbol{c}}}$. Next, we bound each of these jumps as

$$|\omega_{\boldsymbol{c}}|\langle[\![q^*]\!]\rangle^2_{\gamma_{\boldsymbol{c}}} \leq C|\omega_{\boldsymbol{c}}||\kappa_{\boldsymbol{c}}|^{-1}\|q^*\|^2_{0,\kappa_{\boldsymbol{c}}\cup K_{\boldsymbol{c}}} = C2^{2r}\|q^*\|^2_{0,\Omega}\,,$$

since $|\omega_{\boldsymbol{c}}||\kappa_{\boldsymbol{c}}|^{-1} = 2^{2r}$, and then (5.16) follows.

Given (5.13) the proof of [ABW15, Lemma 4.1] implies (5.14). The reverse follows using only $\Pi_G q = q$ for $q \in G$. □

Remark 5.3. *For a single corner patch we conclude from* (5.15) *that the spurious mode on the (refined) corner patches in Figure 5.2 is given by the function connecting the (uniformly stable) average free spaces on* $\omega_{\boldsymbol{c}} \coloneqq [0,\lambda]\times[0,\lambda]$ *and* $\Omega \setminus \omega_{\boldsymbol{c}}$*, that is,*

$$q_B \coloneqq \chi_{\omega_{\boldsymbol{c}}} - \frac{|\omega_{\boldsymbol{c}}|}{|\Omega\setminus\omega_{\boldsymbol{c}}|}\chi_{\Omega\setminus\omega_{\boldsymbol{c}}}\,.$$

Hence for small enough λ *we have* $\beta_{\mathcal{P}_0} = \beta_{\mathcal{P}_1} = \ldots = \beta_{\mathcal{P}_r}$*.*

Remark 5.4. *We stress the fact that β_G only depends on how refined the partition $\mathcal{P}_0$ is. This is reflected by the factor 2^r in β_G. This unfortunate behaviour can be easily solved by limiting the number of refinements and instead moving λ closer to the nodes $\boldsymbol{c}$, since β_G is independent of λ.*

The next result shows the existence of a divergence preserving interpolant on partitions that contain (refined) corner patches.

Lemma 5.5. *Let $G \subset M_{\mathcal{P}}$ be defined as in Lemma 5.2. Then, there exists $\boldsymbol{u}_I \in \boldsymbol{Q}^c_{1,\mathcal{P}}$ such that*

$$(\operatorname{div}(\boldsymbol{u} - \boldsymbol{u}_I), q)_\Omega = 0 \quad \textit{for all} \quad q \in G\,, \tag{5.17}$$

and

$$|\boldsymbol{u} - \boldsymbol{u}_I|_{1,\Omega} \leq (1 + C\beta_G^{-1}) \inf_{\boldsymbol{v}_{\mathcal{P}} \in \boldsymbol{Q}^c_{1,\mathcal{P}}} |\boldsymbol{u} - \boldsymbol{v}_{\mathcal{P}}|_{1,\Omega}\,. \tag{5.18}$$

Proof. Let $(\boldsymbol{\phi}_{\mathcal{P}}, \chi_{\mathcal{P}}) \in \boldsymbol{Q}^c_{1,\mathcal{P}} \times G$ be the solution of the following auxiliary problem:

$$\begin{aligned} (\nabla \boldsymbol{\phi}_{\mathcal{P}}, \nabla \boldsymbol{v})_\Omega - (\operatorname{div} \boldsymbol{v}, \chi_{\mathcal{P}})_\Omega &= (\nabla \boldsymbol{u}, \nabla \boldsymbol{v})_\Omega \quad \text{for all } \boldsymbol{v} \in \boldsymbol{Q}^c_{1,\mathcal{P}}\,, \\ (\operatorname{div} \boldsymbol{\phi}_{\mathcal{P}}, q)_\Omega &= (\operatorname{div} \boldsymbol{u}, q)_\Omega \quad \text{for all } q \in G\,. \end{aligned} \tag{5.19}$$

The well-posedness of this problem is a consequence of (5.13). Then, defining $\boldsymbol{u}_I \coloneqq \boldsymbol{\phi}_{\mathcal{P}}$, (5.17) follows immediately from (5.19). Moreover, since $(\boldsymbol{u}_I, \chi_{\mathcal{P}})$ is a finite element approximation of $(\boldsymbol{u}, 0)$, (5.18) follows by standard arguments, see e.g. [GR86, p.115].□

5.1.4. Numerical confirmation (part 1)

In this section we show the improvement of β_G over $\beta_{\mathcal{P}_0}$. For simplicity we restrict the presentation of β_G to partitions on the unit square $\Omega = (0,1)\times(0,1)$. To this end, we define a parametrized (by $\lambda > 0$), refined corner patch $\mathcal{P}^c_r$ as the tensor-product of the following one-dimensional interval subdivision of $[0,1]$. The parameter $\lambda < 1/2$ separates a coarse and a fine region in $[0,1]$. The interval $[0,\lambda]$ is split into 2^r intervals of length $h \coloneqq \lambda/2^r$ and $[\lambda,1]$ remains unsplit. Figure 5.2 shows $\mathcal{P}_0 = \mathcal{P}^c_r (r = 0,1,2)$ as continuous lines and the uniform refinement $\mathcal{P}$ of $\mathcal{P}_0$ is indicated by the dashed lines. The subspace $G \subset M_{\mathcal{P}_0}$ additionally imposes the continuity across the edges $\mathcal{E}_{\mathcal{C}}$.

We have computed β_G and $\beta_{\mathcal{P}_0}$ for different levels of refinements while letting $\lambda \to 0$. The results are depicted in Figure 5.4. The constant β_G remains independent of λ, as predicted by Lemma 5.2.

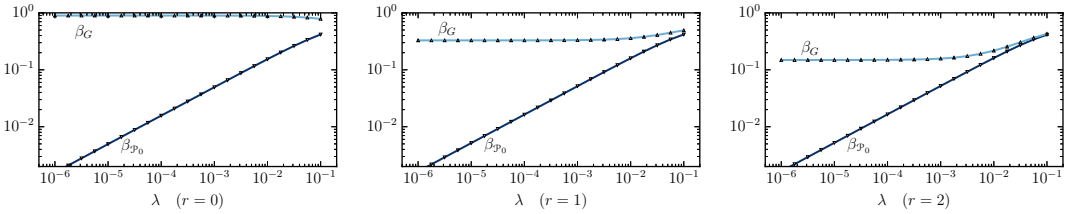

Fig. 5.4. Refined corner patches, from left to right $r = 0, 1, 2$ times refined.

5.2. The stabilised method for the Oseen equation

The stabilised method proposed in this chapter reads:

Find $(\boldsymbol{u}_\mathcal{P}, p_\mathcal{P}) \in \boldsymbol{Q}^c_{1,\mathcal{P}} \times M_\mathcal{P}$ such that

$$\mathfrak{B}_s(\boldsymbol{u}_\mathcal{P}, p_\mathcal{P}; \boldsymbol{v}_\mathcal{P}, q_\mathcal{P}) = (\boldsymbol{f}, \boldsymbol{v}_\mathcal{P})_\Omega \quad \text{for all} \quad (\boldsymbol{v}_\mathcal{P}, q_\mathcal{P}) \in \boldsymbol{Q}^c_{1,\mathcal{P}} \times M_\mathcal{P}\,, \tag{5.20}$$

where

$$\mathfrak{B}_s(\boldsymbol{u}, p; \boldsymbol{v}, q) \coloneqq \mathfrak{B}(\boldsymbol{u}, p; \boldsymbol{v}, q) + s_v(\boldsymbol{u}, \boldsymbol{v}) - s_p(p, q)\,, \tag{5.21}$$

and s_v and s_p are symmetric, positive semi-definite bilinear forms aimed at stabilising velocity and pressure, respectively. In order to prove stability and a priori estimates we need to make assumptions on s_v and s_p. For this purpose, we define

$$|\boldsymbol{v}|^2_{s_v} \coloneqq s_v(\boldsymbol{v}, \boldsymbol{v}) \quad \text{and} \quad \|\boldsymbol{v}\|^2_{a+s} \coloneqq \|\boldsymbol{v}\|^2_a + |\boldsymbol{v}|^2_{s_v}\,, \tag{5.22}$$

and the bilinear form

$$s_v^{div}(\boldsymbol{u}; \boldsymbol{v}) \coloneqq \sum_{K \in \mathcal{P}} \gamma_K (\kappa_K(\operatorname{div} \boldsymbol{u}), \operatorname{div} \boldsymbol{v})_K\,, \quad \gamma_K \geq 0\,, \tag{5.23}$$

where $\kappa_\omega \coloneqq \mathrm{id} - \langle\cdot\rangle_\omega$ denotes the fluctuation operator. Then, the main assumptions on s_v and s_p are now stated.

Assumption 5.6. *Let $\boldsymbol{v}, \boldsymbol{w} \in \boldsymbol{V}$. There exists a positive constant c_s, which may depend on the data, but is independent of the mesh, such that*

$$s_v(\boldsymbol{w}, \boldsymbol{v}) \leq c_s |\boldsymbol{w}|_{s_v} |\boldsymbol{v}|_{1,\Omega}\,. \tag{5.24}$$

Furthermore, s_v is assumed to satisfy

$$s_v(\boldsymbol{w}, \boldsymbol{v}) \leq s_v(\boldsymbol{w}, \boldsymbol{w})^{1/2} s_v(\boldsymbol{v}, \boldsymbol{v})^{1/2}\,, \tag{5.25}$$

$$s_v^{div}(\boldsymbol{v}; \boldsymbol{v}) \leq s_v(\boldsymbol{v}, \boldsymbol{v})\,, \tag{5.26}$$

where s_v^{div} is given by the LPS-like term (5.23).

The pressure stabilisation is given by

$$s_p(p,q) \coloneqq \frac{\alpha_p}{4} \sum_{M\in\mathcal{P}_0} S_M(p,q) + \frac{\alpha_p}{4} \sum_{\gamma_{\boldsymbol{c}}\in\mathcal{E}_{\mathcal{C}}} S_{\gamma_{\boldsymbol{c}}}(p,q)\,, \tag{5.27a}$$

with $\alpha_p \geq \alpha$ (α given below in (5.28)) and

$$S_M(p,q) \coloneqq \sum_{e\in\mathcal{E}_M} \frac{|M|}{4|e|}([\![p]\!],[\![q]\!])_e\,, \tag{5.27b}$$

$$S_{\gamma_{\boldsymbol{c}}}(p,q) \coloneqq \frac{\min\{|K|,|K'|\}}{|\gamma_{\boldsymbol{c}}|}([\![p]\!],[\![q]\!])_{\gamma_{\boldsymbol{c}}}\,, \tag{5.27c}$$

where $K, K' \in \mathcal{P}$ such that $\gamma_{\boldsymbol{c}} = K \cap K'$.

Remark 5.7. *For $q \in G$ we realise that $s_p(q,q) = 0$. Consequently, s_p is only relevant to functions not in G. Moreover, if the mesh $\mathcal{P}_0$ does not contain corner patches, then $S_{\gamma_{\boldsymbol{c}}} \coloneqq 0$ and the present term s_p appears as an extension of the one from [LS13] to the Oseen equation.*

5.2.1. Stability of the method

The stability and convergence will be analysed using the norm

$$|||(\boldsymbol{v},q)|||^2 \coloneqq \|\boldsymbol{v}\|_{a+s}^2 + \alpha\|q\|_{0,\Omega}^2 + s_p(q,q) \quad \text{with} \quad \alpha \coloneqq \frac{1}{c_a^2 + c_s^2}\,, \tag{5.28}$$

with c_a and c_s defined by (5.8) and (5.24), respectively.

This section is devoted to proving that method (5.20) is stable with a stability constant depending only on β_G. The first step towards this result is stated next.

Lemma 5.8. *Let $q_{\mathcal{P}} \in M_{\mathcal{P}}$, $p \in H^1(\Omega)$ and Π_G be the projection from Lemma 5.2. Then, the following holds*

$$\frac{1}{16}\alpha_p\|q_{\mathcal{P}} - \Pi_G q_{\mathcal{P}}\|_{0,\Omega}^2 \leq s_p(q_{\mathcal{P}}, q_{\mathcal{P}})\,, \tag{5.29}$$

$$s_p(q_{\mathcal{P}}, q_{\mathcal{P}}) \leq C\alpha_p \sum_{K\in\mathcal{P}} \left(\|p - q_{\mathcal{P}}\|_{0,K}^2 + |e_{1,K}|^2\|\partial_{t_1}p\|_{0,K}^2 + |e_{2,K}|^2\|\partial_{t_2}p\|_{0,K}^2\right), \tag{5.30}$$

where $e_{1,K}$ and $e_{2,K}$ are two non-parallel edges of K, and $\partial_{t_i}(i = 1,2)$ are partial derivatives in their directions and C is a constant independent of mesh, angles, and data.

Proof. We start with (5.29). This proof uses notation and conventions from Figure 5.5. Our assumptions on the partitions $\mathcal{P}$ and $\mathcal{P}_0$ imply that every selected edge $\gamma_{\boldsymbol{c}} \in \mathcal{E}_{\mathcal{C}}$ satisfies $\gamma_{\boldsymbol{c}} \subset M \cap M'$ where $M, M' \in \mathcal{P}_0$ and $|M| \leq |M'|$. For readability we define $\omega_{\gamma_{\boldsymbol{c}}} \coloneqq M \cup M'$. Now, from its definition $\Pi_G q$ is given by

$$\Pi_G q\big|_M = \begin{cases} \langle q \rangle_{\omega_{\gamma_{\boldsymbol{c}}}} & \text{if } M \subset \omega_{\gamma_{\boldsymbol{c}}}\,, \\ \langle q \rangle_M & \text{otherwise.} \end{cases} \tag{5.31}$$

Therefore, bound (5.29) follows once we prove the local bounds

$$2\alpha_p \|q_{\mathcal{P}} - \langle q_{\mathcal{P}} \rangle_M\|_{0,M}^2 \leq \alpha_p\, S_M(q_{\mathcal{P}}, q_{\mathcal{P}})\,, \tag{5.32a}$$

$$\frac{1}{16}\alpha_p \big\|q_{\mathcal{P}} - \langle q_{\mathcal{P}} \rangle_{\omega_{\gamma_{\boldsymbol{c}}}}\big\|_{\omega_{\gamma_{\boldsymbol{c}}}}^2 \leq \alpha_p \big(S_M + S_{M'} + S_{\gamma_{\boldsymbol{c}}}\big)(q_{\mathcal{P}}, q_{\mathcal{P}})\,. \tag{5.32b}$$

The first estimate follows from multiplying (4.18) through by α_p. We recall notation to prepare the proof of (5.32b).

Let $M \in \mathcal{P}_0$ be a macro element such that $M \not\subset \omega_{\gamma_{\boldsymbol{c}}}$, $\gamma_{\boldsymbol{c}} \in \mathcal{E}_{\mathcal{C}}$. Then, we recall $M_{\mathcal{P}}(M) \subset L_0^2(M)$ and its orthogonal basis (cf. proof of Lemma 4.5):

$$\phi_{1,M} \coloneqq \chi_{K_1} - \chi_{K_2}\,, \quad \phi_{2,M} \coloneqq \chi_{K_1 \cup K_2} - \chi_{K_3 \cup K_4} \quad \text{and} \quad \phi_{3,M} \coloneqq \chi_{K_3} - \chi_{K_4}\,,$$

where χ_ω is the characteristic function of ω. Moreover, $r_a \coloneqq (q_{\mathcal{P}} - \langle q_{\mathcal{P}} \rangle_M)|_M$ belongs to $M_{\mathcal{P}}(M)$ and can be written as $r_a = \sum_{i=1}^3 \alpha_i \phi_i$ with appropriate coefficients α_i.

To prove (5.32b), we fix an edge $\gamma_{\boldsymbol{c}} \in \mathcal{E}_{\mathcal{C}}$ and let $r_b \coloneqq \big(q_{\mathcal{P}} - \langle q_{\mathcal{P}} \rangle_{\omega_{\gamma_{\boldsymbol{c}}}}\big)\big|_{\omega_{\gamma_{\boldsymbol{c}}}}$. Then

$$r_b = \alpha_0 \phi_0 + r_a + r_a'\,,$$

where $\phi_0 = |M|^{-1}\chi_M - |M'|^{-1}\chi_{M'}$, $r_a = \sum_{i=1}^3 \alpha_i \phi_{i,M}$ and $r_a' = \sum_{i=1}^3 \alpha_i' \phi_{i,M'}$. Using (5.32a), the definition of ϕ_0 and $|K| \leq |K'|$ (since $|M| \leq |M'|$) we get

$$\big(S_M + S_{M'} + S_{\gamma_{\boldsymbol{c}}}\big)(q_{\mathcal{P}}, q_{\mathcal{P}}) \geq 2\|r_a\|_{0,M}^2 + 2\big\|r_a'\big\|_{0,M'}^2 + \frac{|K|}{|\gamma_{\boldsymbol{c}}|}\|[\![r_b]\!]\|_{0,\gamma_{\boldsymbol{c}}}^2\,. \tag{5.33}$$

It only remains to bound the last term. Using $[\![r_b]\!]_{\gamma_{\boldsymbol{c}}}, [\![\phi_0]\!]_{\gamma_{\boldsymbol{c}}} \in \mathbb{P}_0(\gamma_{\boldsymbol{c}})$ and the linearity

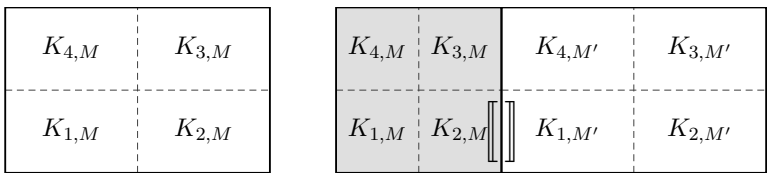

Fig. 5.5. A macro element $M \in \mathcal{P}_0$ (left) and set $\omega_{\gamma_{\boldsymbol{c}}}$ (right) with cells $K_{i,M} \in \mathcal{P}$.

of the jump, followed by $ab \leq \frac{1}{4}a^2 + b^2$ we obtain

$$\begin{aligned}\frac{\|[\![r_b]\!]\|^2_{0,\gamma_{\boldsymbol{c}}}}{|\gamma_{\boldsymbol{c}}|} &= \Big([\![\alpha_0\phi_0]\!]_{\gamma_{\boldsymbol{c}}} + \alpha_2 - \alpha_2' - \alpha_1 - \alpha_1'\Big)^2 \\ &= [\![\alpha_0\phi_0]\!]^2_{\gamma_{\boldsymbol{c}}} + 2[\![\alpha_0\phi_0]\!]_{\gamma_{\boldsymbol{c}}}\big(\alpha_2 - \alpha_2' - \alpha_1 - \alpha_1'\big) + \big(\alpha_2 - \alpha_2' - \alpha_1 - \alpha_1'\big)^2 \\ &\geq \frac{1}{2}[\![\alpha_0\phi_0]\!]^2_{\gamma_{\boldsymbol{c}}} - \big(\alpha_2 - \alpha_2' - \alpha_1 - \alpha_1'\big)^2 \\ &\geq \frac{1}{2}[\![\alpha_0\phi_0]\!]^2_{\gamma_{\boldsymbol{c}}} - 4\big(\alpha_2^2 + \alpha_2'^2 + \alpha_1^2 + \alpha_1'^2\big)\,,\end{aligned}$$

and conclude

$$\frac{|K|}{|\gamma_{\boldsymbol{c}}|}\|[\![r_b]\!]\|^2_{0,\gamma_{\boldsymbol{c}}} \geq \frac{|K|}{2|\gamma_{\boldsymbol{c}}|}\|[\![r_b]\!]\|^2_{0,\gamma_{\boldsymbol{c}}} \geq \frac{|K|}{4}[\![\alpha_0\phi_0]\!]^2_{\gamma_{\boldsymbol{c}}} - 2|K|\big(\alpha_2^2 + \alpha_2'^2 + \alpha_1^2 + \alpha_1'^2\big). \tag{5.34}$$

Now, using the definition of ϕ_0 and $|K| = |M|/4$ we get

$$\frac{|K|}{4}[\![\alpha_0\phi_0]\!]^2_{\gamma_{\boldsymbol{c}}} = \alpha_0^2\frac{|M|}{16}\left(\frac{1}{|M|} + \frac{1}{|M'|}\right)^2 \geq \frac{\alpha_0^2}{16}\left(\frac{1}{|M|} + \frac{1}{|M'|}\right) = \frac{1}{16}\|\alpha_0\phi_0\|^2_{0,\omega_{\gamma_{\boldsymbol{c}}}}, \tag{5.35}$$

and, since $|M| \leq |M'|$

$$\begin{aligned}2|K|\big(\alpha_1^2 + \alpha_1'^2 + \alpha_2^2 + \alpha_2'^2\big) &\leq \frac{|M|}{2}(\alpha_1^2 + \alpha_2^2) + \frac{|M'|}{2}(\alpha_1'^2 + \alpha_2'^2) \\ &\leq \|r_a\|^2_{0,M} + \big\|r_a'\big\|^2_{0,M}\,.\end{aligned} \tag{5.36}$$

Inserting (5.34)–(5.36) into (5.33) and using that ϕ_0 is orthogonal to $\phi_{i,M}$, $\phi_{i,M'}, i = 1,2,3$ leads to

$$\big(S_M + S_{M'} + S_{\gamma_{\boldsymbol{c}}}\big)(q_{\mathcal{P}}, q_{\mathcal{P}}) \geq \|r_a\|^2_{0,M} + \big\|r_a'\big\|^2_{0,M} + \frac{1}{16}\|\alpha_0\phi_0\|^2_{0,\omega_{\gamma_{\boldsymbol{c}}}} \geq \frac{1}{16}\|r_b\|^2_{0,\omega_{\gamma_{\boldsymbol{c}}}}\,,$$

which proves (5.32b).

Finally, using $p \in H^1(\Omega)$, and $[\![p]\!]_e = 0$ a.e. on $e \in \mathcal{E}_{\mathcal{P}}$, and the trace estimate (2.3b) (Section 2.2.1) we bound each jump as follows:

$$\begin{aligned}\frac{|K|}{|e_i|}\|[\![p - q_{\mathcal{P}}]\!]\|^2_{0,e_i} &\leq 2\sum_{K\colon e_i\subset K}\|p - q_{\mathcal{P}}\|_{0,K}\Big(\|p - q_{\mathcal{P}}\|_{0,K} + 2|e_j|\,\|\boldsymbol{t}_j\cdot\nabla\eta_p\|_{0,K}\Big) \\ &\leq 4\sum_{K\colon e_i\subset K}\Big(\|p - q_{\mathcal{P}}\|^2_{0,K} + 2|e_j|^2\|\boldsymbol{t}_j\cdot\nabla\eta_p\|^2_{0,K}\Big)\,,\end{aligned}$$

where $i = 1, j = 2$ or $i = 2, j = 1$. Then, we sum over the edges across which s_p contains jumps and note for each $K \in \mathcal{P}$, that s_p contains jumps across at least two and at most three different edges. This proves estimate (5.30) and finishes the proof.□

We now present the main stability result.

Theorem 5.9. *Let Assumption 5.6 be satisfied, let $|||\cdot|||$ be defined by (5.28), and s_p by (5.27) with $\alpha_p \geq \alpha$. Then,*

$$\sup_{(\boldsymbol{v},q)\in \boldsymbol{Q}^c_{1,\mathcal{P}}\times M_{\mathcal{P}}} \frac{\mathfrak{B}_s(\boldsymbol{w},r;\boldsymbol{v},q)}{|||(\boldsymbol{v},q)|||} \geq \mu_s |||(\boldsymbol{w},r)||| \quad \textit{for all} \quad (\boldsymbol{w},r)\in \boldsymbol{Q}^c_{1,\mathcal{P}}\times M_{\mathcal{P}}\,, \tag{5.37}$$

where $\mu_s = \beta_G^2/[2(1+\beta_G)(17+16\beta_G)]$ where β_G is the constant from (5.13). Hence, Problem (5.20) is well-posed.

Proof. Let $(\boldsymbol{w},r)\in \boldsymbol{Q}^c_{1,\mathcal{P}}\times M_{\mathcal{P}}$ be given. First, from the definition of $\mathfrak{B}_s$ it follows that

$$\mathfrak{B}_s(\boldsymbol{w},r;\boldsymbol{w},-r) = \|\boldsymbol{w}\|^2_{a+s} + s_p(r,r)\,. \tag{5.38}$$

Additionally, given $\boldsymbol{w}_\delta \in \boldsymbol{Q}^c_{1,\mathcal{P}}$, using (5.8), (5.24) and $\alpha := 1/(c_a^2+c_s^2)$ we get

$$\begin{aligned}\mathfrak{B}_s(\boldsymbol{w},r;-\boldsymbol{w}_\delta,0) &= (a+s_v)(\boldsymbol{w},-\boldsymbol{w}_\delta) + (\operatorname{div}\boldsymbol{w}_\delta,r)_\Omega \\ &\geq -\sqrt{c_a^2+c_s^2}\|\boldsymbol{w}\|_{a+s}|\boldsymbol{w}_\delta|_{1,\Omega} + (\operatorname{div}\boldsymbol{w}_\delta,r)_\Omega \\ &\geq -\frac{1}{2}\|\boldsymbol{w}\|^2_{a+s} - \frac{1}{2\alpha}|\boldsymbol{w}_\delta|^2_{1,\Omega} + (\operatorname{div}\boldsymbol{w}_\delta,r)_\Omega. \end{aligned}\tag{5.39}$$

Next, we choose $\boldsymbol{w}_\delta$. By (5.14) there exists $\boldsymbol{z}\in \boldsymbol{Q}^c_{1,\mathcal{P}}$ such that $|\boldsymbol{z}|_{1,\Omega}=1$ and

$$(\operatorname{div}\boldsymbol{z},r)_\Omega \geq \beta_G\|r\|_{0,\Omega} - (1+\beta_G)\|r-\Pi_G r\|_{0,\Omega}.$$

Defining $\boldsymbol{w}_\delta := \delta\alpha\|r\|_{0,\Omega}\boldsymbol{z}$ with $\delta>0$ to be chosen, this last estimate, (5.29) and $\alpha\leq\alpha_p$ give

$$\begin{aligned}(\operatorname{div}\boldsymbol{w}_\delta,r)_\Omega &\geq \beta_G\delta\alpha\|r\|^2_{0,\Omega} - (1+\beta_G)\delta\alpha\|r\|_{0,\Omega}\alpha_p^{-1/2}C_1^{-1/2}s_p(r,r)^{1/2} \\ &\geq \beta_G\delta\alpha\|r\|^2_{0,\Omega} - \frac{\alpha}{2C_1}\delta^2(1+\beta_G)^2\|r\|^2_{0,\Omega} - \frac{1}{2}s_p(r,r)\,, \end{aligned}\tag{5.40}$$

and $|\boldsymbol{w}_\delta|_{1,\Omega} = \delta\alpha\|r\|_{0,\Omega}$ where $C_1 = 1/16$. We then define $(\boldsymbol{v},q) := (\boldsymbol{w}-\boldsymbol{w}_\delta,-r)$, and (5.38), (5.39) and (5.40) yield

$$\begin{aligned}\mathfrak{B}_s(\boldsymbol{w},r;\boldsymbol{v},q) &\geq \frac{1}{2}\Big[\|\boldsymbol{w}\|^2_{a+s}+s_p(r,r)\Big] + \left[\beta_G - \frac{\delta(1+\beta_G)^2}{2C_1}\right]\delta\alpha\|r\|^2_{0,\Omega} - \frac{1}{2\alpha}|\boldsymbol{w}_\delta|^2_{1,\Omega} \\ &= \frac{1}{2}\Big[\|\boldsymbol{w}\|^2_{a+s}+s_p(r,r)\Big] + \beta_G\left[1 - \frac{\delta(1+\beta_G)^2}{2C_1\beta_G} - \frac{\delta}{2\beta_G}\right]\delta\alpha\|r\|^2_{0,\Omega} \\ &\geq \frac{\delta\beta_G}{2}\Big(\|\boldsymbol{w}\|^2_{a+s}+s_p(r,r)+\alpha\|r\|^2_{0,\Omega}\Big)\,, \end{aligned}$$

where the choice $\delta := \beta_G C_1/(C_1+(1+\beta_G)^2)$ and $\delta\beta_G\leq 1$ imply the last estimate.

On the other hand, using (5.8) and (5.24) shows $\|\boldsymbol{z}\|_{a+s}\leq\alpha^{-1/2}|\boldsymbol{z}|_{1,\Omega}$ for all $\boldsymbol{z}\in \boldsymbol{Q}^c_{1,\mathcal{P}}$. Therefore, the definition of $\boldsymbol{w}_\delta$ and $|||\cdot|||$ give

$$|||(\boldsymbol{v},q)||| \leq |||(\boldsymbol{w},r)||| + \|\boldsymbol{w}_\delta\|_{a+s} \leq |||(\boldsymbol{w},r)||| + \delta\alpha^{1/2}\|r\|_{0,\Omega} \leq (1+\delta)|||(\boldsymbol{w},r)|||\,,$$

which proves the stated stability condition with $\mu_s = \delta\beta_G/(2+2\delta)$. Recalling $C_1 = 1/16$ proves the result. □

Remark 5.10. *We stress the fact that the stability constant μ_s only depends on β_G which is independent of mesh properties and data of the problem. Furthermore, the stability estimate* (5.37) *is valid independently of the relation of c_a and c_s. In [MT15] velocity stabilisation terms that satisfy* (5.24) *with $c_s \leq Cc_a$ are used. We avoid this assumption, as large stabilisation parameters may be optimal for some problems (cf. [JJLR14]).*

5.2.2. A priori estimates

This section is devoted to the a priori analysis of (5.20). We use $\Pi_{M_\mathcal{P}} \colon L^2(\Omega) \to M_\mathcal{P}$ to denote the L^2-projection into $M_\mathcal{P}$ satisfying

$$(p - \Pi_{M_\mathcal{P}} p, 1)_K = 0 \quad \text{for all} \quad K \in \mathcal{P}\,. \tag{5.41}$$

Theorem 5.11. *Let us suppose the solution $(\boldsymbol{u}, p)$ of* (5.2) *satisfies $p \in H^1(\Omega)$. Let s_v satisfy Assumption 5.6 and let s_p be defined by* (5.27) *with $\alpha_p \geq \alpha$. Then, if $\boldsymbol{u}_I \in \boldsymbol{Q}^c_{1,\mathcal{P}}$ is the interpolant defined in Lemma 5.5, then*

$$\begin{aligned}
|||(\boldsymbol{u} - \boldsymbol{u}_\mathcal{P}, p - p_\mathcal{P})||| \leq (1 + C\mu_s^{-1})\Big\{ & s_v(\boldsymbol{u}, \boldsymbol{u}) + s_v(\boldsymbol{u} - \boldsymbol{u}_I, \boldsymbol{u} - \boldsymbol{u}_I) + \sigma \|\boldsymbol{u} - \boldsymbol{u}_I\|^2_{0,\Omega} \\
& + \sum_{K \in \mathcal{P}} \Big(\Big(\frac{1}{\alpha + \alpha_p} + \nu + \frac{b^2_{\infty,K} C^2_\Omega}{\nu + \sigma C^2_\Omega} \Big) |\boldsymbol{u} - \boldsymbol{u}_I|^2_{1,K} \\
& + \Big(\alpha + \alpha_p + \frac{1}{\nu + \gamma_K} \Big) \|p - \Pi_{M_\mathcal{P}} p\|^2_{0,K} + \alpha_p \sum_{i=1,2} |e_{i,K}|^2 \|\partial_{t_i} p\|^2_{0,K} \Big) \Big\}^{1/2},
\end{aligned} \tag{5.42}$$

where $e_{i,K}, \partial_{t_i}$ $(i = 1, 2)$ are defined in Lemma 5.8, and the constant C is independent of mesh and data.

Proof. As usual, we split the errors

$$(\boldsymbol{u} - \boldsymbol{u}_\mathcal{P}, p - p_\mathcal{P}) = (\boldsymbol{u} - \boldsymbol{u}_I, p - \Pi_{M_\mathcal{P}} p) - (\boldsymbol{u}_\mathcal{P} - \boldsymbol{u}_I, p_\mathcal{P} - \Pi_{M_\mathcal{P}} p) =: (\boldsymbol{\eta}_v, \eta_p) - (\boldsymbol{\xi}_v, \xi_p).$$

Using definition (5.22) the interpolation error satisfies

$$|||(\boldsymbol{\eta}_v, \eta_p)|||^2 = \nu |\boldsymbol{\eta}_v|^2_{1,\Omega} + \sigma \|\boldsymbol{\eta}_v\|^2_{0,\Omega} + s_v(\boldsymbol{\eta}_v, \boldsymbol{\eta}_v) + \alpha \|\eta_p\|^2_{0,\Omega} + s_p(\eta_p, \eta_p)\,.$$

Similar to (5.30) the term $s_p(\eta_p, \eta_p)$ is bounded by the last two terms in (5.42). To bound the discrete error $(\boldsymbol{\xi}_v, \xi_p)$, from Theorem 5.9 there exists $(\boldsymbol{w}_\mathcal{P}, r_\mathcal{P}) \in \boldsymbol{Q}^c_{1,\mathcal{P}} \times M_\mathcal{P}$

with $|||(\boldsymbol{w}_{\mathcal{P}}, r_{\mathcal{P}})||| = 1$ and

$$\begin{aligned}\mu_s |||(\boldsymbol{\xi}_v, \xi_p)||| &\leq \mathfrak{B}_s(\boldsymbol{\xi}_v, \xi_p; \boldsymbol{w}_{\mathcal{P}}, r_{\mathcal{P}}) \\ &= \mathfrak{B}(\boldsymbol{\eta}_v, \eta_p; \boldsymbol{w}_{\mathcal{P}}, r_{\mathcal{P}}) - s_v(\boldsymbol{u}_I, \boldsymbol{w}_{\mathcal{P}}) + s_p(\Pi_{M_{\mathcal{P}}} p, r_{\mathcal{P}}) \,,\end{aligned} \tag{5.43}$$

where we used (5.2) and (5.20). We estimate the right-hand side term by term. Using (5.25) and $|||(\boldsymbol{w}_{\mathcal{P}}, r_{\mathcal{P}})||| = 1$ shows

$$\begin{aligned}-s_v(\boldsymbol{u}_I, \boldsymbol{w}_{\mathcal{P}}) &= s_v(\boldsymbol{\eta}_v, \boldsymbol{w}_{\mathcal{P}}) + s_v(\boldsymbol{u}, \boldsymbol{w}_{\mathcal{P}}) \leq s_v(\boldsymbol{\eta}_v, \boldsymbol{\eta}_v)^{1/2} + s_v(\boldsymbol{u}, \boldsymbol{u})^{1/2} \,, \\ s_p(\Pi_{M_{\mathcal{P}}} p, r_{\mathcal{P}}) &\leq s_p(\Pi_{M_{\mathcal{P}}} p, \Pi_{M_{\mathcal{P}}} p)^{1/2} \,,\end{aligned} \tag{5.44}$$

and applying $p \in H^1(\Omega)$ and (5.30) the right-hand sides of the last two inequalities are bounded by the first two and last two terms of (5.42). Next, using (5.7) we get

$$\begin{aligned}\nu(\nabla \boldsymbol{\eta}_v, \nabla \boldsymbol{w}_{\mathcal{P}})_\Omega + \sigma(\boldsymbol{\eta}_v, \boldsymbol{w}_{\mathcal{P}})_\Omega &\leq \Big(\nu |\boldsymbol{\eta}_v|_{1,\Omega}^2 + \sigma \|\boldsymbol{\eta}_v\|_{0,\Omega}^2\Big)^{1/2} \|\boldsymbol{w}_{\mathcal{P}}\|_a, \\ (\boldsymbol{b} \cdot \nabla \boldsymbol{\eta}_v, \boldsymbol{w}_{\mathcal{P}})_\Omega &\leq \left(\sum_{K \in \mathcal{P}} b_{\infty,K}^2 |\boldsymbol{\eta}_v|_{1,\Omega}^2 \right)^{1/2} \frac{C_\Omega}{(\nu + \sigma C_\Omega^2)^{1/2}} \|\boldsymbol{w}_{\mathcal{P}}\|_a.\end{aligned} \tag{5.45}$$

Moreover, for every $K \in \mathcal{P}$ we have

$$(\operatorname{div} \boldsymbol{w}_{\mathcal{P}}, \eta_p)_K \leq \sqrt{2} |\boldsymbol{w}_{\mathcal{P}}|_{1,K} \|\eta_p\|_{0,K} \,. \tag{5.46}$$

On the other hand, since $(\eta_p, \langle \operatorname{div} \boldsymbol{w}_{\mathcal{P}} \rangle_K)_K = 0$, we get

$$(\operatorname{div} \boldsymbol{w}_{\mathcal{P}}, \eta_p)_K = (\kappa_K(\operatorname{div} \boldsymbol{w}_{\mathcal{P}}), \eta_p)_K \leq \|\kappa_K(\operatorname{div} \boldsymbol{w}_{\mathcal{P}})\|_{0,K} \|\eta_p\|_{0,K} \,. \tag{5.47}$$

Then, using the inequality $ab \leq \sqrt{t}|ab| + \sqrt{1-t}|ab|$ with $t = \nu/(\nu + \gamma_K)$ to combine (5.46) and (5.47) leads to

$$(\operatorname{div} \boldsymbol{w}_{\mathcal{P}}, \eta_p)_K \leq \Big(\sqrt{2\nu} |\boldsymbol{w}_{\mathcal{P}}|_{1,K} + \sqrt{\gamma_K} \|\kappa_K(\operatorname{div} \boldsymbol{w}_{\mathcal{P}})\|_{0,K} \Big) (\nu + \gamma_K)^{-1/2} \|\eta_p\|_{0,K}.$$

Summing over all $K \in \mathcal{P}$ and employing (5.22), (5.23) and Assumption (5.26) we arrive at

$$(\operatorname{div} \boldsymbol{w}_{\mathcal{P}}, \eta_p)_\Omega \leq C \left(\sum_{K \in \mathcal{P}} \frac{1}{\nu + \gamma_K} \|\eta_p\|_{0,K}^2 \right)^{1/2} \|\boldsymbol{w}_{\mathcal{P}}\|_{a+s} \,. \tag{5.48}$$

Finally, since $\Pi_G r_{\mathcal{P}} \in G$, we can apply (5.17) and (5.29) to conclude

$$\begin{aligned}(\operatorname{div} \boldsymbol{\eta}_v, r_{\mathcal{P}})_\omega &= (\operatorname{div} \boldsymbol{\eta}_v, r_{\mathcal{P}} - \Pi_G r_{\mathcal{P}})_\omega \\ &\leq \sqrt{2} |\boldsymbol{\eta}_v|_{1,\omega} \|r_{\mathcal{P}} - \Pi_G r_{\mathcal{P}}\|_{0,\omega} \leq C \alpha_p^{-1/2} |\boldsymbol{\eta}_v|_{1,\omega} s_p(r_{\mathcal{P}}, r_{\mathcal{P}})|_\omega^{1/2} \,,\end{aligned} \tag{5.49}$$

where $\omega = M \in \mathcal{P}_0$, or $\omega = M \cup M'$ if $\gamma_{\boldsymbol{c}} \subset M \cap M'$ for one $\gamma_{\boldsymbol{c}} \in \mathcal{E}_{\mathcal{C}}$. On the other

hand, for any subset $\omega \subset \Omega$ we have

$$(\operatorname{div} \boldsymbol{\eta}_v, r_{\mathcal{P}})_\omega \leq \|\operatorname{div} \boldsymbol{\eta}_v\|_{0,\omega} \|r_{\mathcal{P}}\|_{0,\omega} \leq \alpha^{-1/2} |\boldsymbol{\eta}_v|_{1,\omega} \alpha^{1/2} \|r_{\mathcal{P}}\|_{0,\omega} \,. \tag{5.50}$$

Following the same steps as for (5.48), with $t = \alpha/(\alpha + \alpha_p)$ we combine (5.49) and (5.50) to arrive at

$$(\operatorname{div} \boldsymbol{\eta}_v, r_{\mathcal{P}})_\Omega \leq C \Big(\sum_{K \in \mathcal{P}} \frac{1}{\alpha + \alpha_p} \|\boldsymbol{\eta}_v\|_{0,K}^2 \Big)^{1/2} \Big(\alpha \|r_{\mathcal{P}}\|_{0,\Omega}^2 + s_p(r_{\mathcal{P}}, r_{\mathcal{P}}) \Big)^{1/2} . \tag{5.51}$$

The result follows on collecting the estimates (5.43)–(5.45), (5.48), and (5.51). □

We close this section with a few remarks on Theorem 5.11.

1) A reduced proof of (5.42) also implies a best approximation result. More precisely, if the property (5.17) of $\boldsymbol{u}_I$ (and hence (5.49)) is not used, then the terms involving $\boldsymbol{u} - \boldsymbol{u}_I$ become

$$\inf_{\boldsymbol{v}_{\mathcal{P}} \in \boldsymbol{Q}^c_{1,\mathcal{P}}} |\boldsymbol{u} - \boldsymbol{v}_{\mathcal{P}}|_{s_v}^2 + \sum_{K \in \mathcal{P}} \left(\frac{1}{\alpha} + \nu + \frac{b_{\infty,K}^2 C_\Omega^2}{\nu + \sigma C_\Omega^2} \right) |\boldsymbol{u} - \boldsymbol{v}_{\mathcal{P}}|_{1,K}^2 + \sigma \|\boldsymbol{u} - \boldsymbol{v}_{\mathcal{P}}\|_{0,K}^2 \,.$$

   This result extends, for instance, [MT15, Theorem 4.4] to the non-inf-sup stable pair $\boldsymbol{Q}^c_{1,\mathcal{P}} \times M_{\mathcal{P}}$ on anisotropic meshes. On the other hand, the results in [Bra08] for the $\boldsymbol{Q}^c_1 \times \mathbb{Q}^c_1$ pair do not show the data dependency $b_{\infty,\Omega}^2 C_\Omega^2/(\nu + \sigma C_\Omega^2)$ which is achieved by penalising a fluctuation of $\nabla \boldsymbol{u}$. But, the therein defined LPS norm does not control $\|p\|_{0,\Omega}$ (see also the appendix in [MPP03] for a similar issue) and a priori estimates require $p \in H^2(\Omega)$.

2) The choice $\alpha_p > \alpha$ is motivated by the fact that it leads stability constants which are independent of the data of the problem, and the inclusion of the pressure stabilisation term in the energy norm allows an error estimate containing $1/(\alpha + \alpha_p)$. This is a better bound than $1/\alpha$, which for $\sigma = 0$ behaves like ν^{-1}.

3) The error estimate contains $s_v(\boldsymbol{\eta}_v, \boldsymbol{\eta}_v)^{1/2}$ which may be much smaller for the pure grad-div term than its crude bound $c_s |\boldsymbol{\eta}_v|_{1,\Omega}$. This, as well, provides more flexibility for the choice of γ_K (see [JJLR14] for a detailed discussion of this issue in the case of the Stokes problem).

4) If the mixed method using $\boldsymbol{Q}^c_{1,\mathcal{P}} \times G$ is to be used as an approximation space, then the proof of a priori estimate (5.42) changes, since we need to replace $\Pi_{M_{\mathcal{P}}}$ by Π_G. Hence, (5.47) requires Assumption (5.26) to be replaced as follows. We observe

that G has a locally constant basis $\{\phi_j\}_{j=1}^{\dim G}$ and define $\omega_j \coloneqq \operatorname{supp}\phi_j$, where either $\omega_j = M$ or $\omega_j = M \cup M'$ with $M, M' \in \mathcal{P}_0$. Now, defining

$$s_v^G(\boldsymbol{u};\boldsymbol{v}) \coloneqq \sum_{j=1}^{\dim G} \gamma_{\omega_j}\big(\kappa_{\omega_j}(\operatorname{div}\boldsymbol{u}), \operatorname{div}\boldsymbol{v}\big)_{\omega_j},$$

we can replace assumption (5.26) by $s_v^G(\boldsymbol{u};\boldsymbol{v}) \leq s_v(\boldsymbol{u};\boldsymbol{v})$. The latter definitions directly imply (5.47) with κ_{ω_j} instead of κ_K. Then, (5.48) changes to

$$(\operatorname{div}\boldsymbol{w}_{\mathcal{P}}, \eta_p)_\Omega \leq C\bigg(\sum_{j=1}^{\dim G} \frac{1}{\nu+\gamma_{\omega_j}}\|p-\Pi_G p\|_{0,\omega_j}^2\bigg)^{1/2} \|\boldsymbol{w}_{\mathcal{P}}\|_{a+s}.$$

On the other hand, estimate (5.49) is not needed as $(\operatorname{div}\boldsymbol{\eta}_v, r_G)_\omega = 0$ by definition.

5.3. Examples of stabilisation terms for the velocity

The previous sections, in particular Section 5.2, leave the choice of velocity stabilisation terms flexible. Below we define the stabilisation terms used in the numerical experiments.

Option one. Let $\boldsymbol{b}_K \coloneqq \langle \boldsymbol{b}\rangle_K$ and define

$$s_v(\boldsymbol{u},\boldsymbol{v}) \coloneqq \sum_{M\in\mathcal{P}_0} \gamma_M(\kappa_M(\operatorname{div}\boldsymbol{u}), \operatorname{div}\boldsymbol{v})_M + \sum_{K\in\mathcal{P}} \frac{1}{|\boldsymbol{b}_K|}(\kappa_K(\boldsymbol{b}_K\cdot\nabla\boldsymbol{u}), \boldsymbol{b}_K\cdot\nabla\boldsymbol{v})_K, \tag{5.52}$$

where γ_M is chosen as one of the following options

$$\gamma_M \coloneqq \max\big\{1, \mathrm{Pe}_{\mathcal{P}_0}^{\min}\big\}, \tag{5.53a}$$

$$\gamma_M \coloneqq 1 + ind(M)\mathrm{Pe}_M^{\min} \quad \text{and} \quad ind(M) \coloneqq 1 - \frac{\rho_M|M|}{\max_{\omega\in\mathcal{P}_0}|\omega|}, \tag{5.53b}$$

with local and global (minimal) Péclet numbers defined by $\mathrm{Pe}_{\mathcal{P}_0}^{\min} \coloneqq \min_{M\in\mathcal{P}_0}\mathrm{Pe}_M^{\min}$ and $\mathrm{Pe}_M^{\min} \coloneqq \nu^{-1}b_{\infty,M}\min\{h_{x,M}, h_{y,M}\}$. The inverse euclidean length $|\boldsymbol{b}_K|^{-1}$ is introduced to have a proper physical scaling.

The choice (5.53b) is motivated by the fact that the minimal global Péclet number does not contain information about local phenomena. Then the introduction of the $ind(\cdot)$ function ensures that γ_M varies significantly with local geometric properties of M. In fact $\gamma_M \approx 1$ in large shape-regular elements and $\gamma_M \approx 1 + \mathrm{Pe}_M^{\min}$ in highly stretched elements and small corner elements, which is the desirable behaviour.

Remark 5.12. *The stabilisation term* (5.52) *satisfies Assumption 5.6 and the continuity estimate* (5.24) *with* $c_s = (b_{\infty,\Omega} + \max_{M\in\mathcal{P}_0} 2\gamma_M)^{1/2}$. *On the other hand, defining* s_v *by* (5.52) *guarantees that* $s_v(\boldsymbol{u},\boldsymbol{u})$ *and* $s_v(\boldsymbol{\eta}_u,\boldsymbol{\eta}_u)$, *appearing in the a priori estimate* (5.42), *can be bounded in an optimal way.*

Option two. We also consider the following stabilisation

$$s_v(\boldsymbol{u},\boldsymbol{v}) \coloneqq \sum_{M\in\mathcal{P}_0} (\kappa_M(\partial_x \boldsymbol{u}), \delta_x \partial_x \boldsymbol{v})_M + (\kappa_M(\partial_y \boldsymbol{u}), \delta_y \partial_y \boldsymbol{v})_M \,, \tag{5.54}$$

where (δ_x, δ_y) are given by

$$\begin{aligned}
\delta_{K,x} &\coloneqq \nu^{-1} b_{\infty,K}^2 h_{K,x}^2 \min\Big\{1, \mathrm{Pe}_{\mathrm{min},K}^{-1}\Big\}\,,\\
\delta_{K,y} &\coloneqq \nu^{-1} b_{\infty,K}^2 h_{K,y}^2 \min\Big\{1, \mathrm{Pe}_{\mathrm{min},K}^{-1}\Big\}\,,\\
\mathrm{Pe}_{\mathrm{min},K} &\coloneqq \nu^{-1} \min\{h_{K,x}, h_{K,y}\} b_{\infty,K}\,.
\end{aligned}$$

This term has been introduced and analysed in [Bra08] for the $\boldsymbol{Q}_1^c \times \mathbb{Q}_1^c$ pair. It satisfies Assumption 5.6 with $c_s = \max\{\delta_x, \delta_y\}^{1/2}$ and $\gamma_K = \gamma_M \coloneqq \frac{1}{2}\min\{\delta_x, \delta_y\}$, which is obtained from

$$\begin{aligned}
\sum_{K\subset M} \|\kappa_K(\operatorname{div}\boldsymbol{u})\|_{0,K}^2 &\le \|\kappa_M(\operatorname{div}\boldsymbol{u})\|_{0,M}^2\\
&= \big\|\partial_x \boldsymbol{u}_1 + \partial_y \boldsymbol{u}_2 - \langle \partial_x \boldsymbol{u}_1\rangle_M - \langle \partial_y \boldsymbol{u}_2\rangle_M\big\|_{0,M}^2\\
&\le 2\|\partial_x \boldsymbol{u}_1 - \langle \partial_x \boldsymbol{u}_1\rangle_M\|_{0,M}^2 + 2\big\|\partial_y \boldsymbol{u}_2 - \langle \partial_y \boldsymbol{u}_2\rangle_M\big\|_{0,M}^2\,.
\end{aligned}$$

5.4. Numerical verification

In this section we report numerical results confirming our theoretical findings. We present the results of two different experiments approximating a solution of (5.1) with non-homogeneous boundary conditions in the domain $\Omega \coloneqq (0,1)\times(0,1)$.

Example 1. We define $\boldsymbol{b} = (-1,-1)^\top$, $\nu = 10^{-6}$, $\sigma = 0$ and choose the right-hand-side $\boldsymbol{f}$ and boundary conditions such that the exact solution is given by

$$\boldsymbol{u} \coloneqq \begin{pmatrix} \frac{1-\exp(-y/\nu)}{1-\exp(-1/\nu)} - y \\ \frac{1-\exp(-x/\nu)}{1-\exp(-1/\nu)} - x \end{pmatrix} \quad \text{and} \quad p \coloneqq \sin(x-1/2)\sin(y-1/2)\,. \tag{5.55}$$

Example 2. We define $\boldsymbol{b} = (-1,-1)^\top$, $\nu = 10^{-6}$, $\sigma = 1$ and choose the right-hand-side $\boldsymbol{f}$ and boundary conditions such that the exact solution is given by

$$\boldsymbol{u} \coloneqq \begin{pmatrix} 1 - \exp\Big(-y\frac{1+\sqrt{1+4\nu}}{2\nu}\Big) \\ 1 - \exp\Big(-x\frac{1+\sqrt{1+4\nu}}{2\nu}\Big) \end{pmatrix} \quad \text{and} \quad p \coloneqq \sin(x-1/2)\sin(y-1/2)\,. \tag{5.56}$$

In both cases the right-hand-side $\boldsymbol{f}$ is independent of ν, which makes the results independent of the quadrature rules employed.

For the experiments we define parametrized partitions containing a corner patch. Let $\mathcal{P}_{N,\lambda}$ (N divisible by 4, and $\lambda \in (0, 1/2]$) be the tensor-product of the one-dimensional interval subdivision that splits each of the intervals $[0, \lambda]$ and $[\lambda, 1]$ into $N/2$ intervals of equal length, cf. Figure 5.1 (right) where $\mathcal{P}_{4,\lambda}$ is shown. The mesh $\mathcal{P}_{N,\lambda}$ is a Shishkin-mesh, but we choose λ to be larger than the Shishkin parameter $2\nu \ln N \leq 10^{-5}$.

Our aim is to explore how robust the methods with the previously defined stabilisation terms and parameters are with respect to the choice of λ. This is why we chose a wide range for λ from $\lambda = 1/2$ (a shape-regular mesh) to $\lambda = 10^{-4}$ (a highly anisotropic corner patch with minimal aspect ratio $\varrho \approx 10^{-4}$).

The purpose of the tables is to show how different stabilised methods perform compared to the interpolation and best approximation errors, respectively. To this end, the entries of a table show relative errors defined by

$$E_u^{rel} := \frac{|\boldsymbol{u} - \boldsymbol{u}_{\mathcal{P}}|_{1,\Omega}}{|\boldsymbol{u} - I_{\mathcal{P}}\boldsymbol{u}|_{1,\Omega}}, \quad E_p^{rel} := \frac{\|p - p_{\mathcal{P}}\|_{0,\Omega}}{\|p - \Pi p\|_{0,\Omega}} \quad \text{and} \quad E_{nat}^{rel} := \frac{|||(\boldsymbol{u} - \boldsymbol{u}_{\mathcal{P}}, p - p_{\mathcal{P}})|||}{|||(\boldsymbol{u} - I_{\mathcal{P}}\boldsymbol{u}, p - \Pi p)|||},$$

where $|||\cdot|||$ is defined in (5.28). Here $I_{\mathcal{P}}\boldsymbol{u} \in \boldsymbol{Q}^c_{1,\mathcal{P}}$ stands for the nodal interpolant of $\boldsymbol{u}$, and $\Pi \in \{\Pi_{M_{\mathcal{P}}}, \Pi_G\}$ are the projections defined earlier, chosen depending on whether we use pair $\boldsymbol{Q}^c_{1,\mathcal{P}} \times M_{\mathcal{P}}$ or $\boldsymbol{Q}^c_{1,\mathcal{P}} \times G$. The last row shows the value of the *denominators* used to define E_u^{rel} and E_p^{rel}. For E_{nat}^{rel} this value changes for different stabilisation parameters and terms and is therefore not shown. The first two columns show the used velocity stabilisation term s_v and parameter γ_M (where appropriate). The columns 3–5 and 6–8 show relative errors obtained when using the pair $\boldsymbol{Q}^c_{1,\mathcal{P}} \times G$ and $\boldsymbol{Q}^c_{1,\mathcal{P}} \times M_{\mathcal{P}}$ with s_p ($\alpha_p = 1$), respectively.

Since the results for Ex. 1 and Ex. 2 are qualitatively similar, we only show results for Ex. 2 in Tables 5.1–5.9. The tables present experiments using $N = 4, 8$ and 16 as a mesh parameter. Qualitatively similar results are obtained for all three cases. From the tables we observe that the different stabilisation terms cause a comparable behaviour of the pressure errors.

The robustness is mostly due to the second term in (5.52). As a matter of fact, removing this term makes the error in pressure depend on λ in a more pronouced way. On the other hand, the velocity errors do not seem to differ much. This is why we provide plots of obtained velocity profiles in Figures 5.6–5.9. We note that the present stabilisation term s_v given by (5.52) always produces a profile that is smoother, almost free of oscillations; whereas the profile obtained from the method using s_v given by (5.54) presents large oscillations. Naturally, the two choices for

γ_M in (5.53) give different results on shape-regular meshes, cf. the plots for $\lambda = 1/2$. However, on anisotropic meshes the behaviour is similar and oscillations and overshoots are significantly reduced.

Table 5.1. Relative errors for Example 2, mesh $(N, \lambda) = (4, 0.5)$

		$\boldsymbol{Q}^c_{1,\mathcal{P}} \times G$			$\boldsymbol{Q}^c_{1,\mathcal{P}} \times M_{\mathcal{P}}, \alpha_p = 1$		
s_v	γ_M	E_p^{rel}	E_u^{rel}	E_{nat}^{rel}	E_p^{rel}	E_u^{rel}	E_{nat}^{rel}
(5.54)	–	3.25	1.0000	1.0000	8.54	1.0000	1.0000
(5.52)	(5.53a)	7.17	1	1.0000	13.67	1	1.0000
(5.52)	(5.53b)	6.49	1.0000	1.0000	13.67	1.0000	1.0000
denominator		$5.19 \cdot 10^{-2}$	999.9965	–	$2.72 \cdot 10^{-2}$	999.9965	–

Table 5.2. Relative errors for Example 2, mesh $(N, \lambda) = (4, 10^{-2})$

		$\boldsymbol{Q}^c_{1,\mathcal{P}} \times G$			$\boldsymbol{Q}^c_{1,\mathcal{P}} \times M_{\mathcal{P}}, \alpha_p = 1$		
s_v	γ_M	E_p^{rel}	E_u^{rel}	E_{nat}^{rel}	E_p^{rel}	E_u^{rel}	E_{nat}^{rel}
(5.54)	–	1.06	1.0000	1.0000	5.94	1.0000	1.0000
(5.52)	(5.53a)	8.95	1.0000	1.0000	13.84	1.0000	1.0000
(5.52)	(5.53b)	7.35	1.0000	1.0000	11.37	1.0000	1.0000
denominator		$7.94 \cdot 10^{-2}$	999.8005	–	$5.14 \cdot 10^{-2}$	999.8005	–

Table 5.3. Relative errors for Example 2, mesh $(N, \lambda) = (4, 10^{-4})$

		$\boldsymbol{Q}^c_{1,\mathcal{P}} \times G$			$\boldsymbol{Q}^c_{1,\mathcal{P}} \times M_{\mathcal{P}}, \alpha_p = 1$		
s_v	γ_M	E_p^{rel}	E_u^{rel}	E_{nat}^{rel}	E_p^{rel}	E_u^{rel}	E_{nat}^{rel}
(5.54)	–	1.00	1.0017	1.0022	6.04	1.0007	1.0014
(5.52)	(5.53a)	1.00	1.0000	1.0000	1.54	1.0000	1.0000
(5.52)	(5.53b)	1.00	1.0000	1.0000	1.54	1.0000	1.0000
denominator		$7.94 \cdot 10^{-2}$	979.7964	–	$5.20 \cdot 10^{-2}$	979.7964	–

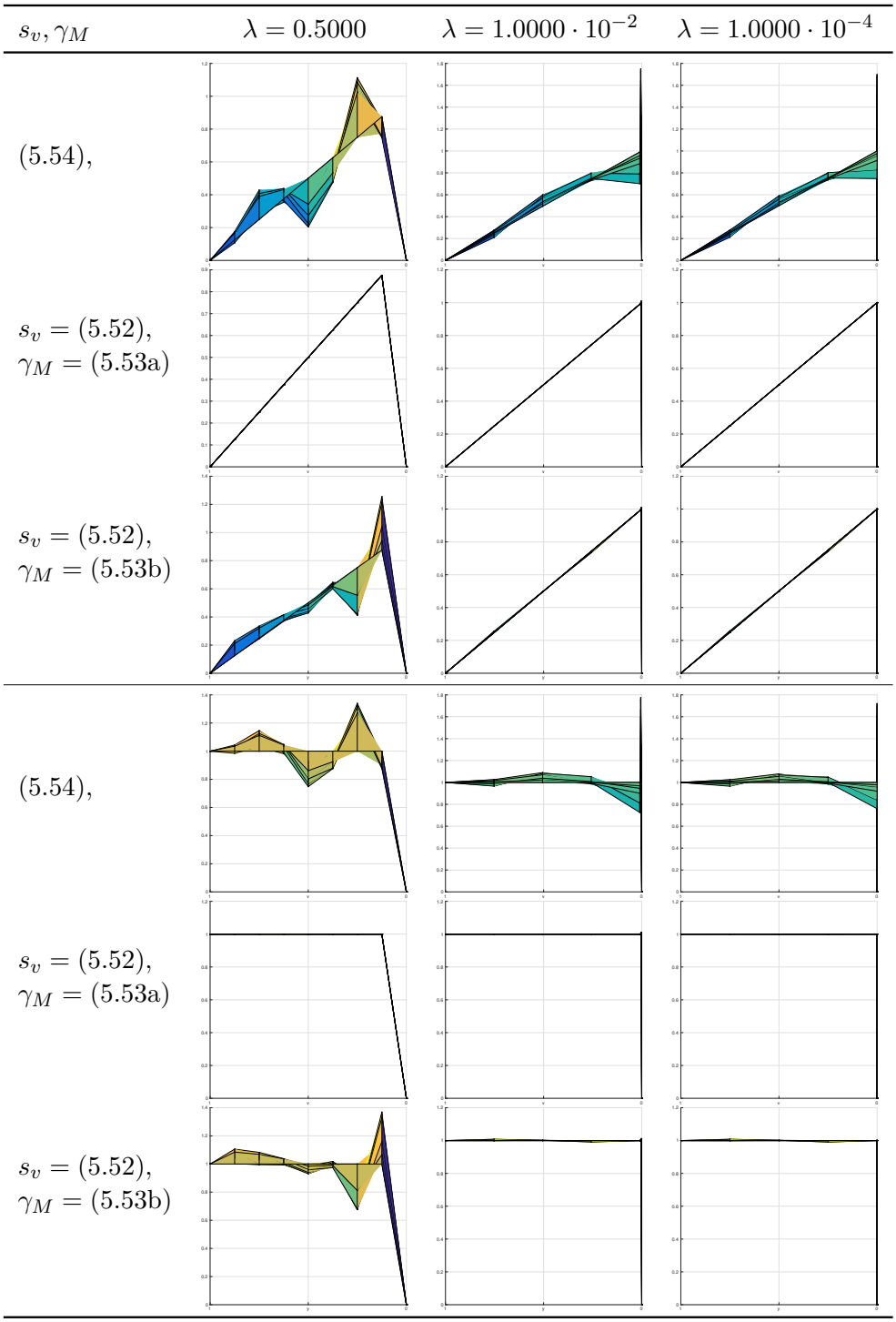

Fig. 5.6. Side profiles on meshes ($N = 8$). Using $\boldsymbol{Q}^c_{1,\mathcal{P}} \times G$.

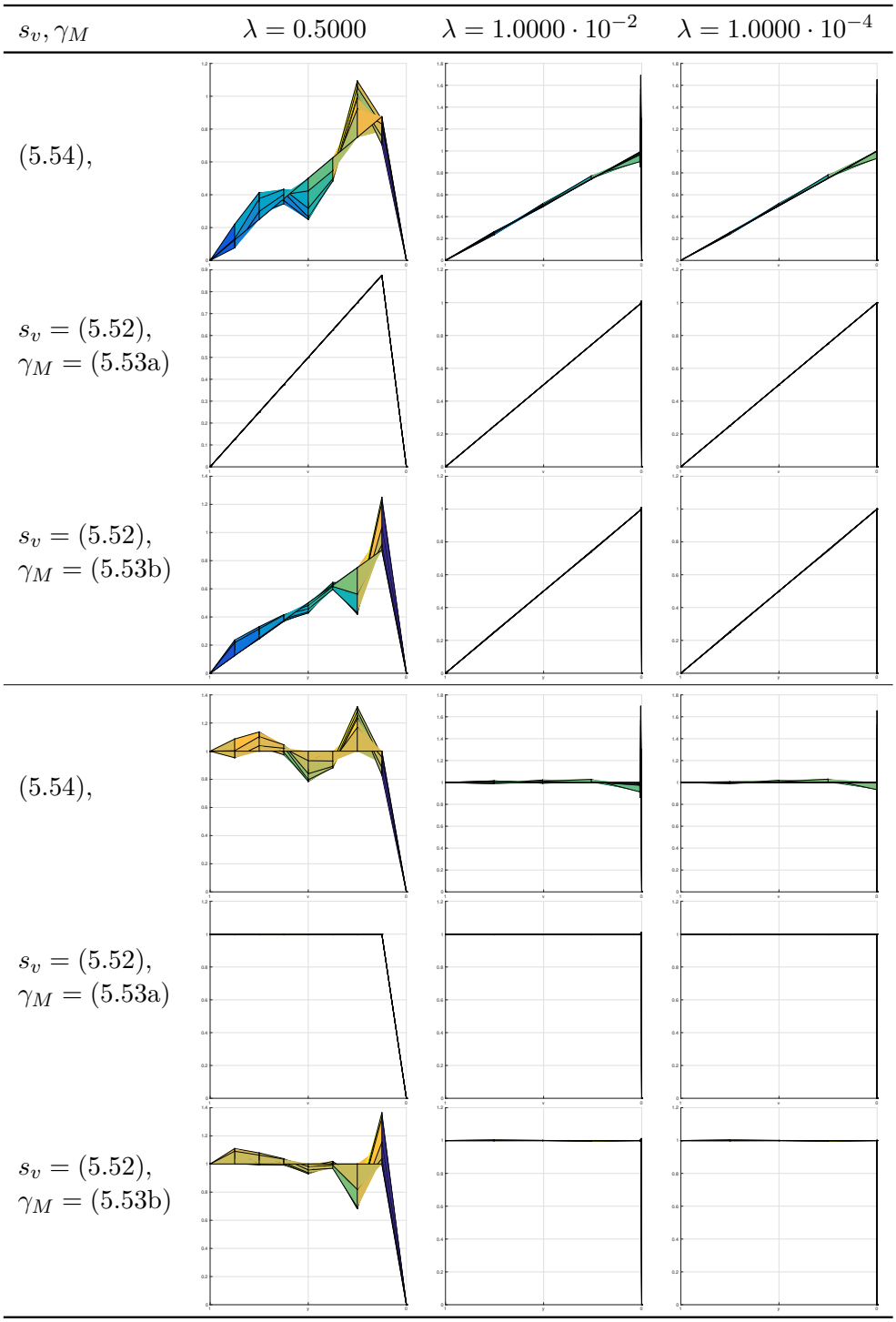

Fig. 5.7. Side profiles on meshes ($N = 8$). Using $\boldsymbol{Q}^c_{1,\mathcal{P}} \times M_{\mathcal{P}}$ with s_p and $\alpha_p = 1$.

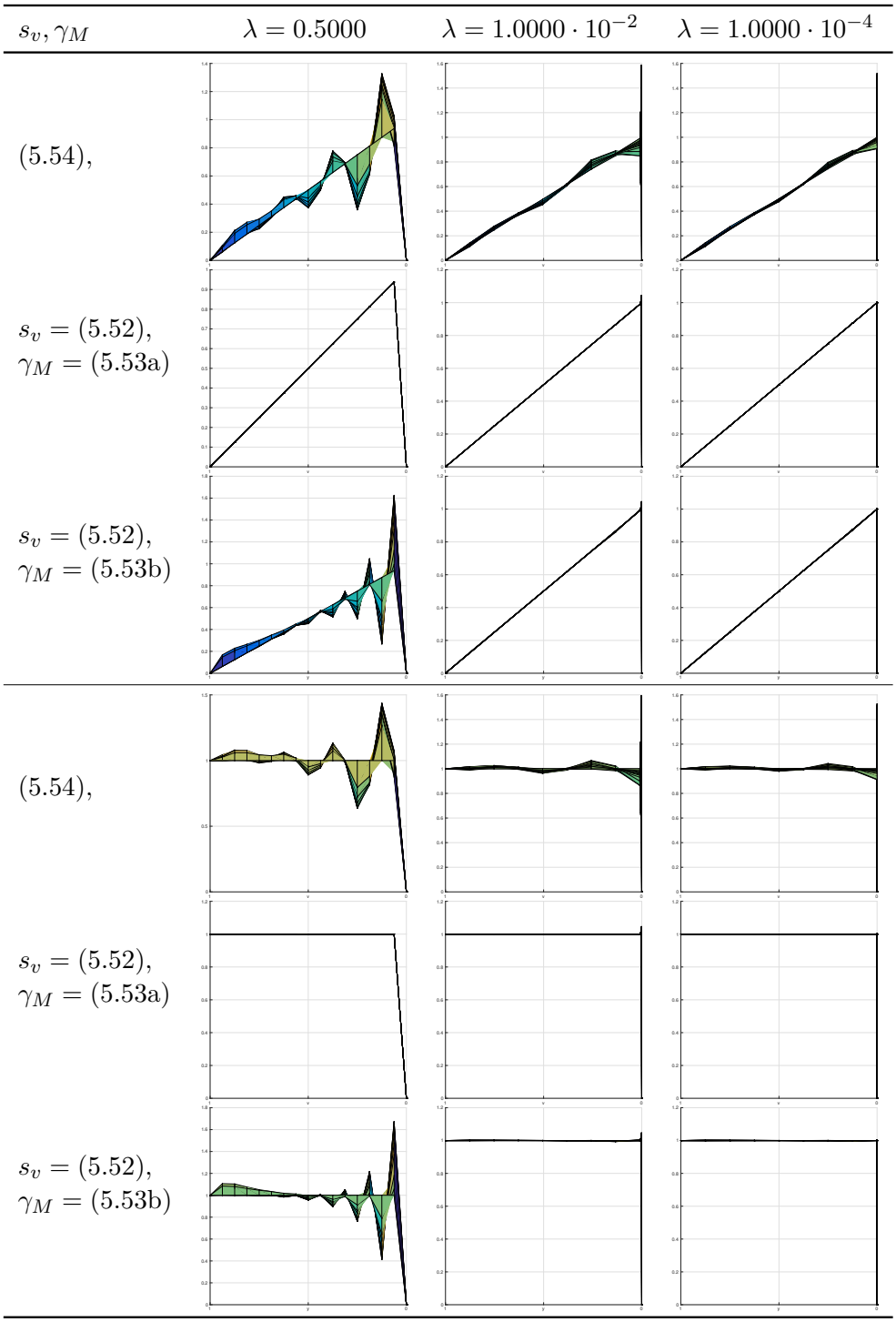

Fig. 5.8. Side profiles on meshes ($N = 16$). Using $\boldsymbol{Q}^c_{1,\mathcal{P}} \times G$.

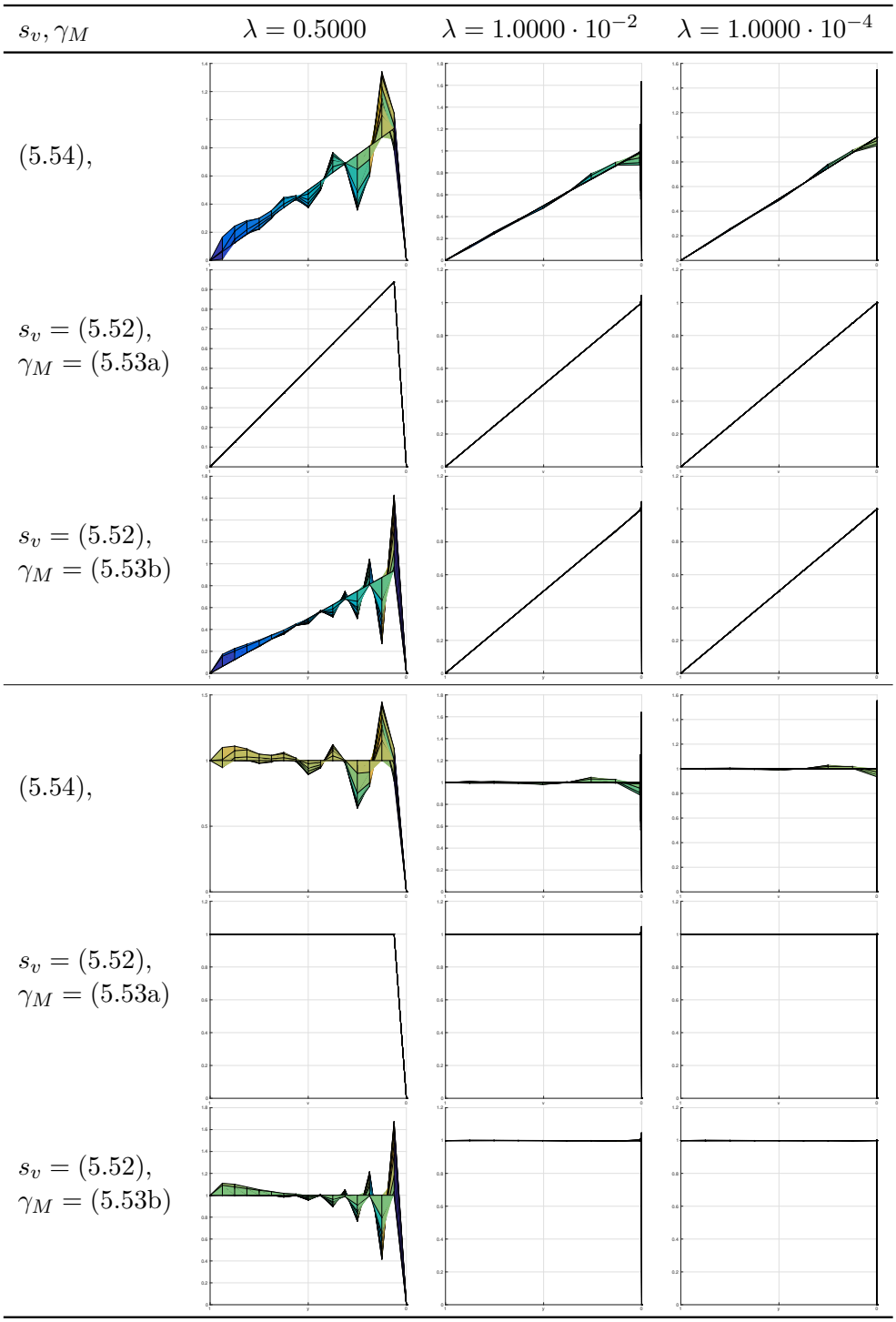

Fig. 5.9. Side profiles on meshes ($N = 16$). Using $\boldsymbol{Q}^c_{1,\mathcal{P}} \times M_{\mathcal{P}}$ with s_p and $\alpha_p = 1$.

Table 5.4. Relative errors for Example 2, mesh $(N, \lambda) = (8, 0.5)$

		$\boldsymbol{Q}^c_{1,\mathcal{P}} \times G$			$\boldsymbol{Q}^c_{1,\mathcal{P}} \times M_{\mathcal{P}}, \alpha_p = 1$		
s_v	γ_M	E_p^{rel}	E_u^{rel}	E_{nat}^{rel}	E_p^{rel}	E_u^{rel}	E_{nat}^{rel}
(5.54)	–	5.79	1.0000	1.0000	13.73	1.0000	1.0000
(5.52)	(5.53a)	13.69	1.0000	1.0000	27.08	1.0000	1.0000
(5.52)	(5.53b)	9.58	1.0000	1.0000	21.04	1.0000	1.0000
denominator		$2.72 \cdot 10^{-2}$	999.9925	–	$1.37 \cdot 10^{-2}$	999.9925	–

Table 5.5. Relative errors for Example 2, mesh $(N, \lambda) = (8, 10^{-2})$

		$\boldsymbol{Q}^c_{1,\mathcal{P}} \times G$			$\boldsymbol{Q}^c_{1,\mathcal{P}} \times M_{\mathcal{P}}, \alpha_p = 1$		
s_v	γ_M	E_p^{rel}	E_u^{rel}	E_{nat}^{rel}	E_p^{rel}	E_u^{rel}	E_{nat}^{rel}
(5.54)	–	1.40	1.0002	1.0001	7.47	1.0002	1.0001
(5.52)	(5.53a)	27.93	1.0000	1.0000	53.35	1.0000	1.0000
(5.52)	(5.53b)	28.01	1.0000	1.0000	53.77	1.0000	1.0000
denominator		$5.12 \cdot 10^{-2}$	999.6004	–	$2.68 \cdot 10^{-2}$	999.6004	–

Table 5.6. Relative errors for Example 2, mesh $(N, \lambda) = (8, 10^{-4})$

		$\boldsymbol{Q}^c_{1,\mathcal{P}} \times G$			$\boldsymbol{Q}^c_{1,\mathcal{P}} \times M_{\mathcal{P}}, \alpha_p = 1$		
s_v	γ_M	E_p^{rel}	E_u^{rel}	E_{nat}^{rel}	E_p^{rel}	E_u^{rel}	E_{nat}^{rel}
(5.54)	–	1.22	1.0219	1.0078	6.73	1.0152	1.0077
(5.52)	(5.53a)	1.10	1.0000	1.0000	3.62	1.0000	1.0000
(5.52)	(5.53b)	1.10	1.0000	1.0000	3.39	1.0000	1.0000
denominator		$5.19 \cdot 10^{-2}$	959.1668	–	$2.72 \cdot 10^{-2}$	959.1668	–

Table 5.7. Relative errors for Example 2, mesh $(N, \lambda) = (16, 0.5)$

		$\boldsymbol{Q}^c_{1,\mathcal{P}} \times G$			$\boldsymbol{Q}^c_{1,\mathcal{P}} \times M_{\mathcal{P}}, \alpha_p = 1$		
s_v	γ_M	E_p^{rel}	E_u^{rel}	E_{nat}^{rel}	E_p^{rel}	E_u^{rel}	E_{nat}^{rel}
(5.54)	–	7.81	1.0000	1.0000	18.08	1.0000	1.0000
(5.52)	(5.53a)	26.03	1.0000	1.0000	51.91	1.0000	1.0000
(5.52)	(5.53b)	12.27	1.0000	1.0000	28.01	1.0000	1.0000
denominator		$1.37 \cdot 10^{-2}$	999.9845	–	$6.89 \cdot 10^{-3}$	999.9845	–

Table 5.8. Relative errors for Example 2, mesh $(N, \lambda) = (16, 10^{-2})$

		$\boldsymbol{Q}^c_{1,\mathcal{P}} \times G$			$\boldsymbol{Q}^c_{1,\mathcal{P}} \times M_{\mathcal{P}}, \alpha_p = 1$		
s_v	γ_M	E_p^{rel}	E_u^{rel}	E_{nat}^{rel}	E_p^{rel}	E_u^{rel}	E_{nat}^{rel}
(5.54)	–	1.08	1.0006	1.0001	3.38	1.0006	1.0001
(5.52)	(5.53a)	41.24	1.0000	1.0000	81.59	1.0000	1.0000
(5.52)	(5.53b)	41.51	1.0000	1.0000	82.18	1.0000	1.0000
denominator		$2.68 \cdot 10^{-2}$	999.2002	–	$1.35 \cdot 10^{-2}$	999.2002	–

Table 5.9. Relative errors for Example 2, mesh $(N, \lambda) = (16, 10^{-4})$

		$\boldsymbol{Q}^c_{1,\mathcal{P}} \times G$			$\boldsymbol{Q}^c_{1,\mathcal{P}} \times M_{\mathcal{P}}, \alpha_p = 1$		
s_v	γ_M	E_p^{rel}	E_u^{rel}	E_{nat}^{rel}	E_p^{rel}	E_u^{rel}	E_{nat}^{rel}
(5.54)	–	1.03	1.0514	1.0162	2.15	1.0516	1.0161
(5.52)	(5.53a)	2.43	1.0000	1.0000	9.00	1.0000	1.0000
(5.52)	(5.53b)	2.47	1.0000	1.0000	8.89	1.0000	1.0000
denominator		$2.72 \cdot 10^{-2}$	916.5163	–	$1.37 \cdot 10^{-2}$	916.5163	–

5.5. Conclusion

In this chapter we have generalised the results from Chapter 4 and [ABW15, LS13] to the lowest order pair $\boldsymbol{Q}^c_1 \times \mathbb{P}_0$ in partitions that contain refined corner patches, and extended this generalisation to the Oseen equation. To analyse the resulting methods we have used, and adapted when necessary, the abstract approach given in [MT15]. This allowed us to present stability and convergence results that are valid both in the inf-sup stable and stabilised cases. A precise definition, by means of a weighted grad-div term enhanced by a penalisation of the convective derivative, of the stabilisation term for the velocity has been proposed, justified, and tested numerically. This new definition seems to outperform some previously known alternatives, at least numerically.

Chapter 6

Conclusions and future work

In this chapter, we first present conclusions, and then we show by numerical experiments that our ideas for future projects are promising.

6.1. Conclusions

Our main goal was to propose methods (alternative to [AC00]) that circumvent the inf-sup deficiency caused by the presence of corner patches in anisotropic meshes.

The first methods and methodology were derived in Chapter 3 for the Stokes problem and the pair $\boldsymbol{Q}^c_{k+1} \times \mathbb{P}_{k-1}$ ($k \geq 1$). The results in [AC00,SSS99,AN04] state that the inf-sup degeneracy does not depend on local aspect ratios, but rather on the combination of the aspect ratio and the presence of corner patches. These results allowed the authors of [AC00] to identify the pressure modes responsible for the undesirable behaviour. We further reduced this number by Corollary 3.15 in Chapter 3. Then, we proved the existence of alternative uniformly inf-sup stable subspaces $\boldsymbol{V}_{\mathcal{P}} \times G$ in Theorem 3.3. We used, as planned, arguments from PPS methods to derive the methods. A secondary effect of the equivalence of stabilisation terms and inf-sup deficiency allowed us to prove that the stabilised methods converge as fast as the methods using the reduced pressure spaces, cf. Remark 3.9.

The second goal was to derive methods for balanced-order pairs that allow corner patches. We saw (Table 1.1) that the stability of such pairs may additionally depend on local aspect ratios, and hence more stabilisation may be required. On anisotropic meshes we were not able to find uniformly inf-sup stable, balanced-order pairs, with the exception of non-conforming pairs. The stabilised method for $\boldsymbol{Q}^c_1 \times \mathbb{P}_0$ proposed in [LS13] is uniformly stable on anisotropic meshes without corner patches, but a few additional jumps (similar to those in Chapter 3) permit the use of corner patches, cf. Chapter 4.

Finally, in Chapter 5 we extended the methods to the Oseen problem. This was

done for the low order case $\boldsymbol{Q}_1^c \times \mathbb{P}_0$ (from Chapter 4). We saw that the general analysis given in [MT15] can be extended to non-inf-sup stable pairs on anisotropic meshes. Furthermore, we made the choice of parameters for the velocity stabilisation terms more flexible and derived a lower bound for the stabilisation parameter of the pressure. It is evident, also from the analysis in [MT15], that a small coefficient α of the pressure norm reduces the given control over the pressure error. The methods we proposed control the full L^2-norm of the pressure, which is an improvement with respect to equal-order methods on anisotropic meshes in [MPP03, AKL08, Bra08]. In fact the method in [AKL08] imposes a restriction on the aspect ratio, and the appendix in [MPP03] suggests that the control depends on the smallest aspect ratio. Furthermore, corner patches are ruled out in [MPP03, AKL08, Bra08] and the convergence of the methods therein requires more regularity than $p \in H^1(\Omega)$. Finally, when $(\boldsymbol{u}_\mathcal{P}, p_\mathcal{P})$ is the solution of the discrete problem, then also the stabilised methods presented satisfy $(\operatorname{div} \boldsymbol{u}_\mathcal{P}, q)_\Omega = 0$ for all $q \in G$, which is due to $s_p(q, q) = 0$ for all $q \in G$. This is in fact a local mass conservation result.

We may conclude that we achieved the goals posed in the introduction. However, the results obtained just open the door for several future research directions. We list these directions here; for some of them we show first experiments in the next sections.

- Extend the results in Chapter 3 to triangles and three-dimensional cases. For the lowest order case $\boldsymbol{P}_2^c \times \mathbb{P}_0$ we will (in Section 6.3) sketch a proof on triangulated corner patches. The stability for higher order pairs on triangular edge patches has not been analysed yet. Therefore, we leave the proof as part of future work. Also the analysis for three dimensional corner patches is part of future work.

- In fact, methods using balanced-order pairs are more desirable. The extension of Chapter 3 to the case $\boldsymbol{P}_2^c \times \mathbb{P}_0$ allows us to propose a local jump-stabilised method (similar to those in Chapter 4 and [LS13]) using the pair $\boldsymbol{P}_1^c \times \mathbb{P}_0$ on anisotropic triangles. Furthermore, we stated in the introduction, that coarse-scale projection stabilisation may be an option to allow stabilised methods using balanced-order pairs of higher degree. We show experiments confirming that this actually works for the $\boldsymbol{Q}_2^c \times \mathbb{P}_1$ and $\boldsymbol{P}_2^c \times \mathbb{P}_1$ pairs (with discontinuous pressures), cf. Section 6.4. Future work is to propose methods for higher (balanced) order pairs $\boldsymbol{Q}_k^c \times \mathbb{P}_{k-1}$ and $\boldsymbol{P}_k^c \times \mathbb{P}_{k-1}, (k \geq 3)$ on anisotropic meshes.

- Once the extensions concerning balanced-order pairs are available for the Stokes problem, the results can be generalised to the Oseen problem as in Chapter 5.

- The methods in Chapter 5 can be used (as presented) to solve the (non-linear)

Navier–Stokes problem. However, a more sophisticated choice of the stabilisation parameter γ_M is part of future research. We perform some preliminary experiments in Section 6.2.

- Some other topics like a posteriori analysis and time dependent problems will also be a subject of future research.

6.2. Numerical experiments for the Navier–Stokes equation

Let $\Omega \coloneqq [-3, 20] \times [-3, 3] \setminus [-1, 1]^2$ for the Navier–Stokes equation

$$\begin{aligned} -\nu \Delta \boldsymbol{u} + \boldsymbol{u} \cdot \nabla \boldsymbol{u} + \nabla p &= \boldsymbol{0} \quad \text{in} \quad \Omega \\ \operatorname{div} \boldsymbol{u} &= 0 \quad \text{in} \quad \Omega \end{aligned} \tag{6.1}$$

using $\nu = 10^{-2}$ subject to the do-nothing condition on $\{20\} \times [-3, 3]$ and the other conditions as shown in Figure 6.1. We approximated the solution of (6.1) on the mesh, that was obtained as the third uniform refinement of the mesh in Figure 6.1 with $\lambda = 4 \cdot 10^{-2}$. The non-linear problem was split into various (linear) problems of Oseen type, which were solved with method (5.20), s_v given by (5.52) with $\gamma_M \coloneqq 1$ and s_p with $\alpha_p = 1$. The obtained approximation $\boldsymbol{u}_{\mathcal{P}} \coloneqq (\boldsymbol{u}_1, \boldsymbol{u}_2)$ shows reasonable streamlines (Figure 6.2) and surface elevations (Figure 6.3).

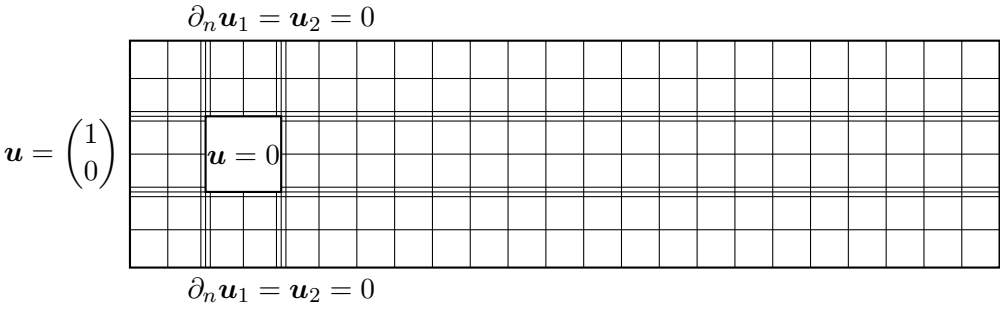

Fig. 6.1. A (coarse) mesh for the Navier–Stokes experiment ($\lambda = 1/8$).

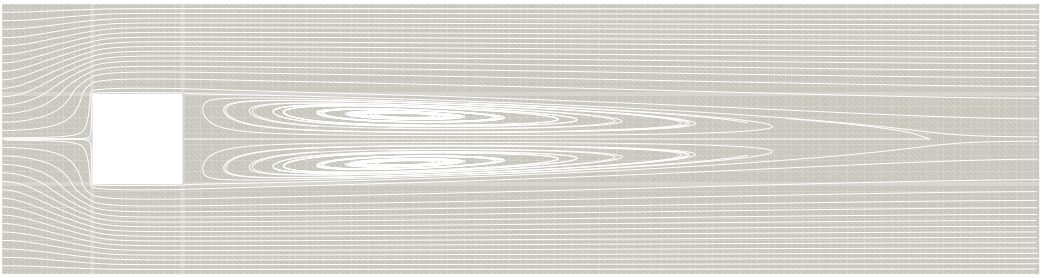

Fig. 6.2. Streamlines of $\boldsymbol{u}_{\mathcal{P}}$ for $\lambda = 4 \cdot 10^{-2}$

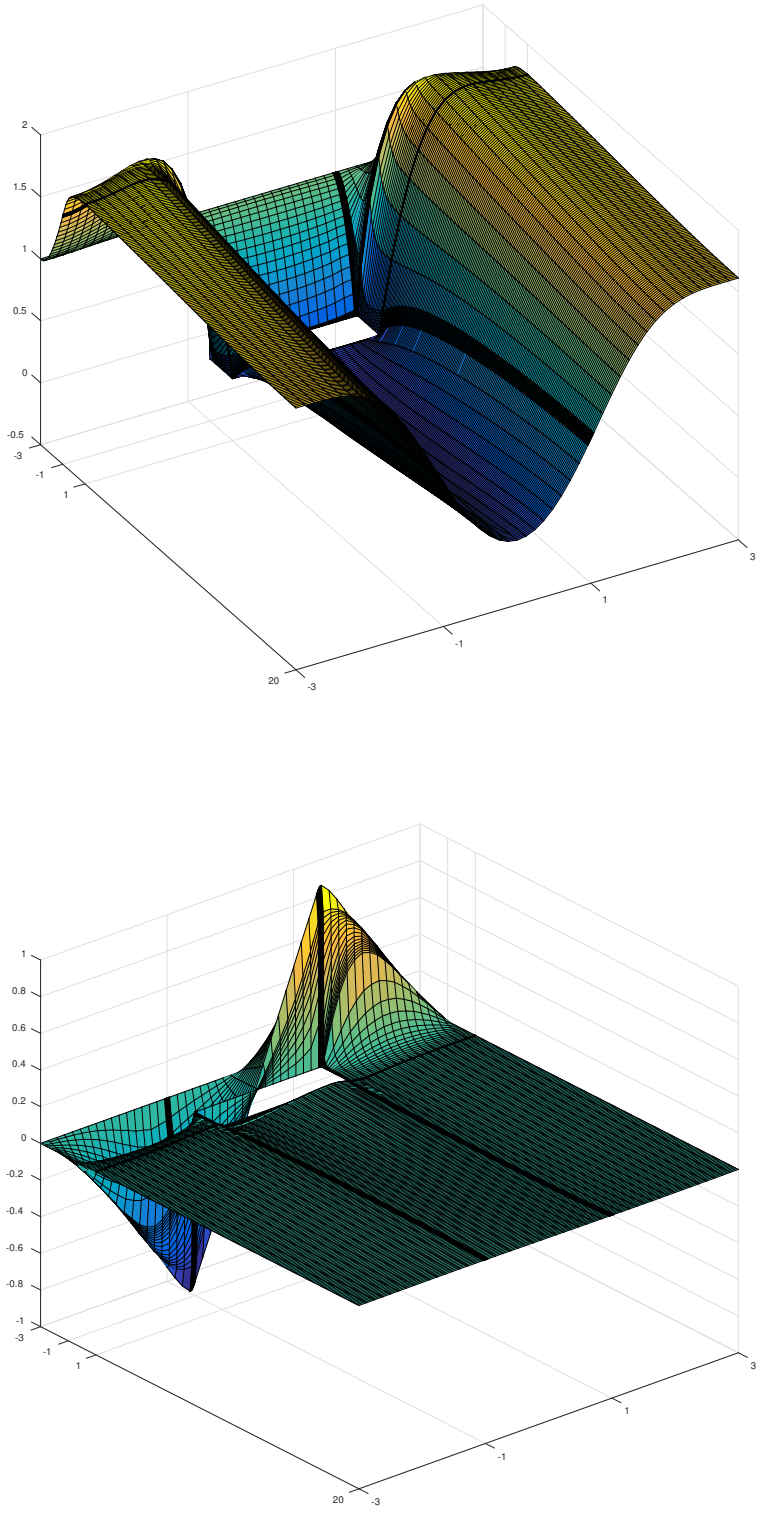

Fig. 6.3. Velocity components $\boldsymbol{u}_1$ (top) and $\boldsymbol{u}_2$ (bottom), $\lambda = 4 \cdot 10^{-2}$

6.3. The $\boldsymbol{P}_2^c \times \mathbb{P}_0$ pair on triangulated corner patches

In Chapter 3 we proved the existence of uniformly inf-sup stable subspaces of $\boldsymbol{V}_{\mathcal{P}} \times M_{\mathcal{P}}$ by restricting the pressure space. The assumptions made on the meshes can be generalised. In fact, the idea of the proofs can be extended to triangles or three-dimensional objects. This is possible because the proof of Corollary 3.15 is independent of the spatial dimension and element shape, as long as uniform inf-sup conditions are satisfied on parts of the mesh. Also, the main ingredient to prove Lemma 3.17 is an anisotropic trace-inverse inequality, which is available on several affine elements (as we saw in Section 2.2.2), and the assumption that the corners are not refined too many times. In the following, we carry out the first step towards an extension to corner patches consisting of triangles.

We have not found proof that the pairs $\boldsymbol{P}_{k+1}^c \times \mathbb{P}_{k-1}$, $(k \geq 2)$ are uniformly inf-sup stable on edge patches. The particular case $\boldsymbol{P}_2^c \times \mathbb{P}_0$ is proven (in [AN04]) to be uniformly inf-sup stable on anisotropic meshes stretched locally in one direction. Hence, we extend the results of Chapter 3 to triangles, but we restrict ourselves to the pair $\boldsymbol{P}_2^c \times \mathbb{P}_0$. To reduce notation, we sketch the sequence of proofs to derive the uniformly inf-sup stable subspace and a stabilised method on one corner patch. The proofs in the presence of multiple, disjoint corner patches then work in an analogous way to Section 3 (using a macro element technique).

Assumptions on the partition:

- Let $\mathcal{P}$ be one of the axis-parallel, corner patches shown in Figure 3.2. Let $\boldsymbol{c}$ be the selected node, let $\omega_{\boldsymbol{c}}$ be the small shaded part, and let $\gamma_{\boldsymbol{c}}$ be an edge on $\partial\omega_{\boldsymbol{c}} \setminus \partial\Omega$.
- Let $\mathcal{T}$ be obtained by splitting each rectangle of $\mathcal{P}$ into exactly two triangles.

The following statements yield the methods. Let $\boldsymbol{V}_{\mathcal{T}} \coloneqq \boldsymbol{P}_{2,\mathcal{T}}^c$ and $M_{\mathcal{T}} \coloneqq \mathbb{P}_{0,\mathcal{T}}$.

- Let $M_{\mathcal{T}}^\star \coloneqq \left\{q \in M_{\mathcal{T}} \colon \langle q \rangle_{\omega_{\boldsymbol{c}}} = 0\right\}$. Then, $\boldsymbol{V}_{\mathcal{T}} \times M_{\mathcal{T}}^\star$ is uniformly inf-sup stable. The proof for axis-parallel, right-angled triangles (e. g. Figure 6.4a) is given in Lemma 6.1 (below). For other meshes (e. g. Figure 6.4b), the local results in [AN04] may be connected by the proof of Corollary 3.15.
- Let $G_\triangle \coloneqq \left\{q \in M_{\mathcal{T}} \colon [\![q]\!]_{\gamma_{\boldsymbol{c}}} = 0\right\}$. Then, $\boldsymbol{V}_{\mathcal{T}} \times G_\triangle$ is uniformly inf-sup stable. The proof of this statement is analogous to the one of Lemma 3.17, but uses the uniform inf-sup condition of $\boldsymbol{V}_{\mathcal{T}} \times M_{\mathcal{T}}^\star$ (derived above) and the trace identity $|e|^{-1}\|q\|_{0,e}^2 = |T|^{-1}\|q\|_{0,T}^2$ where $q \in M_{\mathcal{T}}$.

- The jump stabilisation is again motivated by the following equivalence

$$\left\|q - \Pi_{G_\triangle} q\right\|_{0,\Omega}^2 = \frac{|K||K'|}{|K \cup K'|} [\![q]\!]_{\gamma_{\boldsymbol{c}}}^2 ,$$

  where $\Pi_{G_\triangle}$ is defined as in (3.10) but using $\phi_{\boldsymbol{c}} = |K|^{-1}\chi_K - |K'|^{-1}\chi_{K'}$. The proof of the equivalence is similar to Lemma 3.7, since $\phi_{\boldsymbol{c}}$ satisfies all properties given in Lemma 3.6.

- The convergence is proven in a similar fashion to Chapter 3. The only difference is the use of the trace estimate Lemma 2.3 which holds for triangles (instead of the one for parallelograms).

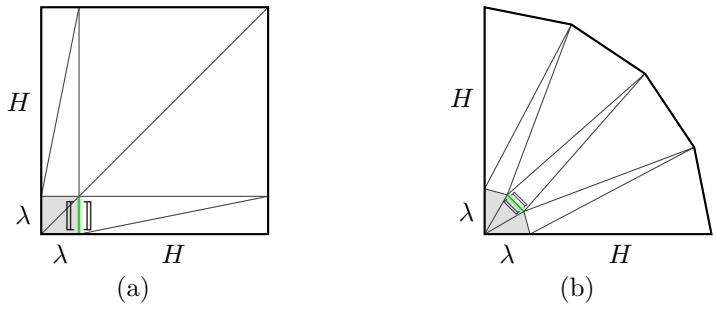

Fig. 6.4. A triangulated and a "circular" corner patch with aspect ratio $\varrho \approx \lambda/H$.

6.3.1. Numerical confirmation

We have computed the stability constants of the unstabilised and the stabilised method using $\boldsymbol{V}_{\mathcal{T}} \times M_{\mathcal{T}}$ on the meshes shown in Figure 6.4 for small parameters λ. The results are shown in Table 6.1 and confirm that there is an inf-sup deficiency depending on the parameter λ and that this deficiency can be cured by penalising a single jump. The numbers were computed by solving the eigenvalue problem (4.25) using the FEniCS software [LMW+12] to assemble the system matrices.

6.3.2. Proof for triangulated corner patches

Lemma 6.1. *Let $\mathcal{P}$ be a partition consisting of axis-aligned rectangles and let $\mathcal{T}$ be a partition obtained by splitting each $K \in \mathcal{P}$ into two triangles. Let*

$$M_{\mathcal{T}}^\star \coloneqq \left\{ q \in M_{\mathcal{T}} \colon \langle q \rangle_{\omega_{\boldsymbol{c}}} = 0 \text{ for } \boldsymbol{c} \in \mathcal{C} \right\} .$$

Then, for all $q \in M_{\mathcal{T}}^\star$ there exists $\boldsymbol{v} \in \boldsymbol{V}_{\mathcal{P}}$ such that $\boldsymbol{v}|_{\omega_{\boldsymbol{c}}} \in \boldsymbol{H}_0^1(\omega_{\boldsymbol{c}})$ for $\boldsymbol{c} \in \mathcal{C}$ and

$$(\operatorname{div} \boldsymbol{v}, q)_\Omega = \|q\|_{0,\Omega}^2 \quad \text{and} \quad |\boldsymbol{v}|_{1,\Omega} \leq C \|q\|_{0,\Omega} .$$

Table 6.1. Stability constants of unstabilised and stabilised systems for $\boldsymbol{P}_2^c \times \mathbb{P}_0$.

	mesh in Fig. 6.4a		mesh in Fig. 6.4b	
λ	$\mu_{\mathcal{T}}$	μ_s	$\mu_{\mathcal{T}}$	μ_s
10^{-1}	$1.32 \cdot 10^{-1}$	$2.81 \cdot 10^{-1}$	$1.44 \cdot 10^{-1}$	$2.25 \cdot 10^{-1}$
10^{-2}	$1.79 \cdot 10^{-2}$	$2.16 \cdot 10^{-1}$	$1.97 \cdot 10^{-2}$	$1.50 \cdot 10^{-1}$
10^{-3}	$1.86 \cdot 10^{-3}$	$2.06 \cdot 10^{-1}$	$2.04 \cdot 10^{-3}$	$1.39 \cdot 10^{-1}$
10^{-4}	$1.87 \cdot 10^{-4}$	$2.05 \cdot 10^{-1}$	$2.05 \cdot 10^{-4}$	$1.38 \cdot 10^{-1}$
10^{-5}	$1.87 \cdot 10^{-5}$	$2.05 \cdot 10^{-1}$	$2.01 \cdot 10^{-5}$	$1.38 \cdot 10^{-1}$

Proof. Let $K = [0, H] \times [0, h]$ and split it as follows:

$$\begin{aligned} T_1 \coloneqq& \left\{(x, y) \in \mathbb{R}^2 \colon 0 \leq x \leq H,\, xh/H \leq y \leq h\right\} \\ =& \left\{(x, y) \in \mathbb{R}^2 \colon 0 \leq y \leq h,\, 0 \leq x \leq yH/h\right\}, \end{aligned}$$

and

$$T_2 \coloneqq \left\{(x, y) \in \mathbb{R}^2 \colon 0 \leq x \leq H,\, 0 \leq y \leq xh/H\right\}.$$

Let $B \in H_0^1(K)$ be the bubble function that is quadratic on T_1 and T_2, and satisfies $B(H/2, h/2) = 1$. On T_1, this function is given by

$$B_1 \coloneqq B|_{T_1} = 4\frac{x}{H}\Big(1 - \frac{y}{h}\Big).$$

Now, let $e \coloneqq \partial T_1 \cap \partial T_2$ and $q \in L_0^2(K) \cap M_{\mathcal{T}}(K)$. Then, using integration by parts we get

$$(\operatorname{div} \boldsymbol{v}, q)_K = \int_e \boldsymbol{v} \cdot [\![\boldsymbol{n} q]\!] \,\mathrm{d}s \quad \text{for} \quad \boldsymbol{v} \in \boldsymbol{H}_0^1(K).$$

Since q is constant on T_1 and T_2, we can write $q = \alpha(\chi_{T_1} - \chi_{T_2})$ where $\alpha \in \mathbb{R}$. Then, choosing

$$\boldsymbol{v} \coloneqq \frac{3}{2}\frac{\|q\|_{0,K}^2}{\|[\![\boldsymbol{n} q]\!]\|_{0,e}^2}[\![\boldsymbol{n} q]\!] B(x, y) = \frac{3}{8}\frac{|K|}{|e|}[\![\boldsymbol{n} q]\!] B(x, y),$$

we get

$$(\operatorname{div} \boldsymbol{v}, q)_K = \|q\|_{0,K}^2 = \alpha^2 |K|.$$

A direct computation yields $\|\partial_x B\|_{0,T_2}^2 = \|\partial_x B\|_{0,T_1}^2$, $\|\partial_y B\|_{0,T_2}^2 = \|\partial_y B\|_{0,T_1}^2$, and

$$\|\partial_x B\|_{0,T_1}^2 = \frac{4h}{3H} \quad \text{and} \quad \|\partial_y B\|_{0,T_1}^2 = \frac{4H}{3h}.$$

Then,

$$
\begin{aligned}
|\boldsymbol{v}|_{1,K}^2 = 2|\boldsymbol{v}|_{1,T_1}^2 &= 2\left(\frac{3|K|}{8|e|}\right)^2 \left((2\alpha n_1)^2 + (2\alpha n_2)^2\right)\left(\|\partial_x B\|_{0,T_1}^2 + \|\partial_y B\|_{0,T_1}^2\right) \\
&= 2\left(\frac{3|K|}{8|e|}\right)^2 4\alpha^2 \frac{4}{3}\left(\frac{h}{H} + \frac{H}{h}\right) \\
&= \frac{3}{2}|K|\alpha^2 \frac{h^2 + H^2}{|e|^2} = \frac{3}{2}\alpha^2|K|\,.
\end{aligned}
$$

Collecting the equalities we get the local inf-sup condition

$$
|\boldsymbol{v}|_{1,K}^{-1}(\operatorname{div}\boldsymbol{v}, r)_K = \sqrt{2/3}\,\|r\|_{0,K}\,.
$$

This proves that the additional local oscillations are controlled by the bubble function B. Then, the result follows using the uniform stability of $\boldsymbol{Q}_2^c \times \mathbb{P}_0$ on edge patches.□

6.4. New locally stabilised methods for balanced order pairs

It is stated in the introduction that balanced-order pairs are inf-sup stable, but their inf-sup constants depend on the aspect ratio (at least for discontinuous pressures). Furthermore, we conjectured that a coarse-scale projection like the pressure stabilisation term used for the $\boldsymbol{Q}_1^c \times \mathbb{P}_0$ pair may cure the dependency on the aspect ratio. In this section we give preliminary arguments and numerical results, that confirm this conjecture.

Preliminary conclusions from our numerical experiments are:

- The Taylor–Hood $\boldsymbol{P}_2^c \times \mathbb{P}_1^c$ pair is inf-sup stable on some anisotropic meshes;
- The pair $\boldsymbol{P}_2^c \times \mathbb{P}_1$ can be stabilised locally to produce a method which is mass-conservative in patches, and stable independently of the aspect ratio;
- The inf-sup deficiency of the $\boldsymbol{Q}_2^c \times \mathbb{P}_1$ pair can be cured by local stabilisation within anisotropic macro elements.

To present the numerical experiments we need the following definitions. By *red refinement* (in two dimensions) we refer to splitting a triangle or parallelogram K into four cells that have the same angles and same shape as the original cell K. The *uniform red refinement* of a partition $\mathcal{P}_0$ refers to the partition that is obtained by applying the red refinement to each $K \in \mathcal{P}_0$. The numerical experiments are carried out on the meshes shown in Figure 6.5. In case of the stabilised methods, the jumps are added only across dashed edges.

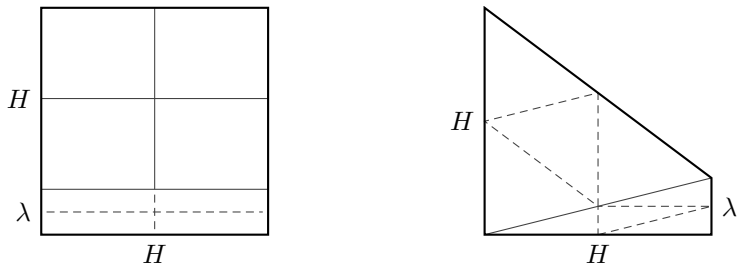

Fig. 6.5. An edge patch and a triangular edge patch with aspect ratio $\varrho \approx \lambda/H$.

6.4.1. The $\boldsymbol{P}_2^c \times \mathbb{P}_1$ pair

Let the partition $\mathcal{P}$ be a uniform red refinement of $\mathcal{P}_0$ consisting of triangles. Let $\boldsymbol{V}_{\mathcal{P}} \coloneqq \boldsymbol{P}^c_{2,\mathcal{P}} \cap \boldsymbol{V}$, let $M_{\mathcal{P}} \coloneqq \mathbb{P}_{1,\mathcal{P}} \cap L^2_0(\Omega)$ be the discontinuous linear polynomials on the fine mesh, and let

$$G \coloneqq \left\{ q \in M_{\mathcal{P}} \colon q \in \mathcal{C}^0(M) \text{ for } M \in \mathcal{P}_0 \right\}.$$

The element $\boldsymbol{V}_{\mathcal{P}} \times G$ seems to be new. On shape-regular meshes we conclude (by the following arguments) that this element is inf-sup stable. In each macro element the pair $\boldsymbol{V}_{\mathcal{P}}(M) \times G(M)$ is the Taylor–Hood element, which is inf-sup stable. By a macro-element technique we conclude the stability of $\boldsymbol{V}_{\mathcal{P}} \times G$.

Conjecture 6.2. *The pair $\boldsymbol{V}_{\mathcal{P}} \times G$ is uniformly stable also on anisotropic meshes without corner patches, and the following equivalence holds*

$$C_1 \|q - \Pi_G q\|^2_{0,M} \leq \sum_{e \in \mathcal{E}_M} \frac{|M|}{4|e|} \|[\![q]\!]\|^2_{0,e} \leq C_2 \|q - \Pi_G q\|^2_{0,M}\,.$$

A consequence of Conjecture 6.2 and $\mathbb{P}^c_1 \subseteq G$ is that the Taylor–Hood pair $\boldsymbol{P}^c_2 \times \mathbb{P}^c_1$ is inf-sup stable on meshes which are uniform red refinements of coarse partitions, and do not possess corner patches.

Furthermore, Conjecture 6.2 allows to prove (as before) the inf-sup deficiency

$$\sup_{\boldsymbol{v} \in \boldsymbol{V}_{\mathcal{P}}} \frac{(\operatorname{div} \boldsymbol{v}, q)_\Omega}{|\boldsymbol{v}|_{1,\Omega}} \geq \beta_G \|\Pi_G q\|_{0,\Omega} - \|q - \Pi_G q\|_{0,\Omega} \quad \text{for all} \quad q \in M_{\mathcal{P}}\,,$$

which justifies a local jump stabilised method for the pair $\boldsymbol{P}^c_2 \times \mathbb{P}_1$. This method is an extension of the one for the $\boldsymbol{P}^c_1 \times \mathbb{P}_0$ pair. The numerical experiment in Table 6.2 confirms the two consequences of Conjecture 6.2, the stability of the Taylor–Hood pair, and of the jump stabilised method on the mesh shown in Figure 6.5b. We penalised the jumps across the dashed edges.

6.4.2. The $\boldsymbol{Q}_2^c \times \mathbb{P}_1$ pair

We also propose local jumps for the $\boldsymbol{Q}_2^c \times \mathbb{P}_1$ pair. This pair is inf-sup stable on shape-regular meshes. On the mesh shown in Figure 6.5a, however, the stability constant of the system behaves like the square of the aspect ratio. Numerical experiments show that adding jumps of the pressure across edges inside anisotropic macro elements removes this deficiency, as we observe in Table 6.2.

Table 6.2. Stability constants of unstabilised and stabilised systems for $\{\boldsymbol{Q}_2^c, \boldsymbol{P}_2^c\} \times \mathbb{P}_1$.

	$\boldsymbol{Q}_2^c \times \mathbb{P}_1$ on Fig. 6.5a		$\boldsymbol{P}_2^c \times \mathbb{P}_1^c$ on Fig. 6.5b	$\boldsymbol{P}_2^c \times \mathbb{P}_1$ on Fig. 6.5b
λ	$\mu_{\mathcal{P}}$	μ_s	$\mu_{\mathcal{P}}$	μ_s
10^{-1}	$2.879 \cdot 10^{-2}$	$2.114 \cdot 10^{-1}$	$6.618 \cdot 10^{-2}$	$6.215 \cdot 10^{-2}$
10^{-2}	$3.333 \cdot 10^{-4}$	$2.191 \cdot 10^{-1}$	$6.018 \cdot 10^{-2}$	$5.702 \cdot 10^{-2}$
10^{-3}	$3.363 \cdot 10^{-6}$	$2.198 \cdot 10^{-1}$	$5.768 \cdot 10^{-2}$	$5.520 \cdot 10^{-2}$
10^{-4}	$3.366 \cdot 10^{-8}$	$2.198 \cdot 10^{-1}$	$5.736 \cdot 10^{-2}$	$5.494 \cdot 10^{-2}$
10^{-5}	$3.366 \cdot 10^{-10}$	$2.198 \cdot 10^{-1}$	$5.732 \cdot 10^{-2}$	$5.491 \cdot 10^{-2}$

Chapter A

Appendix

A.1. Implementation of bases with linear constraints

The implementation of the mixed method using the pair $\boldsymbol{V}_{\mathcal{P}} \times G$ with G defined in Theorem 3.3 requires a basis of G. In this section we show how standard finite element bases and assembly algorithms can be used to assemble the systems for G. More precisely, we describe a general approach to assemble systems for bases arising from linear restrictions.

Let $\mathcal{V} = \operatorname{span}\{\phi_j,\, j = 1 \dots n\}$ denote a (standard) finite element basis and let $\ell\colon \mathcal{V} \to \mathbb{R}$ be a linear functional (constraint). We define $\mathcal{X} \coloneqq \{\Psi \in \mathcal{V}\colon \ell(\Psi) = 0\}$. Our aim is to define a basis $\{\Psi_i\}_i$ of $\mathcal{X}$. First, we realise that $\dim \mathcal{X} \in \{n-1, n\}$. Furthermore, $\dim \mathcal{X} = n \iff \ell(\phi_j) = 0\,, j = 1, \dots, n$ (the case when basis $\{\phi_j\}_{j=1}^n$ already satisfies the constraint imposed by ℓ).

The interesting case is $\dim \mathcal{X} = n - 1$. For each basis function ϕ_j we define the value $w_j \coloneqq \ell(\phi_j)$. Hence, using $\dim \mathcal{X} = n-1$ we have at least one $w_j \neq 0$. In general, we can enumerate the basis such that the first $m-1$ values vanish for some $m \in \{1, \cdots, n\}$, that is,

$$w_j = 0\,(j = 1, \cdots, m-1) \quad \text{and} \quad w_j \neq 0\,(j = m, \cdots, n)\,.$$

Now, the first $m-1$ basis functions Ψ_i are given by

$$\Psi_i = \phi_i \quad \text{for} \quad (i = 1, \dots m-1)\,.$$

If $m = n$, then this is a basis of $\mathcal{X}$. Otherwise, we define the missing functions by

$$\Psi_i = w_i^{-1}\phi_i - w_{i+1}^{-1}\phi_{i+1} \quad \text{for} \quad i = m, \dots n-1\,.$$

Using the linearity of ℓ these functions satisfy the constraint. Also, since $\{\phi_i\}_i$ is a basis, we conclude that $\{\Psi_i\}_i$ is a basis of $\mathcal{X}$. The following vector presentation of the

basis $\{\Psi_i\}_i$ will be useful. We have

$$\begin{pmatrix} \Psi_1 \\ \vdots \\ \Psi_{n-1} \end{pmatrix} = \mathcal{W}^\top \begin{pmatrix} \phi_1 \\ \vdots \\ \phi_n \end{pmatrix} \quad \text{where} \quad \mathcal{W}^\top = \begin{pmatrix} I_{m-1} & \cdot \\ \cdot & W^\top \end{pmatrix} \tag{A.1}$$

or $\mathcal{W}^\top = \begin{pmatrix} I_{m-1} & \mathbf{0}_{(m-1)\times 1} \end{pmatrix}$ if $m = n$. Above, I_{m-1} denotes the identity matrix with $(m-1)$ rows and $W^\top$ is given by

$$\begin{pmatrix} \Psi_m \\ \vdots \\ \Psi_{n-1} \end{pmatrix} = \underbrace{\begin{pmatrix} +w_m^{-1} & -w_{m+1}^{-1} & & \\ & \ddots & \ddots & \\ & & +w_{n-1}^{-1} & -w_n^{-1} \end{pmatrix}}_{=:W^\top} \begin{pmatrix} \phi_m \\ \phi_{m+1} \\ \vdots \\ \phi_n \end{pmatrix}.$$

We obtain the following result.

Corollary A.1. *Let b_h be a linear form and let a_h be bilinear. Then, the assembled matrices and column-vectors*

$$A_\phi = \left[a_h(\phi_i, \phi_j)\right]_{ij}, \quad A_\Psi = \left[a_h(\Psi_i, \Psi_j)\right]_{ij}, \quad B_\Psi = \left[b_h(\Psi_i)\right]_i \quad \textit{and} \quad B_\phi = \left[b_h(\phi_i)\right]_i$$

satisfy the relations

$$B_\Psi = \mathcal{W}^\top B_\phi \quad \textit{and} \quad A_\Psi = \mathcal{W}^\top A_\phi \mathcal{W}.$$

Corollary A.1 shows that the matrices A_Ψ and B_Ψ can be assembled from standard algorithms and matrix multiplications with the weight-matrix $\mathcal{W}$. Evaluating the weights $\ell(\phi_i)$ is the same as calculating a Lagrange multiplier. Multiple linear constraints can be treated one-by-one.

Given the coefficients for basis $\{\Psi_i\}$ (e. g. after solving the restricted system) one can restore the coefficients of the standard basis using identity (A.1), that is,

$$\begin{pmatrix} \alpha_1 & \cdots & \alpha_{n-1} \end{pmatrix} \begin{pmatrix} \Psi_1 \\ \vdots \\ \Psi_{n-1} \end{pmatrix} = \begin{pmatrix} \alpha_1 & \cdots & \alpha_{n-1} \end{pmatrix} \mathcal{W}^\top \begin{pmatrix} \phi_1 \\ \vdots \\ \phi_n \end{pmatrix}.$$

Therefore, the coefficients for the standard basis $\{\phi_i\}_i$ are given by $(\alpha_1 \cdots \alpha_{n-1})\mathcal{W}^\top$. In the multiple constraint setting, say three constraints, the dimension of the constrained basis lies between $n-3$ and n. In this case $\mathcal{W}^\top$ is replaced by $\mathcal{W}_{\ell_1}^\top \mathcal{W}_{\ell_2}^\top \mathcal{W}_{\ell_3}^\top$ with $\mathcal{W}_{\ell_i}^\top$ of appropriate dimension.

Index

Bibliography

[AADL08] G. Acosta, T. Apel, R. G. Durán, and A. L. Lombardi, *Anisotropic error estimates for an interpolant defined via moments*, Computing **82** (2008), no. 1, 1–9.

[ABW15] M. Ainsworth, G. R. Barrenechea, and A. Wachtel, *Stabilization of high aspect ratio mixed finite elements for incompressible flow*, SIAM Journal on Numerical Analysis **53** (2015), no. 2, 1107–1120.

[AC00] M. Ainsworth and P. Coggins, *The stability of mixed hp-finite element methods for Stokes flow on high aspect ratio elements*, SIAM J. Numer. Anal. **38** (2000), no. 5, 1721–1761 (electronic).

[AD99] G. Acosta and R. G. Durán, *The maximum angle condition for mixed and nonconforming elements: application to the Stokes equations*, SIAM J. Numer. Anal. **37** (1999), no. 1, 18–36 (electronic).

[Ada75] R. A. Adams, *Sobolev spaces*, Academic Press, New York, 1975.

[AKL08] T. Apel, T. Knopp, and G. Lube, *Stabilized finite element methods with anisotropic mesh refinement for the Oseen problem*, Appl. Numer. Math. **58** (2008), no. 12, 1830–1843.

[AM08] T. Apel and G. Matthies, *Nonconforming, anisotropic, rectangular finite elements of arbitrary order for the Stokes problem*, SIAM J. Numer. Anal. **46** (2008), no. 4, 1867–1891.

[AMR03] T. Apel and H. Maharavo Randrianarivony, *Stability of discretizations of the Stokes problem on anisotropic meshes*, Math. Comput. Simulation **61** (2003), no. 3-6, 437–447.

[AN04] T. Apel and S. Nicaise, *The inf-sup condition for low order elements on anisotropic meshes*, Calcolo **41** (2004), no. 2, 89–113.

[ANS01] T. Apel, S. Nicaise, and J. Schöberl, *Crouzeix-Raviart type finite elements on anisotropic meshes*, Numer. Math. **89** (2001), no. 2, 193–223.

[Ape99] T. Apel, *Anisotropic finite elements: local estimates and applications*, B. G. Teubner, Stuttgart, 1999.

[BA76] I. Babuška and A. K. Aziz, *On the angle condition in the finite element method.*, SIAM J. Numer. Anal. **13** (1976), 214–226.

[BB98] J. M. Borwein and P. B. Borwein, *Pi and the AGM*, Canadian Mathematical Society Series of Monographs and Advanced Texts, 4, John Wiley & Sons, Inc., New York, 1998.

[BB01] R. Becker and M. Braack, *A finite element pressure gradient stabilization for the Stokes equations based on local projections*, Calcolo **38** (2001), no. 4, 173–199.

[BBF13] D. Boffi, F. Brezzi, and M. Fortin, *Mixed finite element methods and applications*, Springer Series in Computational Mathematics, vol. 44, Springer, Heidelberg, 2013.

[BBGS04] T. Barth, P. Bochev, M. Gunzburger, and J. Shadid, *A taxonomy of consistently stabilized finite element methods for the Stokes problem*, SIAM J. Sci. Comput. **25** (2004), no. 5, 1585–1607.

[BBJL07] M. Braack, E. Burman, V. John, and G. Lube, *Stabilized finite element methods for the generalized Oseen problem*, Comput. Methods Appl. Mech. Engrg. **196** (2007), no. 4-6, 853–866.

[BDG06] P. B. Bochev, C. R. Dohrmann, and M. D. Gunzburger, *Stabilization of low-order mixed finite elements for the Stokes equations*, SIAM J. Numer. Anal. **44** (2006), no. 1, 82–101 (electronic).

[BF91] Franco Brezzi and Michel Fortin, *Mixed and hybrid finite element methods*, Springer Series in Computational Mathematics, vol. 15, Springer-Verlag, New York, 1991.

[BF01] F. Brezzi and M. Fortin, *A minimal stabilisation procedure for mixed finite element methods*, Numer. Math. **89** (2001), no. 3, 457–491.

[BFH06] E. Burman, M. A. Fernández, and P. Hansbo, *Continuous interior penalty finite element method for Oseen's equations*, SIAM J. Numer. Anal. **44** (2006), no. 3, 1248–1274.

[BH82] A. N. Brooks and T. J. R. Hughes, *Streamline upwind/Petrov-Galerkin formulations for convection dominated flows with particular emphasis on the incompressible Navier-Stokes equations*, Comput. Methods Appl. Mech. Engrg. **32** (1982), no. 1-3, 199–259.

[Bla07] J. Blasco, *An anisotropic pressure-stabilized finite element method for incompressible flow problems*, Comput. Math. Appl. **53** (2007), no. 6, 895–909.

[Bla08] ———, *An anisotropic GLS-stabilized finite element method for incompressible flow problems*, Comput. Methods Appl. Mech. Engrg. **197** (2008), no. 45-48, 3712–3723.

[BLR12] M. Braack, G. Lube, and L. Röhe, *Divergence preserving interpolation on anisotropic quadrilateral meshes*, Comput. Methods Appl. Math. **12** (2012), no. 2, 123–138.

[BM99] C. Bernardi and Y. Maday, *Uniform inf-sup conditions for the spectral discretization of the Stokes problem*, Math. Models Methods Appl. Sci. **9** (1999), no. 3, 395–414.

[Bof94] D. Boffi, *Stability of higher order triangular Hood-Taylor methods for the stationary Stokes equations*, Math. Models Methods Appl. Sci. **4** (1994), no. 2, 223–235.

[BR95] R. Becker and R. Rannacher, *Finite element solution of the incompressible Navier-Stokes equations on anisotropically refined meshes*, Fast solvers for flow problems (Kiel, 1994), Notes Numer. Fluid Mech., vol. 49, Vieweg, Braunschweig, 1995, pp. 52–62.

[Bra08] M. Braack, *A stabilized finite element scheme for the Navier-Stokes equations on quadrilateral anisotropic meshes*, M2AN Math. Model. Numer. Anal. **42** (2008), no. 6, 903–924.

[BS08] S. C. Brenner and L. R. Scott, *The mathematical theory of finite element methods*, third ed., Texts in Applied Mathematics, vol. 15, Springer, New York, 2008.

[Bur08] E. Burman, *Pressure projection stabilizations for Galerkin approximations of Stokes' and Darcy's problem*, Numer. Methods Partial Differential Equations **24** (2008), no. 1, 127–143.

[BW15] G. R. Barrenechea and A. Wachtel, *A note on the stabilised Q1-P0 method on quadrilaterals with high aspect ratios*, Proceedings of BAIL 2014 (to appear) (2015).

[CB00] R. Codina and J. Blasco, *Stabilized finite element method for the transient Navier-Stokes equations based on a pressure gradient projection*, Comput. Methods Appl. Mech. Engrg. **182** (2000), no. 3-4, 277–300.

[Cia78] P. G. Ciarlet, *The finite element method for elliptic problems*, North-Holland Publishing Co., Amsterdam, 1978.

[CR73] M. Crouzeix and P.-A. Raviart, *Conforming and nonconforming finite element methods for solving the stationary Stokes equations. I*, Rev. Française Automat. Informat. Recherche Opérationnelle Sér. Rouge **7** (1973), no. R-3, 33–75.

[DB04] C. R. Dohrmann and P. B. Bochev, *A stabilized finite element method for the Stokes problem based on polynomial pressure projections*, Internat. J. Numer. Methods Fluids **46** (2004), no. 2, 183–201.

[DJW89] J. Douglas Jr. and J. P. Wang, *An absolutely stabilized finite element method for the Stokes problem*, Math. Comp. **52** (1989), no. 186, 495–508.

[DL06] R. G. Durán and A. L. Lombardi, *Finite element approximation of convection diffusion problems using graded meshes*, Appl. Numer. Math. **56** (2006), no. 10-11, 1314–1325.

[ESW14] H. C Elman, D. J Silvester, and A. J Wathen, *Finite elements and fast iterative solvers: with applications in incompressible fluid dynamics*, Oxford University Press, 2014.

[FF92] L. P. Franca and S. L. Frey, *Stabilized finite element methods. II. The incompressible Navier-Stokes equations*, Comput. Methods Appl. Mech. Engrg. **99** (1992), no. 2-3, 209–233.

[FFH92] L. P. Franca, S. L. Frey, and T. J. R. Hughes, *Stabilized finite element methods. I. Application to the advective-diffusive model*, Comput. Methods Appl. Mech. Engrg. **95** (1992), no. 2, 253–276.

[FRW14] S. Franz, H.-G. Roos, and A. Wachtel, *A C^0 interior penalty method for a singularly-perturbed fourth-order elliptic problem on a layer-adapted mesh*, Numer. Methods Partial Differential Equations **30** (2014), no. 3, 838–861.

[Gal94] G. P. Galdi, *An introduction to the mathematical theory of the Navier–Stokes equations*, vol. 1, Springer, Berlin, 1994.

[Geo03] E. H. Georgoulis, *Discontinuous Galerkin methods on shape-regular and anisotropic meshes*, 2003, D.Phil. Thesis, University of Oxford.

[GLOS05] T. Gelhard, G. Lube, M. A. Olshanskii, and J.-H. Starcke, *Stabilized finite element schemes with LBB-stable elements for incompressible flows*, J. Comput. Appl. Math. **177** (2005), no. 2, 243–267.

[GR86] V. Girault and P.-A. Raviart, *Finite element methods for Navier Stokes equations*, Springer, Berlin, 1986.

[Gri85] P. Grisvard, *Elliptic problems in nonsmooth domains*, Monographs and Studies in Mathematics, vol. 24, Pitman (Advanced Publishing Program), Boston, MA, 1985.

[GS00] P. M. Gresho and R. L. Sani, *Incompressible flow and the finite element method, isothermal laminar flow*, John Wiley and Sons, Chichester, 2000.

[HF87] T. J. R. Hughes and L. P. Franca, *A new finite element formulation for computational fluid dynamics. VII. The Stokes problem with various well-posed boundary conditions: symmetric formulations that converge for all velocity/pressure spaces*, Comput. Methods Appl. Mech. Engrg. **65** (1987), no. 1, 85–96.

[HFB86] T. J. R. Hughes, L. P. Franca, and M. Balestra, *A new finite element formulation for computational fluid dynamics. V. Circumventing the Babuška-Brezzi condition: a stable Petrov-Galerkin formulation of the Stokes problem accommodating equal-order interpolations*, Comput. Methods Appl. Mech. Engrg. **59** (1986), no. 1, 85–99.

[HS90] P. Hansbo and A. Szepessy, *A velocity-pressure streamline diffusion finite element method for the incompressible Navier-Stokes equations*, Comput. Methods Appl. Mech. Engrg. **84** (1990), no. 2, 175–192.

[HSV12] A. Hannukainen, R. Stenberg, and M. Vohralík, *A unified framework for a posteriori error estimation for the Stokes problem*, Numer. Math. **122** (2012), no. 4, 725–769.

[JJLR14] E. W. Jenkins, V. John, A. Linke, and L. G. Rebholz, *On the parameter choice in grad-div stabilization for the Stokes equations*, Adv. Comput. Math. **40** (2014), no. 2, 491–516.

[JS86] C. Johnson and J. Saranen, *Streamline diffusion methods for the incompressible Euler and Navier-Stokes equations*, Math. Comp. **47** (1986), no. 175, 1–18.

[Kno09] P. Knobloch, *On the application of local projection methods to convection-diffusion-reaction problems*, BAIL 2008—boundary and interior layers, Lect. Notes Comput. Sci. Eng., vol. 69, Springer, Berlin, 2009, pp. 183–194.

[Kno10] ———, *A generalization of the local projection stabilization for convection-diffusion-reaction equations*, SIAM J. Numer. Anal. **48** (2010), no. 2, 659–680.

[KS92] N. Kechkar and D. J. Silvester, *Analysis of locally stabilized mixed finite element methods for the Stokes problem*, Math. Comp. **58** (1992), no. 197, 1–10.

[KT13] P. Knobloch and L. Tobiska, *Improved stability and error analysis for a class of local projection stabilizations applied to the Oseen problem*, Numer. Methods Partial Differential Equations **29** (2013), no. 1, 206–225.

[Kun00] G. Kunert, *An a posteriori residual error estimator for the finite element method on anisotropic tetrahedral meshes*, Numer. Math. **86** (2000), no. 3, 471–490.

[Lin14] A. Linke, *On the role of the Helmholtz decomposition in mixed methods for incompressible flows and a new variational crime*, Comput. Methods Appl. Mech. Engrg. **268** (2014), 782–800.

[LMW+12] A. Logg, K.-A. Mardal, G. N. Wells, et al., *Automated solution of differential equations by the finite element method*, Springer, 2012.

[LR13] A. Linke and L. G. Rebholz, *On a reduced sparsity stabilization of grad-div type for incompressible flow problems*, Comput. Methods Appl. Mech. Engrg. **261/262** (2013), 142–153.

[LS13] Q. Liao and D. Silvester, *Robust stabilized Stokes approximation methods for highly stretched grids*, IMA J. Numer. Anal. **33** (2013), no. 2, 413–431.

[Mal81] D. S. Malkus, *Eigenproblems associated with the discrete LBB condition for incompressible finite elements*, Internat. J. Engrg. Sci. **19** (1981), no. 10, 1299–1310.

[MPP03] S. Micheletti, S. Perotto, and M. Picasso, *Stabilized finite elements on anisotropic meshes: a priori error estimates for the advection-diffusion and the Stokes problems*, SIAM J. Numer. Anal. **41** (2003), no. 3, 1131–1162 (electronic).

[MS09] S. Mao and Z. Shi, *Error estimates of triangular finite elements under a weak angle condition*, J. Comput. Appl. Math. **230** (2009), no. 1, 329–331.

[MST07] G. Matthies, P. Skrzypacz, and L. Tobiska, *A unified convergence analysis for local projection stabilisations applied to the Oseen problem*, M2AN Math. Model. Numer. Anal. **41** (2007), no. 4, 713–742.

[MT15] G. Matthies and L. Tobiska, *Local projection type stabilization applied to inf-sup stable discretizations of the Oseen problem*, IMA J. Numer. Anal. **35** (2015), no. 1, 239–269.

[PS85] J. Pitkäranta and T. Saarinen, *A multigrid version of a simple finite element method for the Stokes problem*, Math. Comp. **45** (1985), no. 171, 1–14.

[Riv81] T. J. Rivlin, *An introduction to the approximation of functions*, Dover Publications Inc., New York, 1981.

[RST08] H.-G. Roos, M. Stynes, and L. Tobiska, *Robust numerical methods for singularly perturbed differential equations*, second ed., Springer Series in Computational Mathematics, vol. 24, Springer-Verlag, Berlin, 2008.

[RT92] R. Rannacher and S. Turek, *Simple nonconforming quadrilateral Stokes element*, Numer. Methods Partial Differential Equations **8** (1992), no. 2, 97–111.

[Sil94] D. Silvester, *Optimal low order finite element methods for incompressible flow*, Comput. Methods Appl. Mech. Engrg. **111** (1994), no. 3-4, 357–368.

[SK90] D. J. Silvester and N. Kechkar, *Stabilised bilinear-constant velocity-pressure finite elements for the conjugate gradient solution of the Stokes problem*, Comput. Methods Appl. Mech. Engrg. **79** (1990), no. 1, 71–86.

[SO97] M. Stynes and E. O'Riordan, *A uniformly convergent Galerkin method on a Shishkin mesh for a convection-diffusion problem*, J. Math. Anal. Appl. **214** (1997), no. 1, 36–54.

[SS96] R. Stenberg and M. Suri, *Mixed hp finite element methods for problems in elasticity and Stokes flow*, Numer. Math. **72** (1996), no. 3, 367–389.

[SS98] D. Schötzau and C. Schwab, *Mixed hp-FEM on anisotropic meshes*, Math. Models Methods Appl. Sci. **8** (1998), no. 5, 787–820.

[SS11] D. J. Silvester and V. Simoncini, *An optimal iterative solver for symmetric indefinite systems stemming from mixed approximation*, ACM Trans. Math. Software **37** (2011), no. 4, Art. 42, pp. 1–22.

[SSS99] D. Schötzau, C. Schwab, and R. Stenberg, *Mixed hp-FEM on anisotropic meshes. II. Hanging nodes and tensor products of boundary layer meshes*, Numer. Math. **83** (1999), no. 4, 667–697.

[ST08] M. Stynes and L. Tobiska, *Using rectangular Q_p elements in the SDFEM for a convection-diffusion problem with a boundary layer*, Appl. Numer. Math. **58** (2008), no. 12, 1789–1802.

[SW94] D. Silvester and A. Wathen, *Fast iterative solution of stabilised Stokes systems. II. Using general block preconditioners*, SIAM J. Numer. Anal. **31** (1994), no. 5, 1352–1367.

[TL91] L. Tobiska and G. Lube, *A modified streamline diffusion method for solving the stationary Navier-Stokes equation*, Numer. Math. **59** (1991), no. 1, 13–29.

[Tob09] L. Tobiska, *Recent results on local projection stabilization for convection-diffusion and flow problems*, BAIL 2008—boundary and interior layers, Lect. Notes Comput. Sci. Eng., vol. 69, Springer, Berlin, 2009, pp. 55–75.

[WH03] T. Warburton and J. S. Hesthaven, *On the constants in hp-finite element trace inverse inequalities*, Comput. Methods Appl. Mech. Engrg. **192** (2003), no. 25, 2765–2773.

[WS93] Andrew Wathen and David Silvester, *Fast iterative solution of stabilised Stokes systems. I. Using simple diagonal preconditioners*, SIAM J. Numer. Anal. **30** (1993), no. 3, 630–649.